Univerza v Ljubljani

Fakulteta za elektrotehniko

Denis Pavliha

Enotna programska oprema za načrtovanje zdravljenja tumorjev z elektrokemoterapijo

DOKTORSKA DISERTACIJA

Mentor: prof. dr. Damijan Miklavčič

Solkan in Ljubljana, 2013

University of Ljubljana

Faculty of Electrical Engineering

Denis Pavliha

Integrated Treatment Planning Software for Electrochemotherapy of Tumors

DOCTORAL DISSERTATION

Mentor: prof. Damijan Miklavčič, Ph. D.
(University of Ljubljana, Slovenia)

Solkan and Ljubljana, 2013

nonotu Karlotu

PREFACE

The present PhD thesis is a result of procedure design and research, and algorithm development and validation performed during the PhD study period at the Laboratory of Biocybernetics, Faculty of Electrical Engineering, University of Ljubljana. The results of the performed work have been published in (or have been submitted to) the following international journals:

Article 1: PATIENT-SPECIFIC TREATMENT PLANNING OF ELECTROCHEMOTHERAPY: PROCEDURE DESIGN AND POSSIBLE PITFALLS
PAVLIHA Denis, KOS Bor, ŽUPANIČ Anže, MARČAN Marija, SERŠA Gregor, MIKLAVČIČ Damijan
Bioelectrochemistry 87: 265-273, 2012.

Article 2: ELECTROPORATION-BASED TREATMENT PLANNING FOR DEEP-SEATED TUMORS BASED ON AUTOMATIC LIVER SEGMENTATION OF MRI IMAGES
PAVLIHA Denis, M. MUŠIČ Maja, SERŠA Gregor, MIKLAVČIČ Damijan
PLOS ONE: resubmitted after minor revision, 2013.

Article 3: PLANNING OF ELECTROPORATION-BASED TREATMENTS USING WEB-BASED TREATMENT PLANNING SOFTWARE
PAVLIHA Denis, KOS Bor, MARČAN Marija, ŽUPANIČ Anže, SERŠA Gregor, MIKLAVČIČ Damijan
Journal of Membrane Biology: submitted, 2013.

ACKNOWLEDGEMENTS

The research has been supported by the Slovenian Research Agency (ARRS) under a Junior Researcher grant. Research was conducted in the scope of the Electroporation in Biology and Medicine (EBAM) European Associated Laboratory (LEA).

I would like to thank Assoc. Prof. Dr. Alenka Maček-Lebar for seeing my potential and inviting me to join the Laboratory of Biocybernetics as student researcher.

I am deeply indebted to my mentor, Prof. Dr. Damijan Miklavčič, for giving me the possibility to grow professionally and, also, for letting me persuade him that physical presence is not a prerequisite for successful research.

I would like to thank Assist. Dr. Maja M. Mušič for providing the manually segmented liver models, Dr. Bor Kos for numerical calculations of electric field distribution, and Marija Marčan for the 3D virtual electrode insertion interface, and tumor and vessel segmentation.

My appreciation also goes to my co-workers at Laboratory of Biocybernetics for providing a positive working environment.

I would like to thank my parents and nona Elza for directing me into taking the right decisions.

And finally, thank you Alenka for being who you are.

TABLE OF CONTENTS

ABSTRACT

When a biological cell is exposed to an external electric field of sufficient strength, its plasma membrane becomes transiently permeabilized. The phenomenon termed electroporation allows the material from outside or inside the cell to traverse the plasma membrane, which would be otherwise impossible. A paramount electroporation-based application is electrochemotherapy (ECT) which enhances chemotherapy outcome by porating the tumor cells and, thus, allowing the cytostatic drug to enter the cells in larger amounts and destroy them. ECT has already been in clinical practice for treating superficial nodules of skin melanoma metastases; in case of such nodules, the clinician needs to follow standard operating procedures for successful treatment since superficial metastases are easily-accessible. Because ECT is a successful method for local tumor treatment, advances towards treating deep-seated tumors have been made. When treating deep-seated tumors, which are diverse in shape, size, and location, patient-specific treatment planning is required for successful treatment. Based on the radiotherapy example where treatment planning is known to be of paramount importance, we established treatment planning procedure of electroporation-based treatments (e.g. ECT). Deriving from a clinical study where colorectal metastases in the liver were subject to ECT treatment, we implemented and evaluated three possible automatic liver segmentation algorithms that generate three-dimensional liver models from patient's medical images. Optimization of the algorithms was performed on a set of seven patient cases previously manually segmented by a radiologist (i.e. training set), and validation of optimized algorithms was performed on another four patient cases previously manually segmented by a radiologist that were not part of the training set. Validation demonstrated that our implementations of segmentation algorithms can perform liver segmentation of cases that were not part of the training set, as well. Furthermore, we developed web-based treatment planning software with a graphical user interface that allows remote treatment planning to clinicians without engineering knowledge. The software allows generation of treatment plans for ECT remotely: automatic segmentation of liver is possible, as well as loading presegmented cases, which allows clinicians evaluation of already-treated cases.

RAZŠIRJENI POVZETEK V SLOVENSKEM JEZIKU

UVOD

Če biološko celico izpostavimo zunanjemu električnemu polju dovolj visoke jakosti, pride do začasnega povečanja prepustnosti celične membrane (Kotnik et al., 2010). Pojav, ki ga imenujemo elektroporacija (Neumann et al., 1982), omogoča snovem iz okolice, da prehajajo celično membrano, kar bi bilo sicer oteženo ali nemogoče. Ilustracijo pojava elektroporacije prikazuje *Slika 1*.

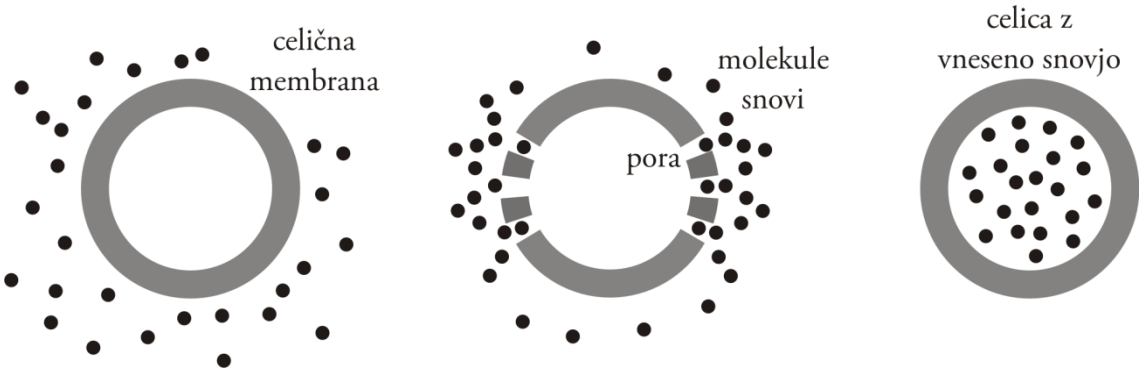

Slika 1: ob prisotnosti električnega polja visoke jakosti se na celični membrani začasno vzpostavijo pore, ki omogočajo molekulam snovi iz okolice prehajanje celične membrane. Po določenem času se pore zaprejo in snov iz okolice ostane vnesena v celici.

Električno polje, ki je predpogoj za pojav elektroporacije, vzpostavimo v okolici ciljne skupine celic tako, da dovedemo kratkotrajne visokonapetostne električne pulze z uporabo generatorja pulzov (tj. elektroporatorja) (Puc et al., 2004). Čeprav vsi mehanizmi, ki so povezani z elektroporacijo, še niso povsem pojasnjeni, pa je elektroporacija že uveljavljena kot splošno uporaben tehnološki postopek celične manipulacije, saj učinkuje na vse vrste celic (tj. živalske, rastlinske in mikroorganizme) (Miklavčič et al., 2012). Elektroporacija je že v rabi na različnih področjih: v medicini za elektrokemoterapijo tumorjev (Serša and Miklavčič, 2008) in atermično ablacijo (Garcia et al., 2011; Rubinsky et al., 2007), gensko terapijo (Heller and Heller, 2010) in drugih (Daugimont et al., 2010; Gusbeth et al., 2009; Toepfl et al., 2007; Ušaj et al., 2010).

Ena pomembnejših aplikacij, ki temelji na pojavu elektroporacije, je elektrokemoterapija (EKT) (Serša et al., 2008). EKT je lokalna metoda zdravljenja raka, ki nadgrajuje kemoterapijo z uporabo elektroporacije: ob prisotnosti dovolj močnega električnega polja pride v področju tumorja do povečanja prepustnosti celične membrane (Serša and Miklavčič, 2008). Pojav omogoči kemoterapevtiku, ki je bil predhodno vbrizgan bolniku intravensko ali sistemsko, da laže prodre v tumorske celice in jih tako uniči. Postopek EKT prikazuje *Slika 2*.

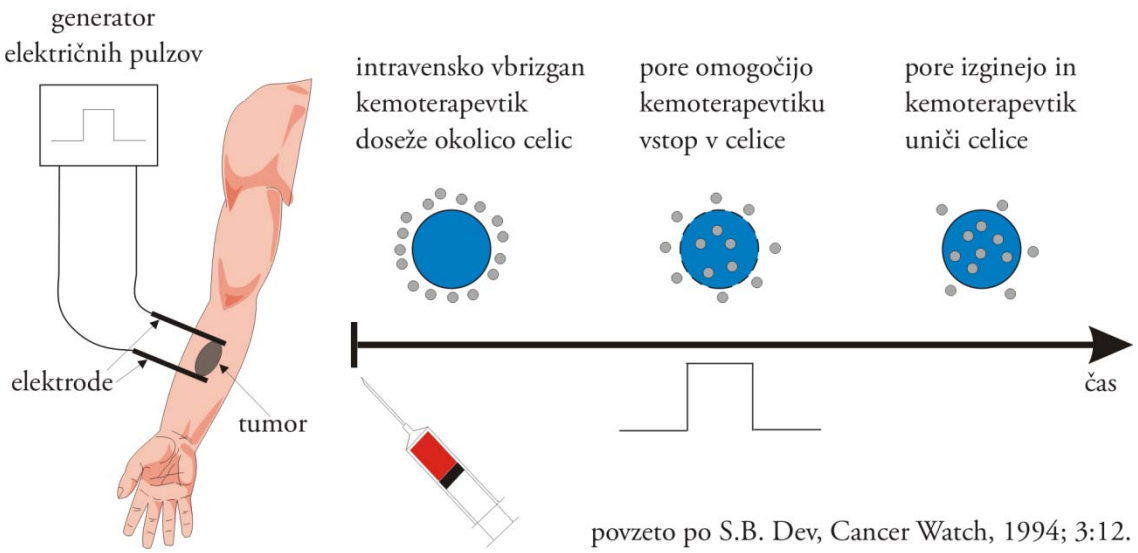

Slika 2: potek zdravljenja tumorjev z elektrokemoterapijo (Maček-Lebar et al., 1998).

EKT je že v klinični rabi za zdravljenje površinskih metastaz kožnega melanoma v več kot sto kliničnih centrih v Evropi (Miklavčič et al., 2012). V primeru zdravljenja površinskih metastaz, ki so enostavno dostopne ter povečini podobnih oblik in relativno majhne velikosti, je za uspešno zdravljenje dovolj, da zdravnik upošteva standardne operativne postopke (SOP), ki narekujejo lastnosti uporabljenih električnih pulzov (amplituda, čas trajanja, ponavljalna frekvenca in število) in uporabo igelnih ali ploščatih elektrod z znanimi dimenzijami, in tako zagotovi uspešno zdravljenje (Mir et al., 2006). Omenjeni način zdravljenja, tj. uporaba SOP za izvedbo EKT, pa ne predvideva zdravljenja globoko ležečih tumorjev, kjer so za zdravljenje potrebne elektrode, ki jih lahko vstavimo posamično ter tako vplivamo na njihov medsebojni položaj in posledično na porazdelitev električnega polja (Miklavčič et al., 1998). Za zdravljenje globoko ležečih tumorjev je torej potrebno bolniku prilagojeno načrtovanje zdravljenja, pri katerem na osnovi medicinskih slik bolnika

(npr. magnetno resonančno slikanje – MRI, ali računalniška tomografija – CT) zgradimo tridimenzionalni model obravnavanega bolnikovega organa skupaj s pripadajočimi strukturami (npr. žile) in patološkim tkivom (tj. tumorjem). Zgrajeni tridimenzionalni model nato uporabimo za izračun porazdelitve električnega polja glede na predvideno konfiguracijo (tj. število in položaj) vstavljenih elektrod. Omenjeni postopek omogoča natančno predvidevanje zadostne pokritosti tumorja z električnim poljem dovolj visoke jakosti, kar je eden od ključnih pokazateljev, ali bo zdravljenje z EKT uspešno (Miklavčič et al., 2006, 1998).

Elektrokemoterapiji sorodna aplikacija, ki prav tako temelji na pojavu elektroporacije, je atermična ireverzibilna elektroporacija (angl. *non-thermal irreversible electroporation* – N-TIRE) (Davalos and Rubinsky, 2008; Garcia et al., 2011; Županič and Miklavčič, 2009). V nasprotju z EKT, kjer ciljno skupino celic uniči kemoterapevtik, dosežemo pri N-TIRE uničenje ciljne skupine celic zgolj s prisotnostjo električnega polja. Vrednost električne poljske jakosti je namreč višja kot pri EKT, kjer so predvidene vrednosti nad *reverzibilnim pragom* (tj. 460 V/cm za jetra) in pod *ireverzibilnim pragom* (tj. 700 V/cm za jetra); za uspešno uničenje tkiva z metodo N-TIRE je torej potrebna izpostavitev celic v tkivu električnemu polju jakosti nad *ireverzibilnim pragom* (Miklavčič et al., 2000; Šel et al., 2005). Ker temelji N-TIRE na pojavu elektroporacije, prav tako potrebuje bolniku prilagojeno načrtovanje zdravljenja za uspešno zdravljenje (Županič and Miklavčič, 2009).

METODE

Postopek načrtovanja zdravljenja z elektrokemoterapijo

Bolniku prilagojeno zdravljenje je že uveljavljeno na področju radioterapije. Radioterapija je do neke mere podobna elektroporaciji, saj prav tako temelji na interakciji fizikalnega dejavnika (radiacija v radioterapiji in električno polje v elektroporaciji) z biološkim tkivom (Lecchi et al., 2008). Radioterapija je metoda zdravljenja raka, pri kateri snop usmerjene energije le-to s sevanjem odloži na ciljno mesto v bolnikovem telesu. Škoda, ki jo snop izsevane energije povzroči, ni omejena na tumorske celice, temveč zajame tudi bližnjo okolico; največja dovoljena količina izsevane energije je tako omejena z največjo količino

sevanja, ki jo izpostavljeno zdravo tkivo ob tumorju še lahko prejme (Tannock et al., 2005). Glavni cilj radioterapije je povzročitev toliko škode tumorskim celicam, da je njihova rast trajno onemogočena in se zato ne morejo več deliti. Postopek zdravljenja z radioterapijo je sestavljen iz korakov, ki jih prikazuje *Tabela 1*.

Tabela 1: vzporednice med radioterapijo in elektrokemoterapijo globoko ležečih tumorjev.

Radioterapija	Elektrokemoterapija globoko ležečih tumorjev
Simulacija: medicinske slike bolnika (CT ali kombinacija CT z MRI ali PET).	Numerični model elektroporacije: modela elektroporacije na celičnem in tkivnem nivoju.
Načrtovanje zdravljenja: določitev ciljnih območij tkiva z razgradnjo slik, določitev omejitev izsevane energije (doza), gradnja geometrije matematičnega modela, izračun ustreznega načrta z numeričnim modeliranjem in optimizacijo (število frakcij, položaj in jakost energijskih snopov).	Načrtovanje zdravljenja: medicinske slike bolnika (CT ali MRI, možnost kombinacije s PET), določitev ciljnih območij tkiva z razgradnjo slik, gradnja geometrije matematičnega modela, izračun ustreznega načrta z numeričnim modeliranjem in optimizacijo (število in položaj uporabljenih elektrod), jakost uporabljenih električnih pulzov.
Preverjanje nastavitev: medicinske slike bolnika (CT ali MRI) so uporabljene za preverjanje položaja bolnika in ciljnih območij tkiva; dodatno je položaj preverjen še z laserji in objekti na koži bolnika, ki služijo kot zaznamki (v kombinaciji z npr. ultrazvokom ali s podobno tehniko slikanja).	Preverjanje nastavitev: optimalni položaji elektrod so poravnani z izvornimi medicinskimi slikami bolnika; položaj elektrod je med operativnim posegom preverjen z ultrazvokom.
Izvedba zdravljenja in nadzor: izsevana energija je usmerjena v bolnikovo telo v skladu z načrtom zdravljenja. Postopek medicinskega slikanja v realnem času je uporabljen za nadzor nad premiki zaradi dihanja bolnika.	Izvedba zdravljenja in nadzor: po vstavitvi elektrod in vbrizganju kemoterapevtika so sproženi električni pulzi; obenem so izvedene meritve tokov in napetosti z namenom zaznavanja morebitnih napak.
Ocena odziva: po izvedenem zdravljenju sledijo meritve velikosti tumorja (ali medicinsko slikanje z uporabo bioloških tumorskih markerjev).	Ocena odziva: po izvedenem zdravljenju sledijo meritve velikosti tumorja (ali medicinsko slikanje z uporabo bioloških tumorskih markerjev) in/ali histološka ocena (primerjava z medicinskimi slikami, dobljenimi pred izvedbo elektrokemoterapije).

Kot prikazuje *Tabela 1*, gre pri primerjavi radioterapije z EKT globoko ležečih tumorjev za podobna postopka zdravljenja. Oba postopka namreč temeljita na načrtovanju zdravljenja glede na bolnikove medicinske slike (npr. CT ali MRI), ki jih uporabimo za določitev ciljnega območja patološkega tkiva, ki ga želimo uničiti. Z razgradnjo medicinskih slik

izdelamo tridimenzionalni model, ki služi kot geometrija matematičnega modela radioterapije (izračun izsevane doze) ali elektroporacije (izračun pokritosti z dovolj visokim električnim poljem pri določenem številu in trajanju pulzov, npr. 8 x 100 μs). Pred izvedbo zdravljenja je izvedeno še preverjanje nastavitev, po sami izvedbi pa ocena odziva tumorja na zdravljenje.

Ker je načrtovanje zdravljenja na področju radioterapije uveljavljen postopek, ki velja za ključni dejavnik za uspešno zdravljenje, smo postopek načrtovanja zdravljenja z EKT zasnovali tako, da temelji na načrtovanju zdravljenja z radioterapijo (Pavliha et al., 2012) in posledično prispeva k lažji uveljavitvi načrtovanja zdravljenja z EKT med končnimi uporabniki (tj. zdravniki).

Uvoz in pred-procesiranje medicinskih slik

Postopek izdelave načrta zdravljenja z EKT se prične z uvozom medicinskih slik bolnika. V okviru postopka uvoza slik, zapisanih v standardnem formatu za shranjevanje in prenos medicinskih slik DICOM (National Electrical Manufacturers Association, 2009), preberemo vse uvožene slike in jih razvrstimo glede na serijo, v okviru katere so bile posnete, in glede na njihov položaj v prostoru (koordinata Z). Omenjeni metapodatki se nahajajo v glavi medicinskih slik kot parametri *SeriesNumber* in *SliceLocation*, in nam omogočajo izbiro serije, ki jo želimo uporabiti za načrtovanje zdravljenja.

Nato izvedemo pred-procesiranje vseh slik (rezin), ki jih vključuje izbrana serija. Postopek pred-procesiranja je izveden na vsaki sliki posebej, zato ga lahko izvajamo večnitno (angl. *multi-threaded*), tj. na več procesorjih ali procesorskih jedrih naenkrat. Pravilna interpretacija medicinskih slik je določena s parametri, ki določajo ciljno območje tkiva (angl. *Volume of Interest – VOI*) in so vključeni v glavi medicinskih slik kot lastnosti *Window Center (WC)* in *Window Width (WW)*. Lastnosti WC in WW uporabimo za transformacijo izvornih medicinskih slik z uporabo sigmoidne funkcije, ki jo opisuje *Enačba 1*.

$$izhod = \frac{rang}{1 + e^{-4\frac{vhod - WC}{WW}}} \qquad \textbf{Enačba 1}$$

Po sigmoidni transformaciji medicinske slike spremenimo tako, da izločimo morebitne neželene učinke zaradi intenzitetne nehomogenosti (Vovk et al., 2007), in sicer z uporabo javno dostopnega algoritma za odpravo nehomogenosti (Zheng et al., 2009). Po odpravi nehomogenosti medicinske slike filtriramo z uporabo povprečevalnega in nato še zameglitvenega Gaussovega filtra ($\sigma = 3$) z velikostjo okna 3 krat 3 pik. Na koncu postopka izvedemo dodatno transformacijo z uporabo sigmoidne funkcije s fiksnimi vrednostmi (*WC = 20000, WW = 100, rang =* 2^{16}), ki zagotovijo, da bo intenziteta medicinskih slik porazdeljena po celotnem šestnajstbitnem območju in z dovolj kontrasta, da bo mogoča razgradnja. Fiksne vrednosti sigmoidne funkcije so bile določene empirično na osnovi podatkov realnih primerov bolnikov. Z izvedbo zadnjega koraka je pred-procesiranje zaključeno in medicinske slike so pripravljene na razgradnjo.

Razgradnja z rastjo regij (angl. *region growing*)

Prvi algoritem, ki smo ga uporabili za razgradnjo medicinskih slik, je postopek rasti regij (angl. *region growing*). Algoritem smo uporabili za avtomatsko razgradnjo jeter, vendar ga lahko uporabimo tudi za razgradnjo drugih organov (Mancas et al., 2005). Rast regij določi, ali je prostorska pika (angl. *voxel*) del ciljne regije tako, da primerja njeno intenziteto z intenziteto začetnega semena, tj. prostorske pike, ki jo na začetku postopka ročno določi uporabnik (zaradi česar algoritma pravzaprav ne moremo opredeliti kot avtomatskega). Rast regij deluje v treh dimenzijah in preverja intenziteto vsake prostorske pike, ki je bila dodana v čakalno vrsto. Delovanje algoritma prikazuje *Slika 3*.

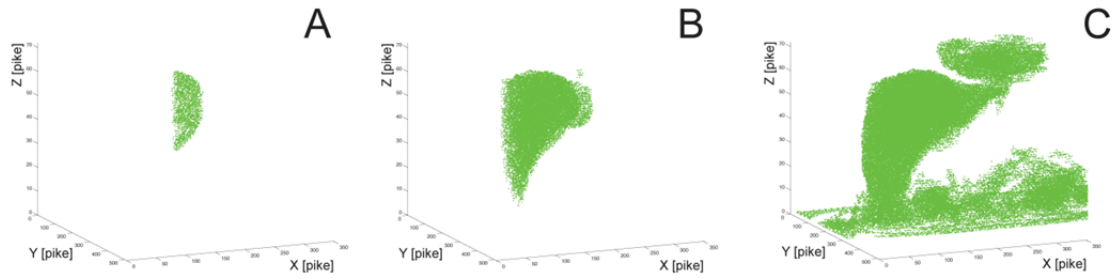

Slika 3: razgradnja z uporabo postopka rasti regij. Prikazan je potek razgradnje jeter po 40.000 (A), 400.000 (B) in vseh (C) obravnavanih prostorskih pikah jeter.

Za uspešno razgradnjo jeter je potrebno dopustiti odstopanje intenzitete prostorskih pik, ki jih želimo vključiti v ciljno območje (tj. jetra), od začetnega semena; v našem primeru smo odstopanje nastavili na vrednost 0.20, kar pomeni, da se nahajajo dopustne intenzitete pik, ki predstavljajo jetra, v območju $0.8 \cdot I_{SEME} < I_{TRENUTNI} < 1.2 \cdot I_{SEME}$, kjer predstavlja I intenziteto prostorske pike in *bit* njeno enoto. Zaradi možnosti puščanja lahko rast regij poleg jeter vključi tudi neželene dele tkiva drugih organov (npr. spodnji del srca, kot to prikazuje *Slika 3*), vendar tovrstne neželene učinke razgradnje odstranimo v naslednjem koraku z uporabo po-procesorja.

Razgradnja z adaptivnim upragovljanjem (angl. *adaptive threshold*)

Drugi možni način razgradnje jeter, ki smo ga preizkusili, je z uporabo adaptivnega upragovljanja. Algoritem temelji na fizični lastnosti organa, tj. zveznosti tkiva med dvema sosednjima rezinama. Algoritem spreminja trenutno obdelovano rezino z uporabo pragovne funkcije, ki ji v vsaki iteraciji spremenimo vrednost praga in obenem primerjamo trenutno rezino (z uporabo normirane križne korelacije) s prejšnjo, že obdelano rezino; končno obdelana trenutna rezina je spremenjena z uporabo pragovne vrednosti, ki je izkazala največjo podobnost s prejšnjo rezino. Delovanje algoritma prikazuje *Slika 4*.

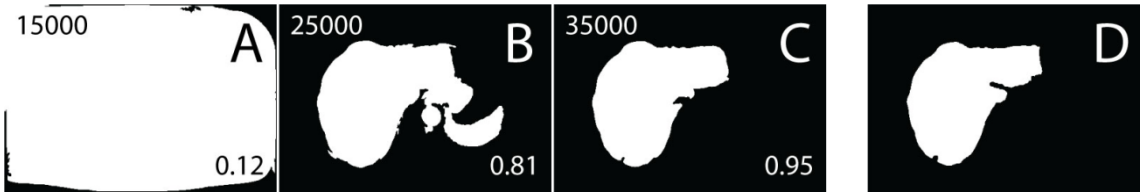

Slika 4: algoritem adaptivnega upragovljanja (angl. *adaptive threshold*); prikazane so tri možne vrednosti (15.000, 25.000, 35.000) praga trenutne rezine (A, B, C) in prejšnja rezina (D).

Algoritem torej upošteva, da se zunanji rob organa, ki ga razgrajujemo, med rezinama spreminja počasi (zvezno), zato predvideva, da je pravilna vrednost praga tista, ki povzroči največjo podobnost s prejšnjo rezino. *Slika 4* prikazuje potek razgradnje trenutne rezine jeter (A, B in C), ki jo primerjamo s prejšnjo, že obdelano rezino (D). Vrednost praga 15.000 bitov izkazuje 12-odstotno podobnost (*Slika 4A*, vrednost 0.12), vrednost praga 25.000 bitov 81-odstotno podobnost (*Slika 4B*, vrednost 0.81), vrednost praga 35.000

bitov pa največjo, 95-odstotno podobnost (*Slika 4C*, vrednost 0.95) glede na prejšnjo, že obdelano rezino (*Slika 4D*).

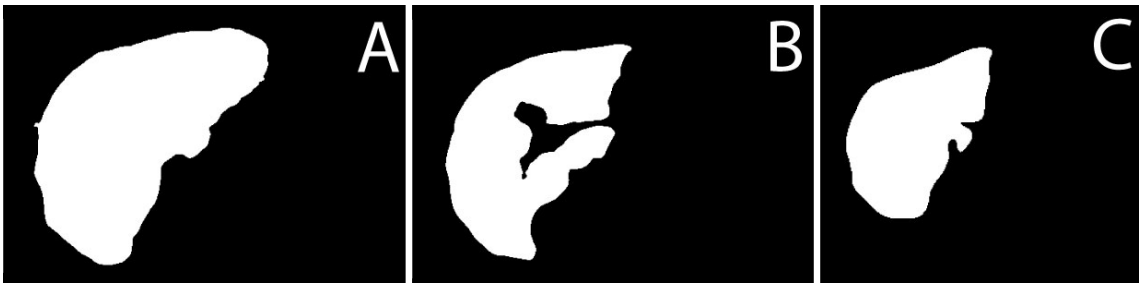

Slika 5: primeri treh predlog (A, B, C), ki so v uporabi pri razgradnji prve rezine jeter z algoritmom adaptivnega upragovljanja.

Ker na začetku delovanja algoritem adaptivnega upragovljanja nima na voljo nobene predhodne rezine, je za prvo primerjavo podobnosti uporabljen nabor šestih predlog, tj. slik s približkom razgrajene rezine organa, ki ga razgrajujemo (npr. jeter). Adaptivno upragovljenje je izvedeno kot primerjava podobnosti z vsemi predlogami, ki so na voljo, prva rezina pa je na koncu primerjav z vsemi predlogami razgrajena glede na največjo izkazano podobnost s katero koli izmed predlog. Primere treh predlog prikazuje *Slika 5*: uporaba predloge torej omogoča avtomatsko inicializacijo vrednosti praga prve rezine in posledično omogoči razgradnjo vseh naslednjih rezin.

Razgradnja z aktivnimi krivuljami – kačami (angl. *active contours*)

Tretji algoritem, ki smo ga uporabili in dodelali za avtomatsko razgradnjo jeter, je algoritem aktivnih (prilagodljivih) krivulj, včasih imenovanih tudi *kače* (angl. *active-deformable contours – snakes*) (Kass et al., 1987). Algoritem temelji na postavitvi aktivne (prilagodljive) krivulje na rezino (medicinsko sliko), ki jo želimo razgraditi. Aktivna krivulja je sestavljena iz točk, ki se nahajajo na mestih prostorskih pik slike in se lahko premikajo po sliki glede na energijo okolice točke. Energija točke in njene okolice je sestavljena iz štirih energijskih prispevkov: elastičnosti (tj. točka aktivne krivulje naj bo glede na obod krivulje čim bliže sredini med dvema sosednjima točkama krivulje), ukrivljenosti (tj. točka aktivne krivulje naj bo čim bliže premici, ki povezuje dve sosednji točki krivulje), magnitudi energije rezine (medicinske slike) in smeri vektorskega polja energije rezine (medicinske slike). Energijo rezine (medicinske slike) izračunamo z uporabo polja gradientnega vektorskega pretoka

(angl. *Gradient Vector Flow – GVF*), ki temelji na zaznanih robovih slike; uporabili smo javno dostopen algoritem izračuna GVF (Xu and Prince, 1998). Primer izračunanega polja GVF prikazuje *Slika 6*.

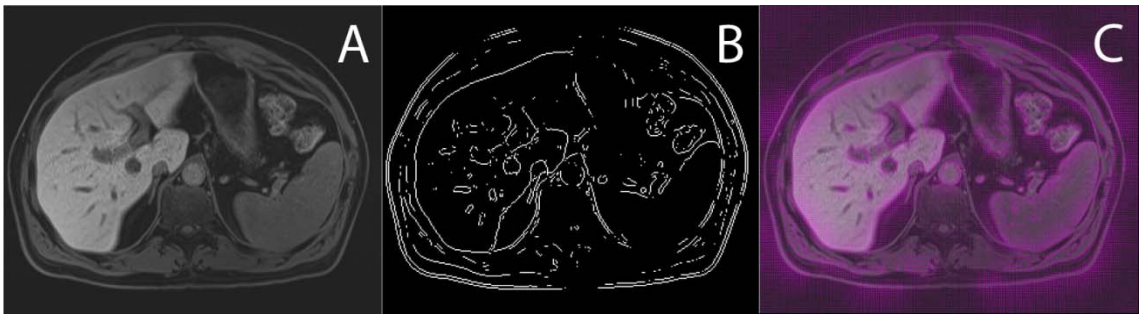

Slika 6: primer izvorne rezine (A), zaznanih robov slike (B) in izračunanega polja GVF (C).

Vsi štirje energijski prispevki so uravnoteženi z uporabo energijskih koeficientov: na osnovi naših izkušenj z optimizacijo algoritmov s podatki realnih primerov bolnikov smo prispevke uravnotežili s koeficienti 1 (elastičnost), 3 (ukrivljenost), 9 (magnituda GVF) in 3 (smer GVF). Vsi energijski prispevki so normirani tako, da se nahajajo v območju vrednosti (0, 1) z namenom njihove medsebojne enakovrednosti. Na osnovi uravnoteženosti energijskih prispevkov je v vsaki iteraciji premika aktivne krivulje izračunana energija v piki, kjer se nahaja točka aktivne krivulje, in v vsaki izmed osmih pik v dvodimenzionalni okolici (tj. na isti rezini). Točka aktivne krivulje je nato premaknjena v piko z najmanjšo energijo; v primeru, da imajo vse okoliške točke večjo energijo od trenutne pike, ostane točka aktivne krivulje na istem mestu. Postopek ponovimo za vse točke aktivne krivulje, ter iterativno ponavljamo dovolj dolgo, da se aktivna krivulja poravna z robom organa, ki ga razgrajujemo (v našem primeru delovanje krivulje zaustavimo po 100 iteracijah).

Ker je delovanje aktivne krivulje dvodimenzionalno (tj. krivulja je dvodimenzionalen objekt, ki se premika po eni rezini), je tridimenzionalna informacija o vseh slikah v zbirki v algoritem vključena tako, da je začetna aktivna krivulja trenutne rezine enaka končni aktivni krivulji prejšnje rezine. Ker ob razgradnji prve rezine nimamo podatka o prejšnji rezini, je za inicializacijo aktivne krivulje uporabljen kar algoritem *adaptivnega upragovljanja*, ki zagotovi razgradnjo prve rezine: dobljeni segment je nato uporabljen za

določitev točk začetne aktivne krivulje, in sicer z uporabo sledenja obrisu območja (Pavešić, 2000).

Po-procesiranje medicinskih slik

Po-procesiranje je namenjeno izločanju napak, do katerih lahko privede postopek razgradnje (npr. puščanje pri algoritmih, ki temeljijo na intenziteti). Razviti po-procesor nam omogoča, da iz razgrajenih medicinskih slik izločimo dele, ki so bili pomotoma vključeni v razgrajeni organ (v primeru jeter gre lahko za srce, ledvice, vranico in okoliško maščobno tkivo).

Po-procesorski algoritem temelji na primerjavi dveh sosednjih rezin z uporabo normirane križne korelacije: algoritem z uporabo erozije loči večje segmente, ki so pravzaprav manjši segmenti, ki so zaradi puščanja povezani med seboj s tanko vezjo. Nato vsakega od segmentov primerja s prejšnjo rezino: če primerjava pokaže, da nekega segmenta s trenutne rezine ni bilo na prejšnji rezini, ga algoritem zavrže. Poudariti je potrebno, da po-procesor ne zavrača segmentov, ki so posledica delitve tkiva na dva segmenta: v primeru, da je prejšnja rezina vključevala le en segment jeter, medtem ko sta na trenutni rezini zaznana dva, bo po-procesor z uporabo normirane križne korelacije ugotovil, da razdeljena segmenta prostorsko ustrezata enemu segmentu s prejšnje rezine in ju obdržal.

Optimizacija in validacija algoritmov za razgradnjo

Ker je ključnega pomena, da izdelajo algoritmi za razgradnjo modele razgrajenega organa pravilno, moramo njihovo delovanje ustrezno ovrednotiti (validirati). Validacijo smo izvedli kot dvostopenjski postopek: najprej smo delovanje algoritmov optimizirali z uporabo podatkovne baze slik sedmih bolnikov, ki jih je ročno razgradila radiologinja, in je služila kot učna množica. Nato smo delovanje optimiziranih algoritmov ovrednotili (validirali) z uporabo nove podatkovne baze slik štirih bolnikov, ki jih je ročno razgradila radiologinja in ni bila del učne množice.

Optimizacijo smo izvedli tako, da smo najprej definirali, kateri parametri vsakega izmed treh algoritmov za razgradnjo jeter (rast regij, adaptivno upragovljanje in aktivne krivulje) so predmet optimizacije; nato smo določili njihova predvidena območja vrednosti in jih

iterativno spreminjali v okviru optimizacije. Rast regij smo optimizirali tako, da smo spreminjali vrednost parametra, ki določa dovoljeno odstopanje intenzitete od intenzitete začetnega semena. Adaptivno upragovljanje smo optimizirali tako, da smo spreminjali vrednost parametra, ki določa velikost maske filtra v okviru pred-procesiranja, in začetni koeficient, ki določa predvideno velikost segmenta na prvi rezini. Aktivne krivulje smo optimizirali tako, da smo spreminjali vrednost vseh štirih koeficientov, ki določajo medsebojno uravnoteženost energijskih prispevkov.

V vsaki iteraciji smo za vsak algoritem razgradnje primerjali trenutno dobljene rezultate z učno množico, tj. ročno razgrajenimi modeli, ki jih je izdelala radiologinja. Primerjavo smo izvedli z uporabo normirane križne korelacije za vsako rezino posebej. Na koncu smo ovrednotili dvoje optimalnih parametrov: specifično optimalne parametre (tj. parametre, ki so optimalni za posamezen primer) in globalno optimalne parametre (tj. parametre, ki so optimalni za vse razgrajene primere).

Po optimizaciji smo algoritme nastavili na vrednosti, ki predstavljajo globalno optimalne parametre. Nato smo delovanje optimiziranih algoritmov ovrednotili z razgradnjo slik dodatnih štirih bolnikov, ki jih je ročno razgradila radiologinja.

Spletni grafični uporabniški vmesnik za načrtovanje zdravljenja z elektrokemoterapijo

Postopek načrtovanja zdravljenja z elektrokemoterapijo smo vključili v spletno programsko opremo, ki vsebuje grafični uporabniški vmesnik za načrtovanje zdravljenja z elektrokemoterapijo (EKT). Ker želimo uporabo programske opreme približati zdravnikom, smo jo razvili tako, da je zahtevana minimalna interakcija uporabnika, saj je to ena od ključnih zahtev za razvoj uporabniku prilagojene programske opreme (Heymann and Degani, 2007). Najzahtevnejše postopke (tj. razgradnjo medicinskih slik, gradnjo geometrije tridimenzionalnega matematičnega modela in izračun porazdelitve električnega polja) smo poenostavili do te mere, da so izvedeni avtomatsko. Potek delovanja spletnega grafičnega uporabniškega vmesnika (angl. *Graphical User Interface – GUI*) za načrtovanje zdravljenja z EKT prikazuje *Slika 7*.

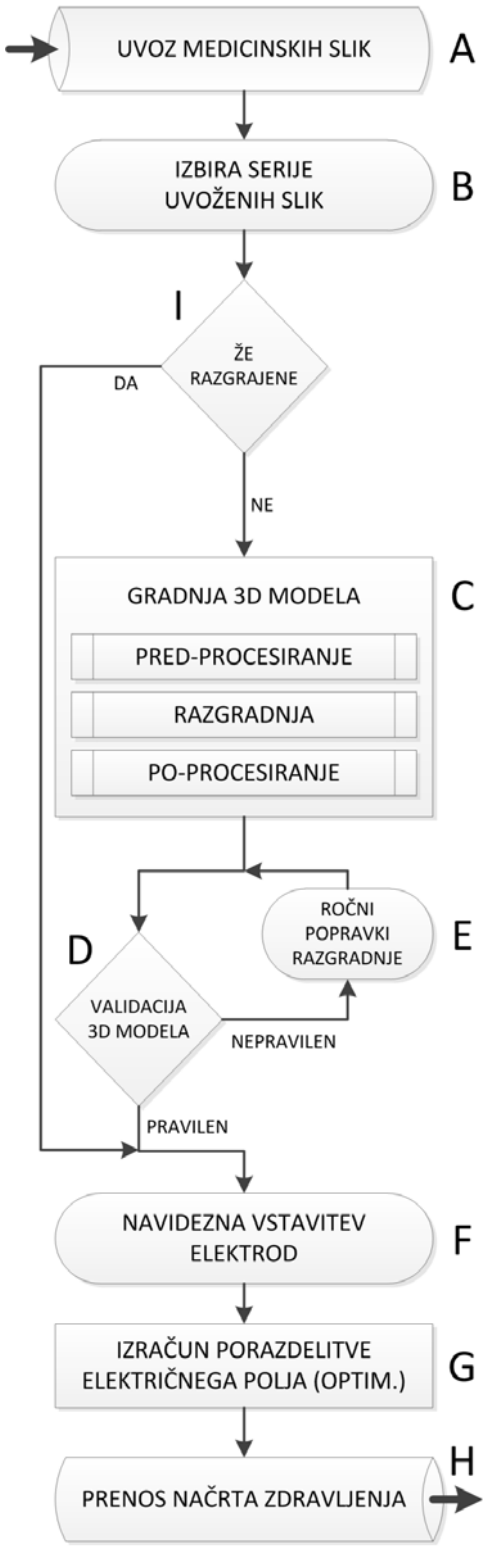

Slika 7: potek delovanja spletnega grafičnega uporabniškega vmesnika za načrtovanje zdravljenja z EKT.

Postopek se prične z uvozom medicinskih slik (*Slika 7A*), ki omogoča nalaganje datotek DICOM prek spletne strani. V primeru, da naložene datoteke vsebujejo več serij bolnikovih slik, GUI omogoči izbiro ustrezne serije (*Slika 7B*). Če so naložene slike že razgrajene (npr. z uporabo tretje programske opreme in razgrajeni segmenti zapisani v obliki standardnega zapisa DICOM), lahko izdelane segmente uporabimo neposredno za načrtovanje EKT (*Slika 7I*). Če slike še niso razgrajene, sledi izvedba postopkov avtomatske razgradnje (*Slika 7C*) glede na izbrano ciljno tkivo (npr. jetra). Ko je zgrajena geometrija tridimenzionalnega matematičnega modela, sledi ročna validacija (tj. končni uporabnik potrdi, da je zgrajeni tridimenzionalni model pravilen, kar preveri s temeljitim pregledom izdelanih kontur vseh rezin) (*Slika 7D*). V primeru, da avtomatsko razgrajeni organ ni pravilno izdelan, ima uporabnik možnost ročnih popravkov (*Slika 7E*). Nato je uporabljen vmesnik za navidezno vstavitev elektrod, kjer določimo število in položaj uporabljenih elektrod za EKT (*Slika 7F*). Sledi izračun porazdelitve električnega polja in optimizacija napetosti in položajev elektrod (*Slika 7G*) ter predstavitev rezultatov v obliki prenosljivega načrta zdravljenja (*Slika 7H*).

REZULTATI

Rezultati optimizacije algoritmov za razgradnjo jeter so podani v *Tabeli 2*, kjer so prikazane podobnosti slik sedmih bolnikov, ki jih je ročno razgradila radiologinja, z avtomatsko razgrajenimi slikami. Vsaka podobnost (P) predstavlja aritmetično sredino podobnosti vseh rezin serije bolnikovih slik. Podobnost je bila izračunana za specifično optimalne parametre (tj. parametre, ki so optimalni za posamezen primer - P_S) in globalno optimalne parametre (tj. parametre, ki so optimalni za vse razgrajene primere - P_G). *Std* predstavlja standardni odklon aritmetične sredine rezin znotraj serije.

Tabela 2: rezultati optimizacije algoritmov za razgradnjo jeter z uporabo aritmetične sredine.

serija	RAST REGIJ				ADAPTIVNO UPRAGOVLJANJE				AKTIVNE KRIVULJE			
	P_S	std(P_S)	P_G	std(P_G)	P_S	std(S_S)	P_G	std(P_G)	P_S	std(P_S)	P_G	std(P_G)
2009122	91.2	*15.9*	**61.1**	*38.9*	72.2	*39.1*	**72.2**	*39.1*	88.2	*22.1*	**68.8**	*36.3*
2010093	92.7	*13.7*	**86.8**	*19.0*	70.1	*38.1*	**68.1**	*40.2*	89.7	*20.7*	**64.5**	*40.1*
2010122	84.7	*19.6*	**79.9**	*19.2*	73.4	*34.5*	**70.1**	*33.9*	84.6	*22.3*	**78.6**	*23.6*
2011022	81.1	*25.5*	**65.7**	*36.0*	74.0	*29.1*	**73.2**	*29.5*	79.4	*29.1*	**67.2**	*37.1*
2011042	86.6	*19.4*	**78.2**	*29.0*	60.0	*35.6*	**40.1**	*41.6*	64.8	*36.6*	**54.8**	*37.9*
2011062	94.4	*2.1%*	**94.2**	*2.9%*	80.2	*13.4*	**80.2**	*13.4*	87.6	*14.1*	**67.9**	*36.6*
2011070	92.5	*4.9%*	**92.5**	*4.9%*	69.3	*37.8*	**69.3**	*37.8*	80.3	*30.9*	**80.3**	*30.9*
aritm.sr.			**79.8%**	*12.7%*			**67.6%**	*12.8%*			**68.8%**	*8.6%*

Ker je lahko predstavitev podobnosti serije z uporabo aritmetične sredine podobnosti vseh rezin v seriji zavajajoča, saj na tovrstno predstavitev rezultatov občutno vplivajo rezine, ki jih algoritmi za razgradnjo niso zaznali (podobnost tovrstnih rezin je 0%), smo rezultate predstavili še z uporabo mediane podobnosti vseh rezin v seriji.

Rezultati so podani v *Tabeli 3*, v kateri so prikazane podobnosti slik sedmih bolnikov, ki jih je ročno razgradila radiologinja, z avtomatsko razgrajenimi slikami. Vsaka podobnost (P) predstavlja mediano podobnosti vseh rezin serije bolnikovih slik. Podobnost je bila izračunana za specifično optimalne parametre (tj. parametre, ki so optimalni za posamezen primer - P_S) in globalno optimalne parametre (tj. parametre, ki so optimalni za vse razgrajene primere - P_G).

Tabela 3: rezultati optimizacije algoritmov za razgradnjo jeter z uporabo mediane.

serija	RAST REGIJ		ADAPTIVNO UPRAGOVLJANJE		AKTIVNE KRIVULJE	
	P_S	P_G	P_S	P_G	P_S	P_G
20091223	95.6%	**79.9%**	92.0%	**92.0%**	94.0%	**82.6%**
20100930	95.9%	**91.8%**	88.8%	**90.0%**	95.3%	**82.5%**
20101221	90.3%	**85.6%**	88.6%	**87.8%**	91.0%	**86.9%**
20110228	88.8%	**84.8%**	83.7%	**83.7%**	88.3%	**86.4%**
20110421	92.6%	**89.2%**	73.6%	**55.4%**	80.2%	**75.6%**
20110624	94.4%	**94.4%**	82.7%	**82.7%**	91.2%	**88.9%**
20110707	93.4%	**93.4%**	87.6%	**87.6%**	91.5%	**91.5%**
mediana		**89.2%**		**87.6%**		**86.4%**

Iz rezultatov (*Tabela 2* in *Tabela 3*) lahko vidimo, da dopušča največ optimizacije algoritem za razgradnjo z rastjo regij, saj omogoča doseganje do 94.4% (aritmetična sredina, standardni odklon 2.1%) oz. do 95.9% (mediana) podobnosti z referenčnim modelom v primeru specifično optimalnih parametrov. Če opazujemo globalno optimalne parametre, je rast regij prav tako za optimizacijo najbolj dopusten algoritem od preizkušenih, saj lahko z njim dosežemo globalne podobnosti z referenčnimi modeli v vrednostih 79.8% (aritmetična sredina, standardni odklon 12.7%) oz. 89.2% (mediana).

Optimizaciji je sledilo končno ovrednotenje (validacija), v okviru katerega smo z uporabo globalno optimalnih parametrov razgradili štiri serije slik bolnikov, ki niso bile del učne množice. Rezultate validacije prikazuje *Tabela 4*.

Tabela 4: rezultati validacije optimiziranih algoritmov za razgradnjo jeter.

serija	RAST REGIJ			ADAPTIVNO UPRAGOVLJANJE			AKTIVNE KRIVULJE		
	P_{AS}	std(P_{AS})	P_{MD}	P_{AS}	std(P_{AS})	P_{MD}	P_{AS}	std(P_{AS})	P_{MD}
V1	**79.4%**	*24.8%*	**87.0%**	**67.3%**	*30.5%*	**76.4%**	**54.5%**	*43.0%*	**79.5%**
V2	**87.1%**	*18.0%*	**92.5%**	**64.5%**	*35.9%*	**79.0%**	**51.7%**	*42.6%*	**70.2%**
V3	**71.3%**	*33.1%*	**85.5%**	**67.5%**	*30.1%*	**78.0%**	**72.8%**	*28.5%*	**81.9%**
V4	**49.6%**	*38.1%*	**70.5%**	**65.9%**	*35.7%*	**81.9%**	**58.2%**	*43.6%*	**83.7%**
	71.9%	*16.2%*	**86.3%**	**66.3%**	*1.4%*	**78.5%**	**59.3%**	*9.4%*	**80.7%**

Tabela 4 prikazuje rezultate validacije – podobnosti (P), predstavljene kot aritmetična sredina (P_{AS}) ali kot mediana (P_{MD}) podobnosti vseh rezin štirih serij bolnikovih slik. Rezultati prikazujejo, da smo z uporabo naših treh algoritmov uspešno razgradili štiri serije bolnikovih slik, ki niso bile del učne množice. Najmanjšo podobnost z referenčnim modelom smo dosegli s serijo *V4* in algoritmom rasti regij (aritmetična sredina podobnosti 49.6% s standardnim odklonom 38.1%, oz. mediana 70.5%) oz. s serijo V2 in algoritmom aktivnih krivulj (aritmetična sredina podobnosti 51.7% s standardnim odklonom 42.6%, oz. mediana 70.2%), kar pomeni, da lahko naši algoritmi razgradijo medicinske slike z jetri tudi v slabih pogojih, vendar z ustrezno manjšo natančnostjo. Največjo podobnost smo dosegli s serijo *V2* in algoritmom rasti regij (aritmetična sredina podobnosti 87.1% s standardnim odklonom 18.0%, oz. mediana 92.5%) in ravno algoritem rasti regij se je izkazal kot globalno najboljši (aritmetična sredina podobnosti 71.9% s standardnim odklonom 16.2%, oz. mediana 86.3%).

Algoritme za avtomatsko razgradnjo jeter smo vključili v grafični uporabniški vmesnik (angl. *Graphical User Interface – GUI*), ki je izdelan kot spletna aplikacija. Uporabniški vmesnik (angl. *front-end*) uporablja hipertekstovni označevalni jezik 5 (angl. *Hyper-Text Markup Language 5 – HTML5*) in JavaScript (JS) za izdelavo vsebin in interakcijo z uporabnikom. Jedro vmesnika (angl. *back-end*) je aplikacija programskega okolja Matlab (Mathworks, Nantick, MA, ZDA), ki jo uporabniški vmesnik zažene prek asinhronega klica JS/XML (angl. *asynchronous JS and XML – AJAX*) z uporabo PHP hiper-tekstovnega pred-procesorja (angl. *PHP HyperText Preprocessor – PHP*; The PHP Group, 2001-2012). Tridimenzionalni prikaz je izveden z uporabo knjižnice *X Toolkit* (XTK; The X Toolkit Developers, 2012), ki temelji na spletni grafični knjižnici – angl. *Web Graphics Libraray* (WebGL). GUI spletne aplikacije za načrtovanje zdravljenja z elektrokemoterapijo prikazuje *Slika 8*, kjer so prikazani trije zasloni: začetni zaslon (*Slika 8A*), vmesnik za izbiro serije (*Slika 8B*, postopek iz *Slike 7B*) in primer zgrajenega tridimenzionalnega modela jeter z žilami in identificiranim tumorjem (*Slika 8C*). Izdelani grafični uporabniški je izrisan na uporabnikovi napravi (tj. v uporabnikovem spletnem brskalniku), medtem ko so vsi izračuni, ki vključujejo razgradnjo medicinskih slik in porazdelitev električnega polja,

izvedeni na strežniku. Omenjeni način delovanja omogoča, da uporabnikova naprava ni obremenjena zaradi delovanja programske opreme.

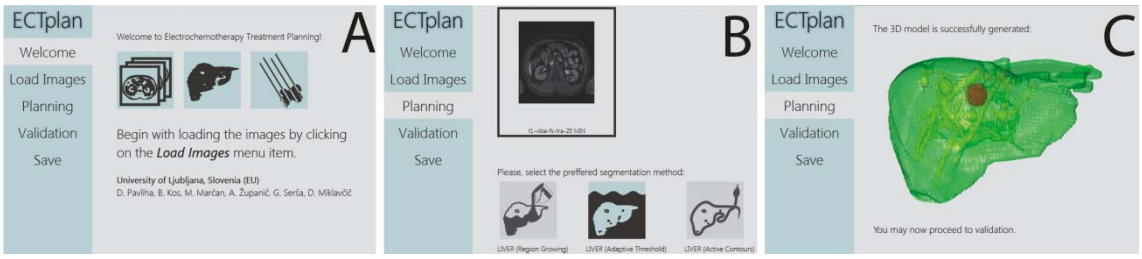

Slika 8: grafični uporabniški vmesnik spletne aplikacije za načrtovanje zdravljenja z EKT.

ZAKLJUČKI

V zadnjem desetletju so aplikacije, ki temeljijo na pojavu elektroporacije, dozorele in dosegle rabo v kliničnem okolju. Elektrokemoterapija (EKT) je sicer že v klinični rabi za zdravljenje površinskih metastaz kožnega melanoma. S predstavljenimi postopki načrtovanja zdravljenja, ki smo jih vpeljali med prvimi, bo tako laže dosegla tudi zdravljenje globoko ležečih tumorjev, kjer je načrtovanje zdravljenja ključnega pomena.

Postopek načrtovanja zdravljenja smo poenotili tako, da smo razvili in ovrednotili algoritme, ki omogočajo avtomatsko razgradnjo medicinskih slik in gradnjo matematičnih tridimenzionalnih modelov želenih organov (npr. jeter). Zaradi modularne zasnove je naknadna vključitev algoritmov za razgradnjo drugih organov enostavna.

Postopke razgradnje in izračuna porazdelitve električnega polja smo vključili v spletno programsko opremo za načrtovanje zdravljenja z EKT, ki vključuje grafični uporabniški vmesnik in omogoča zdravnikom, da izdelajo načrt zdravljenja brez inženirskega predznanja ali neposredne inženirske podpore. Omogočeno je tudi nalaganje že razgrajenih slik, kar omogoča ovrednotenje primerov pacientov, ki so že bili zdravljeni z EKT. Ovrednotenje primerov že zdravljenih pacientov bo omogočilo zdravnikom demonstracijo, da je za uspešno zdravljenje zares ključnega pomena celotna pokritost tumorja z električnim poljem dovolj visoke jakosti. Uporaba programske opreme za načrtovanje zdravljenja z EKT bo tako prispevala k pravilnemu izvajanju zdravljenja z EKT.

IZVIRNI PRISPEVKI K ZNANOSTI

Na osnovi rezultatov te doktorske disertacije prosim za priznanje naslednjih izvirnih prispevkov k razumevanju ožjega znanstvenega področja:

VZPOSTAVITEV POSTOPKOV ZA BOLNIKU PRILAGOJENO NAČRTOVANJE ZDRAVLJENJA GLOBOKO LEŽEČIH TUMORJEV Z ELEKTROKEMOTERAPIJO

Vzpostavili smo postopke bolniku prilagojenega načrtovanja zdravljenja globoko ležečih tumorjev z elektrokemoterapijo, ki so zasnovani na osnovi sorodnih postopkov načrtovanja zdravljenja radioterapije. Postopki načrtovanja zdravljenja, ki smo jih razvili, temeljijo na obdelavi bolnikovih medicinskih slik in razgradnji relevantnih tkiv: obravnavanega organa (npr. jeter), patološkega tkiva (tumorja) in ostalih relevantnih tkiv (npr. žil). Razviti postopki omogočajo učinkovito izvedbo elektrokemoterapije globoko ležečih tumorjev.

OPTIMIZACIJA IN VREDNOTENJE POSTOPKOV ZA AVTOMATSKO RAZGRADNJO MEDICINSKIH SLIK JETER ZA BOLNIKU PRILAGOJENO NAČRTOVANJE ZDRAVLJENJA Z ELEKTROKEMOTERAPIJO

Razvili smo algoritme za avtomatsko razgradnjo jeter z medicinskih slik, ki so v uporabi za načrtovanje bolniku prilagojenega zdravljenja z elektrokemoterapijo. Algoritmi, ki smo jih razvili (rast regij, adaptivno upragovljanje in aktivne konture), so validirani na osnovi radiološkega ekspertnega znanja, in sicer z uporabo sedmih modelov jeter za optimizacijo delovanja in dodatnih štiri modelov jeter za validacijo delovanja optimiziranih algoritmov.

RAZVOJ PROGRAMSKE OPREME ZA BOLNIKU PRILAGOJENO NAČRTOVANJE ZDRAVLJENJA TUMORJEV Z ELEKTROKEMOTERAPIJO

Razvili smo programsko opremo, ki vključuje vse postopke, ki so potrebni za načrtovanje zdravljenja z elektrokemoterapijo: vmesnik za uvoz bolnikovih medicinskih slik, algoritme za avtomatsko razgradnjo medicinskih slik, vmesnik za virtualno vstavitev elektrod, algoritme za izračun porazdelitve električnega polja v tkivih in vmesnik za prikaz izdelanega

načrta zdravljenja. Programska oprema trenutno omogoča avtomatsko razgradnjo dveh tipov tkiva: jeter in kosti. Zaradi modularne zasnove pa omogoča vključitev dodatnih algoritmov za razgradnjo drugih tkiv. S programsko opremo upravljamo prek uporabniku prijaznega grafičnega uporabniškega vmesnika, ki je zasnovan kot spletna stran in zatorej omogoča oddaljeno načrtovanje zdravljenja (tj. telemedicina).

INTRODUCTION

ELECTROPORATION

When the biological cell is exposed to an externally applied electric field of adequate strength, the cell membrane becomes transiently permeabilized (Kotnik et al., 2010). The phenomenon that is termed electroporation (Neumann et al., 1982), sometimes also referred to as electropermeabilization (Šel et al., 2005), allows the material from outside the cell to traverse the plasma membrane, which would be otherwise not possible. Electroporation can be performed by generating external electric field using an electric pulse generator (Puc et al., 2004) that delivers electric pulses in the near proximity of the target group of cells using electrodes (Županič et al., 2008).

Electroporation is considered to be a universal method and platform technology because all types of cells (i.e. animal, plant, and microorganism) can be successfully electroporated (Miklavčič et al., 2012). Many applications of electroporation have been already developed, e.g. electrochemotherapy of tumors (Mir et al., 1991; Serša and Miklavčič, 2008), non-thermal irreversible electroporation for tissue ablation (Garcia et al., 2011; Rubinsky et al., 2007), gene therapy (Heller and Heller, 2010), food preservation (Toepfl et al., 2007), and others (Daugimont et al., 2010; Gusbeth et al., 2009; Ušaj et al., 2010).

CLINICAL APPLICATIONS OF ELECTROPORATION

Electrochemotherapy (ECT)

Currently, the most widely clinically used electroporation-based application is electrochemotherapy (ECT) (Miklavčič et al., 2012) which improves chemotherapy by enhancing uptake of cytotoxic drugs (e.g. bleomycin or cisplatin) due to electroporation (Orlowski et al., 1988; Serša et al., 1995). The procedure is done by first injecting the cytotoxic drug to the patient. Then, the application of electric pulses is performed using an electric pulse generator (i.e. electroporator). In case of intravenous *bolus* injection of the cytotoxic drug, the electric pulses need to be applied at least 8 minutes after injection, i.e.

the time when the cytotoxic drug is expected to reach the pharmacological peak in tumor due to circulation (Mir et al., 2006). Because ECT is based on reversible electroporation (i.e. increase of the plasma membrane permeability is temporary), strength of the applied electric field needs to be above reversible electroporation threshold and below irreversible electroporation threshold (Miklavčič et al., 2006).

ECT has already been in clinical use for treating cutaneous metastases of skin melanoma in more than 100 clinical centers in Europe (Miklavčič et al., 2012). Because cutaneous metastases are small in size, successful ECT treatment is ensured by following standard operating procedures (SOP) which were devised for treating superficial tumor nodules using fixed-geometry needle or plate electrodes (Mir et al., 2006). ECT of cutaneous metastases of skin melanoma proved to be a successful method, with an 85% objective response rate (Mali et al., 2013; Marty et al., 2006).

Recently, however, ECT has been advancing towards treating deep-seated tumors (Miklavčič et al., 2010) in liver (Edhemović et al., 2011), bone (Fini et al., 2011), and brain (Agerholm-Larsen et al., 2011; Linnert et al., 2012; Mahmood and Gehl, 2011). Since deep-seated tumors are not accessible using the type of electrodes used for treating cutaneous metastases, and due to diversity in shape and size of such tumors, ECT of deep-seated tumors requires long-needle electrodes that are inserted individually (i.e. the electrodes are not part of a fixed-geometry electrode array, but are positioned one by one) (Edhemović et al., 2011). The diversity of tumor shape, size and location, and the use of long-needle electrodes impose patient-specific treatment planning for ECT of deep-seated tumors (Pavliha et al., 2012) since SOP are not appropriate for treatment of such tumors.

Non-thermal irreversible electroporation for tissue ablation (N-TIRE)

Another important electroporation-based application is non-thermal irreversible electroporation (N-TIRE) which, like electrochemotherapy, uses electroporation for ablating pathological tissue, i.e. tumors (Županič and Miklavčič, 2009). N-TIRE is a non-thermal ablation technique (Davalos and Rubinsky, 2008) and requires the strength of the applied electric field to reside above irreversible electroporation threshold (Županič and

Miklavčič, 2011) for successful treatment. N-TIRE has been used for ablation of tumors in liver (Charpentier et al., 2011), pancreas (Charpentier et al., 2010), brain (Garcia et al., 2011), and soft-tissue (Neal et al., 2011). When N-TIRE is used for treating deep-seated tumors, patient-specific treatment planning is also needed (Županič et al., 2012).

TREATMENT PLANNING OF ELECTROPORATION-BASED TREATMENTS

Designing the treatment planning procedure

In *Article 1*, we stipulated that electroporation-based treatments such as ECT and N-TIRE require patient-specific treatment planning for treatment of deep-seated tumors (Pavliha et al., 2012) and suggested the treatment planning procedure by exposing parallelisms to radiotherapy (RT) (Lecchi et al., 2008) where treatment planning has been of paramount importance for the success of RT in the last 50 years. RT treatment planning served us as the basis for establishing ECT treatment planning procedure, the latter consisting of patient medical imaging (by Magnetic Resonance Imaging – MRI, or by Computed Tomography – CT), construction of the model geometry, calculation of a suitable plan by numerical modeling and optimization (number and positions of electrodes used), and definition of intensity of the applied electric pulses.

Development and validation of segmentation algorithms

Construction of the model geometry is an important step of ECT treatment planning. The model geometry is generated by performing image segmentation, i.e. extraction of relevant tissue. In *Article 2*, we presented three algorithms that perform automatic liver segmentation for ECT treatment planning. Automatic segmentation of relevant tissue namely enables the end-user (i.e. clinician) to obtain model geometry without the need for manual tissue delineation which is time-consuming (e.g. it may take up to six hours for a clinician to manually delineate relevant tissue of a patient) (Paulides et al., 2010). The functioning of segmentation algorithms was optimized using a training dataset consisting of seven patient cases that were previously manually segmented by a radiologist. Relevant parameters of each algorithm were optimized and optimal parameters were determined

based on similarities of automatically segmented cases to manually segmented cases. Finally, the so obtained optimal parameters were then used to perform automatic segmentation of four additional patient cases that were previously manually segmented by a radiologist, and were not part of the training dataset.

Integrated software with graphical user interface for treatment planning

One of the possibilities to facilitate ECT treatment planning is to develop treatment planning software that embeds execution of all required procedures: import of patient medical images, image segmentation for model geometry generation, possibility of virtual electrode insertion, and calculation of a suitable plan by numerical modeling and optimization. In *Article 3*, we presented development of a web-based ECT treatment planning software with an easy-to-use graphical user interface. The software requires the medical images to be uploaded, and upon selection of the preferred algorithm (e.g. active contours that are optimized for liver segmentation, or fixed thresholding that is optimized for bone segmentation, etc.) the automatically generated 3D model of the relevant organ is presented to the end-user (i.e. clinician). Finally, the end-user determines the number and direction of the electrodes inserted into the generated 3D model, and the calculations of the electric field are executed and presented to the user.

AIMS OF THE DOCTORAL THESIS

The aims of the doctoral thesis are to establish the procedure of electrochemotherapy (ECT) treatment planning, develop validated automatic segmentation algorithms for liver segmentation, and construct integrated electrochemotherapy treatment planning software. Namely, ECT of deep-seated tumors requires patient-specific treatment planning but currently lacks standardization. Therefore, the ECT treatment planning procedure we established may serve as the basis for further ECT treatments. We founded ECT treatment planning procedure on the radiotherapy example where treatment planning has been adopted by the clinicians for more than 50 years.

Despite its complex inner functioning (i.e. the algorithms that form treatment planning are state-of-the-art procedures) patient-specific ECT treatment planning needs to be simplistic from the user's point of view. Therefore, we included validated automatic segmentation algorithms for model generation as part of the developed treatment planning software in order to minimize the time required for generating treatment plans. Moreover, all the procedures which are part of treatment planning (i.e. patient medical images import, image segmentation, virtual electrode insertion, and electric field distribution calculation) are embedded in a web-based graphical user interface of the ECT treatment planning software. The graphical user interface allows the use of the software without engineering or computer knowledge, while the form of a web-based application facilitates treatment planning and contributes to a wide use of electroporation-based treatments since treatment planning can be performed remotely.

SCIENTIFIC ARTICLES

PATIENT-SPECIFIC TREATMENT PLANNING OF ELECTROCHEMOTHERAPY: PROCEDURE DESIGN AND POSSIBLE PITFALLS

PAVLIHA Denis, KOS Bor, ŽUPANIČ Anže, MARČAN Marija, SERŠA Gregor, MIKLAVČIČ Damijan
Bioelectrochemistry 87: 265-273, 2012.

ELECTROPORATION-BASED TREATMENT PLANNING FOR DEEP-SEATED TUMORS BASED ON AUTOMATIC LIVER SEGMENTATION OF MRI IMAGES

PAVLIHA Denis, M. MUŠIČ Maja, SERŠA Gregor, MIKLAVČIČ Damijan
PLOS ONE: submitted, 2013.

PLANNING OF ELECTROPORATION-BASED TREATMENTS USING WEB-BASED TREATMENT PLANNING SOFTWARE

PAVLIHA Denis, KOS Bor, MARČAN Marija, ŽUPANIČ Anže, SERŠA Gregor, MIKLAVČIČ Damijan
Journal of Membrane Biology: submitted, 2013.

ARTICLE 1

Title: Patient-specific treatment planning of electrochemotherapy: Procedure design and possible pitfalls

Authors: PAVLIHA Denis, KOS Bor, ŽUPANIČ Anže, MARČAN Marija, SERŠA Gregor, MIKLAVČIČ Damijan

Publication: Bioelectrochemistry

DOI: 10.1016/j.bioelechem.2012.01.007

Year: 2012

Volume: 87

Number: /

Pages: 265 – 273

Impact factor: 3.759

Ranking:

Category name	Total journals in category	Journal rank in category	Quartile in category
biochemistry & molecular biology	290	90	Q2
biology	85	16	Q1
biophysics	74	17	Q1
electrochemistry	27	8	Q2

Bioelectrochemistry 87 (2012) 265–273

Contents lists available at SciVerse ScienceDirect

Bioelectrochemistry

journal homepage: www.elsevier.com/locate/bioelechem

Patient-specific treatment planning of electrochemotherapy: Procedure design and possible pitfalls

Denis Pavliha [a], Bor Kos [a], Anže Županič [a], Marija Marčan [a], Gregor Serša [b], Damijan Miklavčič [a,*]

[a] University of Ljubljana, Faculty of Electrical Engineering, Tržaška 25, SI-1000 Ljubljana, Slovenia
[b] Institute of Oncology, Zaloška 2, SI-1000 Ljubljana, Slovenia

ARTICLE INFO

Article history:
Received 5 July 2011
Revised 6 January 2012
Accepted 20 January 2012
Available online 28 January 2012

Keywords:
Electrochemotherapy
Electroporation
Treatment planning
Medical imaging
Numerical modeling

ABSTRACT

Electrochemotherapy uses electroporation for enhancing chemotherapy. Electrochemotherapy can be performed using standard operating procedures with predefined electrode geometries, or using patient-specific treatment planning to predict electroporation. The latter relies on realistic computer models to provide optimal results (i.e. electric field distribution as well as electrodes' position and number) and is suitable for treatment of deep-seated tumors.

Since treatment planning for deep-seated tumors has been used in radiotherapy, we expose parallelisms with radiotherapy in order to establish the procedure for electrochemotherapy of deep-seated tumors. We partitioned electrochemotherapy in the following phases: the mathematical model of electroporation, treatment planning, set-up verification, treatment delivery and monitoring, and response assessment. We developed a conceptual treatment planning software that incorporates mathematical models of electroporation. Preprocessing and segmentation of the patient's medical images are performed, and a 3D model is constructed which allows placement of electrodes and implementation of the mathematical model of electroporation.

We demonstrated the feasibility of electrochemotherapy of deep-seated tumors treatment planning within a clinical study where treatment planning contributed to the effective electrochemotherapy treatment of deep-seated colorectal metastases in the liver. The described procedure can provide medical practitioners with information on using electrochemotherapy in the clinical setting. The main aims of this paper are: 1) to present the procedure for treating deep-seated tumors by electrochemotherapy based on patient-specific treatment planning, and 2) to identify gaps in knowledge and possible pitfalls of such procedure.

1. Introduction

When a cell is exposed to a sufficiently intense transient external electric field, the permeability of its membrane is increased [1]. This allows molecules that otherwise lack a membrane transport mechanism to enter the cell. Electroporation, as the phenomenon was named, can therefore be used to control the transport of different molecular species in and out of the cell and even induce controlled cell death if the parameters of the electric field are chosen appropriately [2].

Even though the exact molecular mechanisms of electroporation are not yet fully elucidated, it is being used in several medical applications, e.g. electrochemotherapy [3] (which is currently used in daily clinical practice for treatment of superficial tumor nodules in more than 80 clinical centers around Europe [4]), gene therapy [5], and irreversible electroporation (for non-thermal ablation purposes) [6]. Electrochemotherapy combines cancer drugs, such as bleomycin or cisplatinum, with short high-voltage electric pulses, and achieves approximately 80% objective responses irrespective of the histological type of the tumor [7]. When planning electrochemotherapy, we can choose between two possible treatment planning modes: 1) following standard operating procedures with predefined geometry of electrodes based on models to predict electroporation, or 2) patient-specific treatment planning. Electrochemotherapy based on predefined geometries was described for skin tumors [7] and brain tumors [8,9] and several clinical trials are registered and are ongoing [10,11]. The first deep-seated tumors were treated and reported recently with electrochemotherapy and irreversible electroporation using long needle variable geometry electrodes, which clearly demonstrated that patient-specific treatment planning is needed [12–15].

Other electroporation-based therapies are also at the stage of clinical trials. Researchers have considerably increased the efficacy of electroporation-based gene transfer for gene therapy and DNA vaccination [16–19]. Furthermore, irreversible electroporation has been demonstrated in prostate, liver and brain *in vivo* on experimental animals [20] and in patients [21]. As a non-thermal ablation technique,

* Corresponding author. Tel.: +386 1 4768456; fax: +386 1 4264658.
E-mail addresses: denis.pavliha@fe.uni-lj.si (D. Pavliha), bor.kos@fe.uni-lj.si (B. Kos), anze.zupanic@fe.uni-lj.si (A. Županič), marija.marcan@fe.uni-lj.si (M. Marčan), gsersa@onko-i.si (G. Serša), damijan.miklavcic@fe.uni-lj.si (D. Miklavčič).

1567-5394/$ – see front matter © 2012 Elsevier B.V. All rights reserved.
doi:10.1016/j.bioelechem.2012.01.007

irreversible electroporation can be used to cause cell death while preserving extra-cellular tissue scaffolding [22], which greatly facilitates tissue healing after tissue ablation.

To bring the benefits of all these electroporation-based therapies to patients, treatment planning (predefined geometry-based or patient-specific) is necessary. By taking into account the patient's anatomy and numerically predicting the electroporation effects of the high-voltage electric pulses, optimal position of the electrodes can be determined, thereby assuring adequate electroporation of the tumor and limiting electroporation of the healthy tissue. We have taken radiotherapy treatment planning, that has been of paramount importance in the success of radiotherapy in the last 50 years, as the basis for the design of treatment planning in electrochemotherapy. We have already demonstrated in a proof-of-principle study [15] that anatomically realistic computer models of target tissue can be built based on medical imaging and by using finite element modeling for calculating the electric field distribution in the tissue, an efficient treatment plan can be prepared for treating deep-seated colorectal metastases in the liver. The main aims of this paper thus are: 1) to present procedures for deep-seated tumors electrochemotherapy based on patient-specific treatment planning, and 2) to identify gaps in knowledge and possible pitfalls of such procedures.

2. Background

Patient-specific treatment planning has been successfully introduced to and is widely used in radiotherapy, which like electroporation is also based on the interaction between a physical agent (radiation in radiotherapy, and electric field in electroporation) and biological tissue [23]. Radiotherapy is a cancer-treatment procedure where energy is deposited locally into the patient's body by a targeted radiation beam. The damage caused by the beam is not tumor-specific; the maximum allowed radiation dose to the tumor is thus limited by the dose the healthy tissue along the radiation path can withstand [24]. The main goal of radiotherapy is to cause enough radiation damage so that tumor cells get permanently inhibited and their growth can be delayed infinitively; therefore, tumor cells cannot proliferate further.

Radiotherapy consists of the following steps: simulation, treatment planning, set-up verification, beam delivery, and response assessment [23], as described in Table 1. Simulation is based on the patient's anatomy; the patient is scanned in order to obtain medical images (using e.g. Computed Tomography – CT or Magnetic Resonance Imaging – MRI) in the same position as expected to be when exposed to the radiation beam. Treatment planning starts by using the acquired medical images for generating a three-dimensional model. First, the target volumes are defined by the radiologist based on the image data in order to calculate the appropriate radiation dose, then the treatment plan is developed by numerical modeling and optimization – mathematical models of radiation damage in biological tissues have been developed in the first half of the 20th century and are, with some adjustments, still used today [25]. After the calculations, the plan is transferred to the controller device that manages the functioning of the irradiating device (e.g. a linear accelerator) that delivers the radiation beam. The set-up verification consists of examining the patient's position (e.g. using laser-based detectors) in order to coincide with the scanned medical images, and to reflect consequently the dose data from the generated treatment plan. Finally, beam delivery is executed and response assessment is performed later on by obtaining a new set of medical images and validating the treatment.

For the purposes of establishing procedures for deep seated tumors electrochemotherapy based on patient-specific treatment planning, we can expose parallels between electrochemotherapy and radiotherapy, as already suggested [8]. In radiotherapy, the radiation dose has to be high enough in the tumor volume to kill all the tumor cells, whereas in electrochemotherapy, the electric field in the tumor volume needs to be sufficiently strong, and the exposure long enough, to cause cell membrane electroporation [12]. Similarly to radiotherapy, electrochemotherapy of deep-seated tumors can also be partitioned into several steps: mathematical model of electroporation, treatment planning, set-up verification, treatment, and response assessment (Table 1). Therefore, in establishing procedure for electrochemotherapy of deep-seated tumors based on patient-specific treatment planning, radiotherapy treatment planning can serve as a well-established example.

The first step of designing electrochemotherapy of deep-seated tumors is to create a suitable numerical model of electroporation, at both cellular and tissue levels by determining material properties (electrical conductivity) as well as electroporation mechanisms that are related to the electric field distribution [26]. After patient-specific data are transferred to the model it can be used in the treatment planning procedure. The treatment planning consists of several phases: image import, image pre-processing, segmentation, three-dimensional model generation, electrode placement, implementation of the mathematical model of electroporation, and optimization of the results: the electric field distribution as well as the number of electrodes and electrodes' positions. The position of electrodes needs to be verified intraoperatively as part of the set-up verification in order to assure the treatment plan is accurately followed. Postoperative response assessment is required approximately 4–8 weeks after the treatment in order to determine effectiveness of electrochemotherapy by radiological imaging or tumor histology: if the patient is rescheduled for reoperation (as part of a two stage procedure [27]) the metastasis is resected and also histologically evaluated.

Table 1
Parallelism and similarities between radiotherapy and electrochemotherapy of deep-seated tumors.

Radiotherapy	Electrochemotherapy of deep-seated tumors
Simulation – medical imaging (CT or a combination of CT with MR or PET) of the patient	Mathematical model of electroporation: cell- and tissue-level models of electroporation.
Treatment planning: delineation of target volumes, definition of dose constraints, construction of the mathematical model geometry, calculation of a suitable plan by numerical modeling and optimization – number of fractions, position and intensity of the beams	Treatment planning: medical imaging (CT or MR, possible combination with PET) of the patient, delineation of target volumes, construction of the mathematical model geometry, calculation of a suitable plan by numerical modeling and optimization – number and positions of electrodes used, intensity of the used electric pulses
Set-up verification: medical imaging (CT or MRI) is used for verifying the position of the patient and target tissues, in subsequent session lasers and tattoo marks are used together with ultrasound (US) and other imaging modalities	Set-up verification: optimal electrode positions are registered on the original medical images; electrode positions are verified using intraoperative ultrasound (US)
Treatment delivery and monitoring: radiation is delivered according to the treatment plan, while imaging is used to control for breathing movements	Treatment delivery and monitoring: after electrode insertion and chemotherapeutic injection, electric pulses are delivered, current and voltage are measured to control for possible errors during electric pulse delivery
Response assessment: post-treatment measurement of tumor size or biological tumor markers with medical imaging	Response assessment: post-treatment measurement of tumor size or biological tumor markers with medical imaging and/or histology, compared to pre-treatment medical images.

3. Methodology

3.1. Mathematical model of electroporation

Mathematical modeling on the level of tissues and considering bulk tissue properties has been used in the field of tissue electroporation for more than a decade [28,29]. Initially, the models were focused on determining electric field distribution for different electrode geometries and analyzing the importance of the distribution for the effectiveness of electrochemotherapy. In subsequent studies, a correlation between the strength of the electric field, coverage of the tumor and electrochemotherapy effectiveness was established [30]. Electric field thresholds for reversible and irreversible electroporation were determined for various tissues, including liver [31] and muscle [32] by comparing tissue changes and histology with electric field calculation in geometrically correct models. It needs to be emphasized, however, that threshold values of electric field at which cell membrane electroporation occurs were determined for specific pulse parameters, i.e. most of the time for 8 pulses of 100 μs duration delivered at 1 Hz pulse repetition frequency. However, the electric field amplitude at which membrane permeabilization occurs depends on the pulse parameters (the number and the length of the pulses). Later, electroporation effects on tissue conductivity were incorporated in the mathematical models [33,26,31] which were validated by comparing the predicted and the measured electric currents during electric pulse delivery [33]. Electroporation thresholds (8×100 μs pulses) for liver tissue were determined to be 460 V/cm and 700 V/cm for reversible and irreversible electroporation, respectively [26,31]. In addition to electric field threshold values, which depend greatly on the pulse duration and the number of pulses delivered [34,2,35] but also on the method of detection [36] it has not been yet established how fast and how much the tissue conductivity increases during electroporation [33]. Currently, it is being estimated that during electroporation, the conductivity increases by a factor of 3–4, which yields good agreement between calculated and measured current values. The increase of conductivity was stipulated to correlate with the occurrence of electroporation, which was later demonstrated also in dense cell suspension experiments [37] and *in vivo* [38]. The values of the electric field for irreversible electroporation were later demonstrated to be most probably higher than originally reported [39], but have not yet been equivocally determined.

3.2. Treatment planning software

We developed a proof-of-concept principle computer software in order to fully devise and elaborate treatment planning for electrochemotherapy. The proof-of-concept electrochemotherapy treatment planning software was developed as a Windows (Microsoft, Redmond, USA, 1985–2011) application; the software was constructed in the Microsoft C# programming language within the Microsoft .NET Framework v3.5 (Microsoft, Redmond, USA, 2007) using Microsoft Visual Studio 2008 integrated development environment (Microsoft, Redmond, USA, 2007).

3.2.1. Image import

To generate representative models that can be used as input data for patient-specific electrochemotherapy treatment planning, scanned medical images (e.g. CT or MRI) of the patient are required. A currently commonly used standard for medical imaging is Digital Imaging and Communication in Medicine (DICOM) [40]. DICOM is used as the standard for encapsulating medical images that are obtained from e.g. CT or MRI scanners. Therefore, DICOM images are read and imported into the electrochemotherapy treatment planning software as input data.

Moreover, a conversion of DICOM images is required to allow further image processing. Namely, upon import of the medical images into the electrochemotherapy treatment planning software, the images are deposited into the working storage memory (e.g. memory streams that are located in the Random Access Memory – RAM). If we want to access them as raw data the images need to be converted into such a format; therefore, a conversion from DICOM into some other format, preferably uncompressed raw 8-bit data, is required. In case of the 8-bit format, 8 bits describe a single pixel intensity and a short header is also present to describe the dimensions of the medical images.

At this stage of development, a manual conversion from DICOM to bitmap data using commercially available computer graphics software Adobe Photoshop CS4 (Adobe Systems Inc., San Jose, CA, USA, 2008) is performed. Manual conversion is performed mainly because DICOM is a complex standard and a suitable implementation would require extensive development which has not been possible yet. Nevertheless, bitmap data can be interpreted by our software without problems due to native bitmap implementation in the Microsoft. NET Framework v3.5 (Microsoft, Redmond, USA, 2007). Then, the bitmap data is converted into raw 8-bit data within the electrochemotherapy treatment planning software.

3.2.2. Image pre-processing

Image pre-processing is required to prepare the medical (e.g. CT or MRI) images for image segmentation. Since the segmentation is based on feature extraction, the images are first transformed by means of pre-processing procedures in order to minimize bias of intensities [41]. Because medical images for electrochemotherapy planning purposes may steam from sources with different modalities (e.g. CT or MRI), a single set of pre-processing procedures cannot be implemented; a parameterized pre-processing software module with possibility of dynamically allocating pre-processing procedures is incorporated into the treatment planning software instead.

Pre-processing begins with the analysis of the images; analysis is used to determine the main intensity components that are present in the images, which allows implementation of intensity-based pre-processing procedures, i.e. threshold-based algorithms [42]. Such an analysis begins by showing the electrochemotherapy treatment planning software user (i.e. the attending physician) a histogram of all the intensities that are represented in the medical images' collection. An example of such a histogram is shown in Fig. 1 where relative intensities' representation (ordinate) is presented as a function of the 8-bit intensity range (abscissa).

As seen in Fig. 1, five thresholds delimit six main intensity components: one at the beginning, four in the middle, and one at the end of the 8-bit intensity range. Currently, determination of the thresholds (i.e. gray lines in Fig. 1) is performed manually by the electrochemotherapy treatment planning software user. Up to five thresholds delimiting six most noticeable intensity components by clicking onto the desired targeted positions in the intensity histogram are marked.

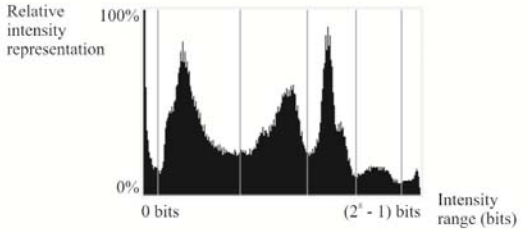

Fig. 1. An example histogram of intensities that are represented in the medical images' collection with manually determined thresholds (gray lines) between the identified main intensity components (peaks of black bars).

In the case of medical images derived from a MRI source, a contrast-enhancement procedure is applied upon the set of medical images. A basic contrast-enhancement procedure is done by performing a non-linear transformation of each pixel of each image in the collection by Eq. (1) where i denotes the *intensity* of a pixel with the range of $0 \le i \le 255$ and a *bit* is its unit:

$$i_N = k \cdot (i_P + 1) \cdot \log_{10}(i_P + 1) \quad (1)$$

i_N is the newly calculated value by using the previous value i_P and a scaling factor k ; in our case, k is empirically set to 0.5. Additionally, because of operating in the 8-bit range of intensities the newly calculated value of i_N is clamped to reside within the interval $0 \le i_N \le 2^8 - 1$. This procedure enhances the contrast in a non-linear way, so that distribution of intensity is changed.

Medical images may contain several unwanted artifacts (e.g. noise, gradient fill anomalies, etc.), which increases the difficulty of medical image segmentation (e.g. edges are not clearly defined) [42]. Moreover, tissue of interest to the application of electrochemotherapy (e.g. tumor, liver, brain, etc.) is most commonly heterogeneously texturized. Therefore, intensities that describe these objects (i.e. tissue) vary due to both tissue heterogeneity (low-frequency variations) and noise (high-frequency variations), making straightforward segmentation impossible (e.g. if we perform threshold-based segmentation without pre-processing, segmentation will result in many more segments than desired).

Regardless of the source of medical images, a noise removal procedure is performed by applying an average-based filter on an intensity matrix in the size of 3×3 pixels. Then, an additional noise removal is executed by applying a median-based filter on an intensity matrix in the size of 3×3 pixels that has previously already been processed using the average-based filter. Finally, the thresholds determined in the procedure of medical images' analysis (Fig. 1) are used to transform the filtered images containing continuous intensities into fully pre-processed images containing up to six discrete intensities (i.e. dithering). Dithering also takes into account heterogeneity of tissue and removes it, hence pre-processing results in homogeneous segments. The transformation is shown in Fig. 2.

As seen in Fig. 2, the pre-processing procedures may however result in non-uniform object surfaces due to source images' anomalies such as unwanted gradient fills (Fig. 2c). Nevertheless, non-uniform object surfaces do not represent a major obstacle as segmentation procedures can overcome such a limitation.

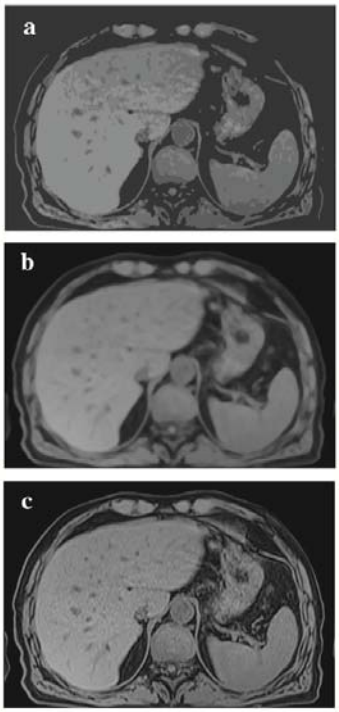

Fig. 2. An example of a CT medical image focusing on the liver; presented are a source image (left – a), a filtered image (middle – b), and a fully pre-processed image (right – c).

3.2.3. Segmentation

Segmentation is a complex procedure for extracting object data (i.e. usable features) from images [41], i.e. determining which part of medical images corresponds to a certain region of interest (ROI) – e.g. the liver or tumors or blood vessels. Such a procedure is performed based on the features identified in the medical images. Due to already pre-processed images, segmentation of objects from medical images is currently being done based on the intensity levels that are present in these images (i.e. threshold-based segmentation). Segments are therefore defined as clusters of pixels that all have the same intensity level [43].

To extract such segments, an algorithm termed *region growing* is applied upon the pre-processed images; the region growing algorithm is initiated by the user who manually places a starting seed on an image (i.e. clicks with the mouse somewhere on the target segment) and then the two-dimensional (i.e. based on each slice/image separately) region growing algorithm marks the desired segment on the selected image. The algorithm first checks all the eight neighboring pixels of the starting seed and if their intensities are equal to the one of the starting seed, they are indexed as being part of the target segment. The procedure is then reapplied until all the neighbors' neighbors are indexed as well, and finished when there are no neighbors with the same intensities as the starting seed left to be indexed.

Different layers of segments can be defined (e.g. liver, vessels, tumors, etc.). Moreover, manual segmentation is possible using common drawing tools (i.e. adding or removing a single or an array of pixels to or from the selected layer), which is helpful for geometries where region growing may lead to unwanted leakage of segments.

Currently, this procedure is only performing a two-dimensional segmentation. A three-dimensional segmentation procedure is, however, planned to be implemented in the final version of the electrochemotherapy treatment planning software in order to allow more robust segmentation procedures based on three-dimensional input data since object comparison will be done on neighboring images and three-dimensional objects will be generated automatically. Moreover, more sophisticated segmentation methods than region growing shall also be considered, e.g. using deformable active contours [44].

3.2.4. Three-dimensional model generation

Before generating a three-dimensional model, segmentation data need to be appropriately post-processed in order to allow construction of a three-dimensional mesh. The post-processing algorithms evaluate all the objects that were identified in the segmentation procedure, and generate an appropriate three-dimensional mesh of the model. Evaluation of objects from the segmentation procedure is done by generating contours in a circular way by a contour-following algorithm that produces contour data as continuous sets of two-dimensional points for each medical image in the collection.

All the two-dimensional points are, finally, used as input data for the Microsoft DirectX SDK-based component that provides objects for mesh generation and visualization within the Microsoft .NET Framework v3.5 (Microsoft, Redmond, USA, 2007). To generate a three-dimensional mesh from multi-plane two-dimensional data, the *marching cubes* algorithm [45] is used. The third dimension information (i.e. step difference of the third dimension between two-dimensional segments) is obtained from the header of the source DICOM images (i.e. the slice thickness parameter).

The electrode configuration is also evaluated and implemented as a model sub-object, so that the generated mesh may be directly applicable for numerical calculations of the electric field distribution using finite-element modeling software [46].

Moreover, the generated three-dimensional model (as example shown in Fig. 3) is useful for the attending surgeon to visualize the patient's anatomy and to determine possible entry directions, which is most important in the electrode placement procedure where guidance of the attending surgeon serves as the main course of action for defining the approximate absolute position of the electrode array [47].

3.2.5. Electrode placement

Determination of the relative electrode placement depends on the size and the shape of targeted tumors. First, the number of electrodes that will be placed in the tumor needs to be determined. Namely, if the shape of the tumor that is planned for treatment is spherically asymmetrical, up to two electrodes may be planned for insertion into the tumor. In case of spherically symmetrical tumors, a single electrode may be planned for insertion into the tumor. However, even spherically symmetrical tumors may be planned for insertion of more than one electrode into the tumor if the electric field coverage could not be achieved using only one electrode being placed in the tumor due to the its size.

Then, an arbitrary number of electrodes are determined for insertion around and into the tumor. Currently, the number and the relative layout of the electrodes are limited based on the recommendations of the attending surgeon who defines possible access directions, hence the plane normal to the electrodes. Determining the number of electrodes is not strictly formalized yet, and more research needs to be performed to this end. However, the current protocol is to keep the total number of electrodes low (also to eliminate the need to manually rewire electrode-generator connections, since the currently available pulse generator has only 6 output connections), and to keep distance between adjacent electrodes below 3 cm. Fig. 4 shows an example of such a placement of the electrodes, where a single electrode was placed into the tumor and four electrodes around it.

After determining the number and the approximate relative layout of the electrodes, electrode parameters (diameter, length of the non-isolated part and the total length of the electrode) are also

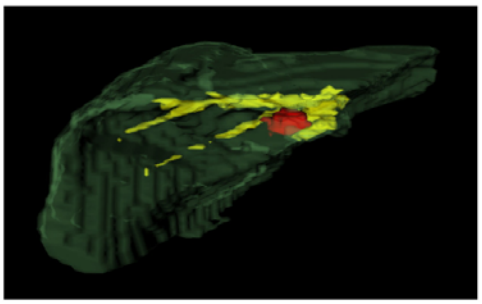

Fig. 3. A generated three-dimensional model of liver with hepatic veins and a tumor (in between the hepatic veins).

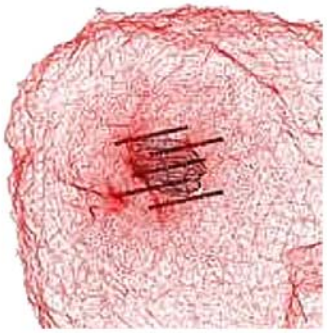

Fig. 4. An example of planned electrode placement for electrochemotherapy treatment.

defined. Finally, data of the defined electrode configuration is inserted into the three-dimensional model for electroporation modeling. The pulses are delivered to the target sequentially on pairs of electrodes, i.e. at each time only two electrodes are active. The data on the positioning and the number of electrodes need to be further supplemented by voltage amplitude of the pulses to be delivered between electrode pairs.

3.2.6. Implementation of the mathematical model of electroporation

It has been demonstrated previously that a sufficiently high local electric field is the major indicator of successful electroporation [29]. Therefore, most efforts in treatment planning and evaluation of electroporation-based treatments are currently devoted to determination of the electric field distribution in the target regions (i.e. tumor and eventually critical tissues). The electric field in conductive media is determined by solving the Laplace equation (2) for the electric potential:

$$\nabla\cdot(\sigma\cdot\nabla\varphi)=0 \tag{2}$$

from which the electric field can be determined by using the Eq. (3):

$$\mathbf{E}=-\nabla\cdot\varphi. \tag{3}$$

Such a field calculation can be performed using numerical methods, e.g. the finite element [48]. We use the commercial Comsol Multiphysics (Comsol AB, Stockholm, Sweden) software, which includes a scripting interface to Matlab (Mathworks, Nantic, MA). The computational domain is split into several subdomains with different conductivities and boundary conditions (e.g. target – tumor tissue, surrounding tissues, electrodes) [33]. The outer boundaries of the computational domain are limited with an insulating boundary condition (4):

$$\mathbf{n}\cdot\mathbf{J}=0 \tag{4}$$

while the interior boundary conditions are defined as either continuity (5) or fixed potential (6).

$$\mathbf{n}\cdot(\mathbf{J}_1-\mathbf{J}_2)=0 \tag{5}$$

$$\mathbf{V}=\mathbf{V}_0 \tag{6}$$

Tissue conductivities are known to change during electroporation [38]; therefore, electroporation is modeled using electric field-dependent conductivity. We used a sequential model to ensure irreversibility of conductivity changes during the duration of one pulse [26,31] while other authors use a simplified field-dependent formulation [49].

3.2.7. Algorithm-based optimization

Optimization is regularly used in radiotherapy treatment planning [50]; both gradient-based and stochastic optimization methods are commonly employed. Since the problem of optimization for electrochemotherapy involves a high number of parameters (pulse voltages, number of electrodes, position of electrodes) and therefore a very large parameter space, genetic algorithms for optimization are especially suitable [51]. The formal approach to optimization requires the formulation of an objective function, which can be a function of one or more parameters. For electrochemotherapy treatment planning, the given objective function (7) which has been proposed previously [12] can be used:

$$F = 100 \cdot V_{Trev} - 10 \cdot V_{Hirrev} \quad (7)$$

where V_{Trev} is the volume fraction of the target tissue above the electroporation threshold (defined as the volume of tissue exposed to electric field above the tissue-specific electroporation threshold divided by the total volume of the tissue), and V_{Hirrev} is the volume fraction of the surrounding healthy tissue above the irreversible electroporation threshold. Additional terms may be added to the objective function on a case-by-case basis. The goal of the optimization is to maximize the objective function, while simultaneously ensuring that other constraints (e.g. maximum current, maximum voltage) are observed. To this end, the optimization algorithm involves changing electrode voltages, the number of electrodes and/or electrode positions. Moreover, the goal of optimization is finding a robust solution which will ensure successful treatment even in the presence of errors or unknowns in the input parameters [52].

3.3. Set-up verification

Set-up verification consists of overlaying the treatment plan, i.e. positioning of electrodes with respect to target tissue, on medical images (CT or MRI) obtained before the treatment (e.g. Fig. 5). Such an overlay in different planes is presented to the surgeon prior to the operation, the access point was determined before starting treatment planning, and then insertion of electrodes intraoperatively using ultrasound or fluoroscopy guidance is performed by the surgeon (Fig. 6a). Electrode positioning is verified by medical imaging and by measuring the depth of electrode insertion (Fig. 6b). Finally, electrodes are connected to the corresponding outputs on the pulse generator and voltages between pairs of electrodes from the treatment plan are programmed and delivered.

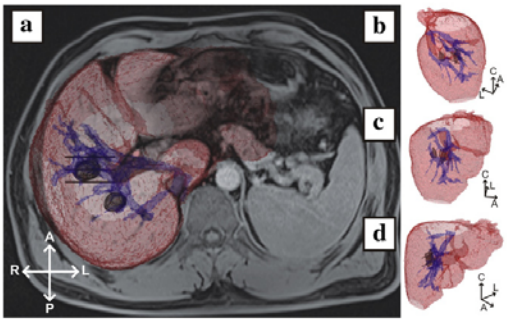

Fig. 5. Overlay (a) of placed electrodes in several viewing angles (b, c, d) as a part of the treatment plan (directions: A as anterior, P as posterior, L as left, R as right, C as cranial).

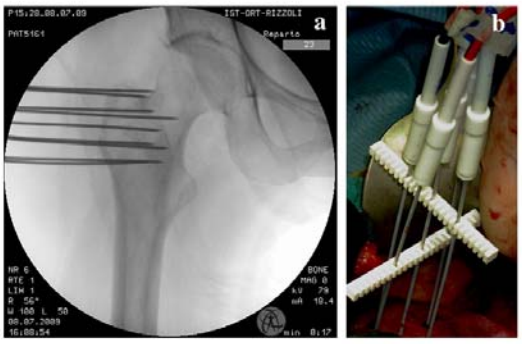

Fig. 6. a: Insertion of electrodes using fluoroscopy guidance. b: Comb-like electrode holders during electrochemotherapy surgery.

3.4. Treatment delivery and monitoring

The patient planned for electrochemotherapy is presently treated intraoperatively. The surgical team mobilizes the liver segment with the metastasis planned for treatment. The long needle electrodes (1.2 mm in diameter with 3 or 4 cm non-insulated tip – IGEA S.r.L., Carpi, MO, Italy) are inserted into the liver tissue and the tumor according to the treatment plan. The insertion of needles is image-guided and verified (as an example, Fig. 6a shows fluoroscopy guidance during bone metastasis electrochemotherapy; ultrasound guidance is used during liver electrochemotherapy). The appropriateness of needle insertion is also verified by measurement of distances between the electrodes and depth of electrode insertion, and compared to the treatment plan (Fig. 6b). Voltage and current between each pair of electrodes are measured for post processing and evaluation.

The needles are inserted using image guidance (which is needed to determine the relative position of the electrode array with respect to the target tissue) and fixed with comb-like holders (Fig. 6b), and then connected to the electric pulse generator (Cliniporator VITAE, IGEA SpA, Carpi, Italy). Thereafter the patient is given 15 000 U/m^2 of bleomycin intravenously in bolus. In the pharmacological peak, i.e. approximately 8 min after bleomycin injection, electric pulses are delivered between the electrode pairs, according to the treatment plan. The delivery of electric pulses is synchronized with the electrocardiogram (ECG); one pulse per heart-beat is delivered. This is done by the ECG triggering device, AccuSync 42 (AccuSync Medical Research Corp., Milford, CT, USA). The ECG synchronization is needed in order to avoid delivery of the electric pulse in the so-called vulnerable period of the ventricles, the T wave [53,54]. If several metastases are being treated the delivery of the electric pulses to all metastases should be performed in the time window after injection of bleomycin when tumor concentration of bleomycin is sufficiently high [55,56].

3.5. Response assessment

Response of metastases to electrochemotherapy is evaluated radiologically (CT or MRI images) and/or by histological analyses. All the patients are followed by CT or MRI imaging for possible changes in the tumor volume and/or the texture of the tumors. They are followed in a monthly period and the images are compared to the pre-treatment ones. So far, on the first 10 patients treated with electrochemotherapy no conclusive data on images were observed to predict the tumor response. Further analyses in this respect are needed. Some of the patients are on two-stage operation [27]. At the first operation, ECT is performed on some of the metastases, while the others are treated by radiofrequency ablation (RFA) or the liver segment is

ligated and scheduled for the removal at the second operation [57]. In such cases, histological analyses are possible for evaluating the histological changes in the treated lesions, especially with respect to the other, non-ECT treated metastases. Preliminary analyses indicate that ECT induces progressive degenerative changes in ECT treated metastases, indicating clinical benefit of the treatment. In some cases, even complete destruction of the treated metastasis was observed, with possible resection of the treated metastasis and no recurrence of the disease in 20 months after the treatment [15].

4. Discussion

In the last decade, electroporation-based therapies have matured, e.g. electrochemotherapy is being routinely used in the clinical setting. As electroporation-based gene therapy [5] and DNA vaccination [18,19] and ablation with irreversible electroporation are developed further [20] it is expected that in the future electroporation will become one of the commonly used clinical methods. Using electroporation for treatment of diseases of internal organs, such as deep-seated tumors, will increase the need of controlling its extent to provide more efficient treatments and minimizing the damage to the healthy tissues.

We described in some detail the development of the procedure and treatment planning software that can provide medical practitioners with the information needed to effectively use electroporation in the clinical setting. Conceptually based on radiotherapy treatment planning tools, the described protocols and algorithms have been intended specifically for electrochemotherapy of deep-seated tumors; however, they are general enough to be useful for all electroporation-based therapies given that specific details are added to the protocols and the objective function [58] is composed of the tumor tissue to be covered with a sufficiently strong electric field (above 460 V/cm, i.e. $V_{THR\text{-}rev}$) minimizing also damage to healthy tissue due to irreversible electroporation ($V_{THR\text{-}irrev}$). Voltage and electrode position/geometry with respect to the distance between electrodes need to be such as to ensure electric field strength higher than the reversible threshold ($V_{THR\text{-}rev}$) and at the same time lower than the irreversible threshold ($V_{THR\text{-}irrev}$) in order to avoid ablation of neighboring vital tissue. Similarly, a well-defined target (i.e. tumor or some other pathological tissue) needs to be determined when planning ablation using non-thermal irreversible electroporation (NTIRE). When planning an NTIRE-based treatment, the resulting electric field strength in the target tissue is required to exceed the irreversible threshold for ablation to be successful. Nevertheless, it is imperative to avoid tissue damage due to thermal effects (i.e. Joule heating) [59]. Furthermore, gene transfer for gene therapy and DNA vaccination [18,19] is another application where it is important for the resulting electric field strength in the target tissue to be above the reversible threshold and at the same time below the irreversible threshold in order to achieve sufficient gene expression [58].

All the above mentioned applications would greatly benefit from treatment planning. The procedural treatment planning software we presented is still in development and is being evaluated at the same time. However, to bring treatment planning into routine clinical use, additional considerations need to be made. First, the treatment planning software needs to be developed as an easy-to-use computer application, in order to simplify the procedure and thus to enable its widespread use. The import of medical images (CT or MRI) has to be simplified; moreover, preprocessing should be a fully automated procedure, so that the attending surgeon does not need special computer skills in order to use the software. Then, segmentation procedures for semi-automatic segmentation of medical images have to incorporate sophisticated methods that would at the same time allow easily performable segmentation (e.g. by using statistical models of organs, or by using deformable active contours). Finally, new methods of three-dimensional mesh generation need to be established in order to adaptively generate a representative three-dimensional mesh regardless of the model being reconstructed (e.g. brain tumor, liver metastases etc.), while at the same time providing the possibility of including electrodes of arbitrary size and position.

The treatment delivery and monitoring itself also requires additional consideration. First, the treatment plan is based on the medical images (CT or MRI) of the patient that are normally acquired a few weeks before the operation; furthermore, the liver may be exposed to substantial flattening from pre-operative image scanning to intra-operative procedure [60]; moreover, during treatment delivery the liver is mobilized so that the attending surgeon can reach the targeted parts of liver for electrodes' insertion. Therefore, currently we cannot accurately match the intra-operative liver position with the generated treatment plan model as abdominal organs are deformable [61]; however, the tracking of such organs could be possible e.g. with small electromagnetically tracked sensors [47]. In the case of electroporation evolving into a percutaneous-only procedure in the future (using e.g. image guided insertion of electrodes) [62], such matching is possible. Nonetheless, in such a case the electrodes should be ultrasound-visible, which can be achieved not only by using appropriate materials (e.g. tungsten) but also by appropriately taking into consideration the scattering effect in correlation with electrodes under ultrasound [63], because materials of surgical instruments have a very high acoustic impedance [61]. Additionally, applied voltage between electrodes and the electric current should be measured during treatment delivery; in that way, conductivity measurements from real cases could be performed, and measurements' results could be re-inserted into the generated treatment plan in order to improve the algorithms used for future treatment plans (i.e. based on real feedback obtained from treatment). Visualization by Current Density Imaging (CDI) and Magnetic Resonance Electrical Impedance Tomography (MREIT) obtained during electroporation pulses might be possible in the future [64,65].

Although the described procedures for deep seated tumors electrochemotherapy based on patient-specific treatment planning rely on the radiotherapy basis, there is also a radiotherapy-specific feature that should not be replicated when planning electrochemotherapy. Namely, since in radiotherapy the damage caused by the radiation beam is not tumor-specific, it is common to plan the radiotherapy treatment to be aimed at not only target tissue (i.e. tumor), but also at a defined amount of the healthy tissue around the tumor (i.e. a safety margin); this safety margin represents a certain amount of the healthy tissue around the tumor that will be damaged by the radiation beam as well in order to assure complete beam coverage of the tumor tissue. Nevertheless, in electrochemotherapy treatment planning such increase of tumor volume is not acceptable because the tumor tissue's conductivity significantly differs from the healthy tissue's conductivity [52]. Therefore, since an exact model of the applied electric field distribution is necessary for the success of electrochemotherapy, an exact model of the patient's tissue needs to be constructed as well.

Implementation of treatment planning among the end-users (i.e. surgeons, physicians, etc.) is a challenging task. To successfully introduce treatment planning, it first needs to be validated in order to determine the accuracy and efficacy of employed procedures. The goal of this validation is to provide a known and well-controlled assessment of uncertainty, which can later be used in the numerical computation phase [47]. Validation of treatment planning is a multi-step procedure. First, segmentation needs to be validated. Validation of segmentation is possible by comparing the output of the segmentation phase to an existing database of segmented medical images; an expert opinion is then required to determine if re-segmentation of medical images using the newly developed treatment planning software matches the segments obtained from the previously available set of segmented images. Alternatively, solely expert opinion could be used to evaluate the accuracy of segmentation. Besides validation

of the segmentation, three-dimensional reconstruction needs to be validated as well. This can be done by imaging (using CT or MRI) a phantom of well-defined dimensions and shape, which is then reconstructed, and the output of the three-dimensional reconstruction is compared to the original object. Since the three-dimensional reconstruction embeds the error of segmentation, segmentation accuracy needs to be already assessed before evaluating three-dimensional reconstruction accuracy. In fact, instead of using a detailed 3D reconstruction, some studies [8] have opted for a rough approximation of the tumor and tissue geometry. While not as accurate, this simplified approach could be of great use in cases where no vital tissues are present in the electrode vicinity and can be based on approximate solutions [66–68].

Part of validation is also the follow-up procedure. To determine objective response after the treatment, the overall treatable and also measurable tumor volume needs to be determined. Pre-operative images (CT or MRI) are used to determine the overall tumor volume. Moreover, in cases of a solitary metastasis, histology should be also considered since assessment of target lesions volume shall not be the only criteria for determining objective response [69]. In our case, as part of a two stage procedure, the follow-up procedure is performed using a second surgery 4–8 weeks after the first electrochemotherapy [15]. The second surgery is necessary to extract the presumably necrotic tissue in order to perform histology and determine success of electrochemotherapy by first performing lesion measurements and then, using e.g. immunohistochemical staining, especially since etiology of necrosis can vary. Preliminary analyses indicate clinical benefit of the treatment, since in some cases even complete destruction of the treated metastasis was observed.

Additionally, several theoretical considerations have been thought of and are used in the simulations and treatment planning for electroporation-based interventions [59,70,71]. Namely, in all the described mathematical models on the tissue level electroporation is considered as a deterministic *all or nothing* response to the electric field: each cell is electroporated if exposed to electric field above electroporation threshold, and not if exposed to electric field bellow threshold. Therefore, current mathematical models of electroporation only predict electroporation based on the distribution of an applied electric field. The electric field strength is compared to a predefined threshold, and distribution is observed in the target area; if the electric field strength exceeds the predefined threshold, electroporation is predicted. However, such a model may be overly simplistic, as it overlooks the stochastic nature of electroporation [72,73]. The sources of stochasticity, for instance cell heterogeneity (e.g. in cell size, shape), cellular density and cellular communication (e.g. gap-junctions) should be included into the models [74]. In that way, more accurate treatment plans could be generated and electrochemotherapy would greatly benefit since more realistic predictions could be achieved. While the mathematical models currently used describe only the electric field distribution and changes in tissue electric properties due to electroporation, it would not be difficult to add a mathematical description of the thermal effects of the electric pulses – thermal effects can be very important for both gene electrotransfer, where due to longer pulses used more energy is deposited in the tissue, and for irreversible electroporation where it is crucial to reside below the thermal damage threshold to achieve good regeneration effects [49,75,76]. Additionally, several other mechanisms have been included in electroporation simulations, namely: mass transfer models for determining molecular uptake or transmembrane transport [77,78] and statistical methods for predicting cell death from electroporation pulses [79], all of which might be useful for specific electroporation-based therapies. Moreover, multiple treatment plans may be generated for each patient e.g. based on the genetic algorithm [80], and compared between and finally assessed with a quantitative criterion such as e.g. conformity index [81], which has already been introduced in radiotherapy.

Using numerical treatment planning protocols could ultimately lead to consistent and predictable effects, thus ensuring a maximally effective treatment. Simultaneously, treatment planning provides a framework for the development of standardized procedures as well as the ability to reduce the uncertainties inherent in the complexity of electroporation-based treatments.

Acknowledgments

This work was supported by the Slovenian Research Agency (ARRS). Research was conducted in the scope of the Electroporation in Biology and Medicine (EBAM) European Associated Laboratory (LEA). The authors thank *IV Oncological Orthopaedic Clinic* of the Rizzoli Institute, Bologna, Italy, for the image (Fig. 6a) on electrode insertion.

References

[1] T. Kotnik, G. Pucihar, D. Miklavčič, Induced transmembrane voltage and its correlation with electroporation-mediated molecular transport, J. Membr. Biol. 236 (2010) 3–13.
[2] A. Pakhomov, D. Miklavčič, M.S. Markov, Advanced Electroporation Techniques in Biology and Medicine, CRC Press, 2010.
[3] G. Serša, D. Miklavčič, M. Čemažar, Z. Rudolf, G. Pucihar, M. Snoj, Electrochemotherapy in treatment of tumours, Eur. J. Surg. Oncol. 34 (2008) 232–240.
[4] R. Magjarević, I. Lacković, D. Miklavčič, Pet godina šire primjene elektrokemoterapije u klinici, Liječničke Novine 97 (2011) 36–39.
[5] L. Heller, R. Heller, Electroporation gene therapy preclinical and clinical trials for melanoma, Curr. Gene Ther. 10 (2010) 312–317.
[6] P. Garcia, T. Pancotto, J. Rossmeisl, N. Henao-Guerrero, N. Gustafson, G. Daniel, et al., Non-thermal irreversible electroporation (N-TIRE) and adjuvant fractionated radiotherapeutic multimodal therapy for intracranial malignant glioma in a canine patient, Technol. Cancer Res. Treat. 10 (2011) 73–83.
[7] M. Marty, G. Serša, J. Garbay, J. Gehl, C. Collins, M. Snoj, et al., Electrochemotherapy – an easy, highly effective and safe treatment of cutaneous and subcutaneous metastases: results of ESOPE (European Standard Operating Procedures of Electrochemotherapy) Study, Eur. J. Cancer Suppl. 4 (2006) 3–13.
[8] F. Mahmood, J. Gehl, Optimizing clinical performance and geometrical robustness of a new electrode device for intracranial tumor electroporation, Bioelectrochemistry 81 (2011) 10–16.
[9] B. Agerholm-Larsen, H. Iversen, P. Ibsen, J. Moller, F. Mahmood, K. Jensen, et al., Preclinical validation of electrochemotherapy as an effective treatment for brain tumors, Cancer Res. 71 (2011) 3753–3762.
[10] EU Clinical Trials Register, https://www.clinicaltrialsregister.eu/, 2011.
[11] ClinicalTrials.gov, http://clinicaltrials.gov/, 2011.
[12] D. Miklavčič, M. Snoj, A. Županič, B. Kos, M. Čemažar, M. Kropivnik, et al., Towards treatment planning and treatment of deep-seated solid tumors by electrochemotherapy, Biomed. Eng. Online 9 (2010).
[13] M. Fini, M. Tschon, M. Alberghini, G. Bianchi, M. Mercuri, L. Campanacci, et al., Cell Electroporation in Bone Tissue, in: S.T. Kee, J. Gehl, E.W. Lee (Eds.), Clinical Aspects of Electroporation, Springer New York, New York, NY, 2011.
[14] J. Rossmeisl, P. Garcia, O. Lanz, N. Henao-Guerrero, R. Davalos, Successful treatment of a large soft tissue sarcoma with irreversible electroporation, J. Clin. Oncol. 29 (2011) E372–E377.
[15] I. Edhemović, E.M. Gadžijev, E. Brecelj, D. Miklavčič, B. Kos, A. Županič, et al., Electrochemotherapy: a new technological approach in treatment of metastases in the liver, Technol. Cancer Res. Treat. 10 (2011) 475–485.
[16] M. Kandušer, D. Miklavčič, M. Pavlin, Mechanisms involved in gene electrotransfer using high- and low-voltage pulses – an in vitro study, Bioelectrochemistry 74 (2009) 265–271.
[17] F. Andre, J. Gehl, G. Serša, V. Preat, P. Hojman, J. Eriksen, et al., Efficiency of high and low voltage pulse combinations for gene electrotransfer in muscle, liver, tumor and skin, Hum. Gene Ther. 19 (2008) 1261–1271.
[18] J.J. Kim, Electroporation-enhanced delivery of DNA vaccines, Bioprocess Int. 9 (2011) 10–14.
[19] N.Y. Sardesai, D.B. Weiner, Electroporation delivery of DNA vaccines: prospects for success, Curr. Opin. Immunol. 23 (2011) 421–429.
[20] P.A. Garcia, J.H. Rossmeisl, R.E. Neal, T.L. Ellis, J.D. Olson, N. Henao-Guerrero, et al., Intracranial nonthermal irreversible electroporation: in vivo analysis, J. Membr. Biol. 236 (2010) 127–136.
[21] G. Onik, B. Rubinsky, Irreversible Electroporation: First Patient Experience Focal Therapy of Prostate Cancer, in: B. Rubinsky (Ed.), Irreversible Electroporation, Springer-Verlag, Berlin Heidelberg, 2010, pp. 235–247.
[22] K.P. Charpentier, F. Wolf, L. Noble, B. Winn, M. Resnick, D.E. Dupuy, Irreversible electroporation of the pancreas in swine: a pilot study, HPB. 12 (2010) 348–351.
[23] M. Lecchi, P. Fossati, F. Elisei, R. Orecchia, G. Lucignani, Current concepts on imaging in radiotherapy, Eur. J. Nucl. Med. Mol. Imaging 35 (2008) 821–837.
[24] I.F. Tannock, R.P. Hill, R.G. Bristow, L. Harrington, The Basic Science of Oncology, 4th ed. McGraw-Hill Medical, 2005.
[25] D.E. Lea, The mechanisms of the induction by radiation of chromosome aberrations in Tradescantia, J. Genet. 44 (1942) 216–245.

[26] D. Šel, D. Cukjati, D. Batiuskaite, T. Slivnik, L. Mir, D. Miklavčič, Sequential finite element model of tissue electropermeabilization, IEEE Trans. Biomed. Eng. 52 (2005) 816–827.
[27] H.D. González, J. Figueras, Practical questions in liver metastases of colorectal cancer: general principles of treatment, HPB. 9 (2007) 251–258.
[28] D. Šemrov, D. Miklavčič, Calculation of the electrical parameters in electrochemotherapy of solid tumours in mice, Comput. Biol. Med. 28 (1998) 439–448.
[29] D. Miklavčič, K. Beravs, D. Šemrov, M. Čemažar, F. Demšar, G. Serša, The importance of electric field distribution for effective in vivo electroporation of tissues, Biophys. J. 74 (1998) 2152–2158.
[30] D. Šemrov, D. Miklavčič, Numerical modeling for in vivo electroporation, Methods Mol. Med. 37 (2000) 63–81.
[31] D. Miklavčič, D. Šemrov, H. Mekid, L. Mir, A validated model of in vivo electric field distribution in tissues for electrochemotherapy and for DNA electrotransfer for gene therapy, Biochim. Biophys. Acta Gen. Subj. 1523 (2000) 73–83.
[32] S. Čorović, A. Županič, S. Kranjc, B. Al Sakere, A. Leroy-Willig, L. Mir, et al., The influence of skeletal muscle anisotropy on electroporation: in vivo study and numerical modeling, Med. Biol. Eng. Comput. 48 (2010) 637–648.
[33] N. Pavšelj, Z. Bregar, D. Cukjati, D. Batiuskaite, L. Mir, D. Miklavčič, The course of tissue permeabilization studied on a mathematical model of a subcutaneous tumor in small animals, IEEE Trans. Biomed. Eng. 52 (2005) 1373–1381.
[34] P. Canatella, J. Karr, J. Petros, M. Prausnitz, Quantitative study of electroporation-mediated molecular uptake and cell viability, Biophys. J. 80 (2001) 755–764.
[35] G. Pucihar, J. Krmelj, M. Reberšek, T. Batista-Napotnik, D. Miklavčič, Equivalent pulse parameters for electroporation, IEEE Trans. Biomed. Eng. 58 (2011) 3279–3288.
[36] H. He, D.C. Chang, Y.-K. Lee, Using a micro electroporation chip to determine the optimal physical parameters in the uptake of biomolecules in HeLa cells, Bioelectrochemistry 70 (2007) 363–368.
[37] M. Pavlin, M. Kandušer, M. Reberšek, G. Pucihar, F. Hart, R. Magjarević, et al., Effect of cell electroporation on the conductivity of a cell suspension, Biophys. J. 88 (2005) 4378–4390.
[38] D. Cukjati, D. Batiuskaite, F. Andre, D. Miklavčič, L. Mir, Real time electroporation control for accurate and safe in vivo non-viral gene therapy, Bioelectrochemistry 70 (2007) 501–507.
[39] E. Maor, A. Ivorra, B. Rubinsky, Non thermal irreversible electroporation: novel technology for vascular smooth muscle cells ablation, PLoS One 4 (2009) E4757.
[40] Medical Imaging & Technology Alliance (a division of NEMA), Digital Imaging and Communications in Medicine – DICOM, http://medical.nema.org/2011.
[41] S. Ahmed, K. Iftekharuddin, A. Vossough, Efficacy of texture, shape, and intensity feature fusion for posterior-fossa tumor segmentation in MRI, IEEE Trans. Inf. Technol. Biomed. 15 (2011) 206–213.
[42] Z. Ma, J. Tavares, R. Jorge, T. Mascarenhas, A review of algorithms for medical image segmentation and their applications to the female pelvic cavity, Comput. Methods Programs Biomed. 13 (2010) 235–246.
[43] M. Mancas, B. Gosselin, B. Macq, Segmentation Using a Region Growing Thresholding, in: Image Processing: Algorithms and Systems IV, Image Processing: Algorithms and Systems IV, San Jose, CA, USA, 2005.
[44] C. Xu, J.L. Prince, Snakes, shapes, and gradient vector flow, IEEE Trans. Image Process. 7 (1998) 359–369.
[45] W.E. Lorensen, H.E. Cline, Marching cubes: a high resolution 3D surface construction algorithm, ACM Comput. Graph. 21 (1987) 163–169.
[46] D. Pahr, P. Zysset, From high-resolution CT data to finite element models: development of an integrated modular framework, Comput. Methods Biomech. Biomed. Engin. 12 (2009) 45–57.
[47] K. Cleary, T. Peters, Image-guided interventions: technology review and clinical applications, Annu. Rev. Biomed. Eng. 12 (2010) 119–142.
[48] N. Pavšelj, D. Miklavčič, Numerical modeling in electroporation based biomedical applications, Radiol. Oncol. 42 (2008) 159–168.
[49] P. Garcia, J. Rossmeisl, R. Neal, T. Ellis, R. Davalos, A parametric study delineating irreversible electroporation from thermal damage based on a minimally invasive intracranial procedure, Biomed. Eng. Online 10 (2011) 34.
[50] V. Bevilacqua, G. Mastronardi, G. Piscopo, Evolutionary approach to inverse planning in coplanar radiotherapy, Image Vis. Comput. 25 (2007) 196–203.
[51] J.H. Holland, Adaptation in Natural and Artificial Systems: An Introductory Analysis with Applications to Biology, Control, and Artificial Intelligence, A Bradford Book, 1992.
[52] B. Kos, A. Županič, T. Kotnik, M. Snoj, G. Serša, D. Miklavčič, Robustness of treatment planning for electrochemotherapy of deep-seated tumors, J. Membr. Biol. 236 (2010) 147–153.
[53] A. Deodhar, T. Dickfeld, G. Single, W. Hamilton, R. Thornton, C. Sofocleous, et al., Irreversible electroporation near the heart: ventricular arrhythmias can be prevented with ECG synchronization, Am. J. Roentgenol. 196 (2011) W330–W335.
[54] B. Mali, T. Jarm, S. Čorović, M. Paulin-Košir, M. Čemažar, G. Serša, et al., The effect of electroporation pulses on functioning of the heart, Med. Biol. Eng. Comput. 46 (2008) 745–757.
[55] L. Mir, J. Gehl, G. Sersa, C. Collins, J. Garbay, V. Billard, et al., Standard operating procedures of the electrochemotherapy: instructions for the use of bleomycin or cisplatin administered either systemically or locally and electric pulses delivered by the Cliniporator (TM) by means of invasive or non-invasive electrodes, Eur. J. Cancer Suppl. 4 (2006) 14–25.
[56] R.T. Dorr, Bleomycin pharmacology: mechanism of action and resistance, and clinical pharmacokinetics, Semin. Oncol. 19 (1992) 3–8.
[57] R. Finch, H. Malik, Z. Hamady, A. Al-Mukhtar, R. Adair, K. Prasad, et al., Effect of type of resection on outcome of hepatic resection for colorectal metastases, Br. J. Surg. 94 (2007) 1242–1248.
[58] A. Županič, S. Čorović, D. Miklavčič, M. Pavlin, Numerical optimization of gene electrotransfer into muscle tissue, Biomed. Eng. Online 9 (2010) 66.
[59] A. Županič, D. Miklavčič, Tissue heating during tumor ablation with irreversible electroporation, Electrotech. Rev. 78 (2011) 42–47.
[60] L.W. Clements, P. Dumpuri, W.C. Chapman, B.M. Dawant, R.L. Galloway, M.I. Miga, Organ surface deformation measurement and analysis in open hepatic surgery: method and preliminary results from 12 clinical cases, IEEE Trans. Biomed. Eng. 58 (2011) 2280–2289.
[61] D. Hawkes, D. Barratt, J. Blackall, C. Chan, P. Edwards, K. Rhode, et al., Tissue deformation and shape models in image-guided interventions: a discussion paper, Med. Image Anal. 9 (2005) 163–175.
[62] S. Phee, K. Yang, Interventional navigation systems for treatment of unresectable liver tumor, Med. Biol. Eng. Comput. 48 (2010) 103–111.
[63] J.M. Mari, C. Cachard, Ultrasonic scanning of straight micro tools in soft biological tissues: methodology and implementation, Ultrasonics 51 (2011) 632–638.
[64] M. Kranjc, F. Bajd, I. Serša, D. Miklavčič, Magnetic resonance electrical impedance tomography for monitoring electric field distribution during tissue electroporation, IEEE Trans. Med. Imaging 30 (2011) 1771–1778.
[65] I. Serša, Enhanced sensitivity current density imaging, J. Magn. Reson. 204 (2010) 219–224.
[66] S. Čorović, M. Pavlin, D. Miklavčič, Analytical and numerical quantification and comparison of the local electric field in the tissue for different electrode configurations, Biomed. Eng. Online 6 (2007).
[67] R. Jimenez, A. Pupo, J. Cabrales, J. Joa, L. Cabrales, J. Nava, et al., 3D stationary electric current density in a spherical tumor treated with low direct current: an analytical solution, Bioelectromagnetics 32 (2011) 120–130.
[68] S. Dev, D. Dhar, W. Krassowska, Electric field of a six-needle array electrode used in drug and DNA delivery in vivo: analytical versus numerical solution, IEEE Trans. Biomed. Eng. 50 (2003) 1296–1300.
[69] M. Fabel, H. Bolte, H. von Tengg-Kobligk, L. Bornemann, V. Dicken, S. Delorme, et al., Semi-automated volumetric analysis of lymph node metastases during follow-up-initial results, Eur. Radiol. 21 (2011) 683–692.
[70] R. Davalos, B. Rubinsky, Temperature considerations during irreversible electroporation, Int. J. Heat Mass Transf. 51 (2008) 5617–5622.
[71] R. Davalos, B. Rubinsky, L. Mir, Theoretical analysis of the thermal effects during in vivo tissue electroporation, Bioelectrochemistry 61 (2003) 99–107.
[72] B. Henslee, A. Morss, X. Hu, G. Lafyatis, L. Lee, Electroporation dependence on cell size: optical tweezers study, Anal. Chem. 83 (2011) 3998–4003.
[73] M. Puc, T. Kotnik, L. Mir, D. Miklavčič, Quantitative model of small molecules uptake after in vitro cell electropermeabilization, Bioelectrochemistry 60 (2003) 1–10.
[74] L. Towhidi, T. Kotnik, G. Pucihar, S. Firoozabadi, H. Mozdarani, D. Miklavčič, Variability of the minimal transmembrane voltage resulting in detectable membrane electroporation, Electromagn. Biol. Med. 27 (2008) 372–385.
[75] I. Lackovič, R. Magjarević, D. Miklavčič, Three dimensional finite element analysis of joule heating in electrochemotherapy and in vivo gene electrotransfer, IEEE Trans. Dielectr. Electr. Insul. 16 (2009) 1338–1347.
[76] N. Pavšelj, D. Miklavčič, Resistive heating and electropermeabilization of skin tissue during in vivo electroporation: a coupled nonlinear finite element model, Int. J. Heat Mass Transf. 54 (2011) 2294–2302.
[77] Y. Granot, B. Rubinsky, Mass transfer model for drug delivery in tissue cells with reversible electroporation, Int. J. Heat Mass Transf. 51 (2008) 5610–5616.
[78] D. Miklavčič, L. Towhidi, Numerical study of the electroporation pulse shape effect on molecular uptake of biological cells, Radiol. Oncol. 44 (2010) 34–41.
[79] A. Goldberg, B. Rubinsky, The effect of electroporation type pulsed electric fields on DNA in aqueous solution, Technol. Cancer Res. Treat. 9 (2010) 423–430.
[80] A. Županič, D. Miklavčič, Optimization and Numerical Modeling in Irreversible Electroporation Treatment Planning, in: Irreversible Electroporation, Springer, Berlin, 2009, pp. 203–222.
[81] L. Feuvret, G. Noel, J. Mazeron, P. Bey, Conformity index: A review, Int. J. Radiat. Oncol. 64 (2006) 333–342.

ARTICLE 2

Title: Electroporation-based Treatment Planning for Deep-seated Tumors based on Automatic Liver Segmentation of MRI images

Authors: PAVLIHA Denis, MUŠIČ M. Maja, SERŠA Gregor, MIKLAVČIČ Damijan

Publication: PLOS ONE

DOI: The paper was submitted on January 3rd, 2013. The manuscript was returned from review on February 18th, 2013, requiring a minor revision prior to publication. The revised manuscript was resubmitted on April 3rd, 2013.

Year: /

Volume: /

Number: /

Pages: /

Impact factor: 4.092

Ranking:

Category name	Total journals in category	Journal rank in category	Quartile in category
biology	85	12	Q1

Electroporation-based Treatment Planning for Deep-seated Tumors based on Automatic Liver Segmentation of MRI images

Denis Pavliha[1], Maja M. Music[2], Gregor Sersa[2], Damijan Miklavcic[1]*

[1] University of Ljubljana, Faculty of Electrical Engineering, Trzaska c. 25, SI-1000 Ljubljana, Slovenia

[2] Institute of Oncology Ljubljana, Zaloska c. 2, SI-1000 Ljubljana, Slovenia

Abstract

Electroporation is the phenomenon that occurs when a cell is exposed to a high electric field, which causes transient cell membrane permeabilization. A paramount electroporation-based application is electrochemotherapy, which is performed by delivering high-voltage electric pulses that enable the chemotherapeutic drug to more effectively destroy the tumor cells. Electrochemotherapy can be used for treating deep-seated metastases (e.g. in the liver, bone, brain, soft tissue) using variable-geometry long-needle electrodes. To treat deep-seated tumors, patient-specific treatment planning of the electroporation-based treatment is required. Treatment planning is based on generating a 3D model of the organ and target tissue subject to electroporation (i.e. tumor nodules). The generation of the 3D model is done by segmentation algorithms. We implemented and evaluated three automatic liver segmentation algorithms: region growing, adaptive threshold, and active contours (snakes). The algorithms were optimized using a seven-case dataset manually segmented by the radiologist as a training set, and finally validated using an additional four-case dataset that was previously not included in the optimization dataset. The presented results demonstrate that patient's medical images that were not included in the training set can be successfully segmented using our three algorithms. Besides electroporation-based treatments, these algorithms can be used in applications where automatic liver segmentation is required.

1. Introduction

Electroporation is the phenomenon that occurs when a biological cell is exposed to an adequately high electric field, which results in the cell membrane becoming transiently permeabilized (Kotnik et al., 2010). Electroporation is considered to be a universal method and platform technology since all types of cells (animal, plant, and microorganisms) can be electroporated (Miklavcic, 2012). A paramount electroporation-based application is electrochemotherapy (Mali et al., 2013; Serša and Miklavčič, 2008) which enhances chemotherapy outcome due to transient permeabilization of targeted cell membranes: because of the externally applied electric field, electroporation facilitates the chemotherapeutic drug diffusion through the plasma membrane into the cells, which would be otherwise hampered, because of the impaired or slow transport of the chemotherapeutics that are used in electrochemotherapy (Sersa et al., 2008).

Electrochemotherapy is performed by high-voltage electric pulses delivery using applicators (i.e. electrodes) that are in contact with (or located near the) target tissue. Electrochemotherapy has already been introduced into clinical use for treating skin melanoma using plate or needle electrodes with a fixed geometry; the use of such electrodes imposes following predefined standard operating procedures for a successful treatment (Marty et al., 2006; Mir et al., 2006). Recently, however, electrochemotherapy has been introduced to clinical trials for treating deep-seated metastases in liver (Edhemovic et al., 2011), bone (Fini et al., 2011), brain (Agerholm-Larsen et al., 2011; Linnert et al., 2012; Mahmood and Gehl, 2011), and soft tissue (Neal, II et al., 2011). Electrochemotherapy of deep-seated tumors imposes the use of variable-geometry long-needle electrodes introduced either percutaneously or during open-surgery (Miklavčič et al., 2012). Hence, only following the standard operating procedures cannot ensure success of the treatment, and patient-specific treatment planning is required for effective electrochemotherapy of deep-seated tumors (Pavliha et al., 2012).

Another important electroporation-based application is termed *non-thermal irreversible electroporation* (N-TIRE) and is used for tissue ablation performed using an externally applied electric field with electric field strengths and higher number of pulses than the

values used for electrochemotherapy (Davalos et al., 2005). Nonetheless, the procedure is technologically very similar to electrochemotherapy and, also, requires patient-specific treatment planning (Županič and Miklavčič, 2009).

To prepare a robust treatment plan for electroporation-based treatments, an anatomical model that is built from medical images (Magnetic Resonance Imaging – MRI) needs to be constructed first (Miklavcic et al., 2010). Construction of such a model is based on the acquisition of the patient's medical images and relies on processing the images in order to perform relevant-tissue extraction (i.e. image segmentation) (Linguraru et al., 2012). Image segmentation, then, serves as the basis for generating a three-dimensional model consisting of the relevant healthy tissue (e.g. liver) and pathological tissue (i.e. tumors) (Pahr and Zysset, 2009). Vessels may also be segmented and included into the model (Chi et al., 2011) since vessel positions have to be taken into account when defining electrodes' entry direction and relative positions. Then, a Finite-Element Model (FEM) is built and using the defined electrode parameters (number, dimensions, position), the distribution of the electrical field is calculated and optimized (Zupanic et al., 2012; Županič et al., 2008) and finally presented to the attending physician.

In order to establish the concept of electroporation-based treatment planning, we follow radiotherapy treatment planning as the basis (Lecchi et al., 2008) using parallelisms and similarities between the planning procedures (Pavliha et al., 2012). Since development of a user-friendly treatment planning would simplify electroporation-based preoperative procedures, we opt towards developing treatment planning software that will not require any prior engineering knowledge from its end-user (e.g. the attending physician). The whole treatment planning software needs to perform as automatically as possible, i.e. with minimum of interaction by the clinician, and the most challenging task is development and implementation of an automatic image segmentation algorithm. Within the clinical study of electrochemotherapy of colorectal metastases in the liver (Edhemovic et al., 2011), we developed treatment planning procedure that includes liver segmentation. After implementing the segmentation algorithms and concluding the segmentation procedures, the latter were additionally modified using optimization results obtained using a training

set of seven cases that were previously manually segmented by a radiologist. Finally, additional four cases were manually segmented by a radiologist and used for the final validation of the segmentation procedures.

In this study, we evaluated three different liver segmentation algorithms that can be used for electroporation-based treatment planning: region growing, adaptive threshold and active contours. Region growing was selected for evaluation because despite its simplicity (i.e. segments are included solely based on their intensities) this algorithm is robust and can provide good results if its basic drawbacks (e.g. oversegmentation due to leakage) are eliminated (Heimann et al., 2004) using a postprocessor. Our implementation of the adaptive threshold algorithm was evaluated because this algorithm is based on a physical property, i.e. continuity of the tissue: segments on two neighboring slices are expected to be minimally different, which although being an intuitive solution which can be used as initialization of other segmentation methods (Casciaro et al., 2012), it proved to be accurate enough to be used as a standalone method for liver segmentation. Finally, the active contours algorithm (Kass et al., 1987) based on the Gradient Vector Flow (GVF) (Xu and Prince, 1998) was evaluated because of its insensitivity for intensity-based anomalies (e.g. inhomogeneity, or thin bonds connecting different segments such as the liver and e.g. kidneys) and possibility of influencing the movement of the contour by balancing the coefficient that influence attraction of the contours by the image or by the contour's inner properties. All three segmentation algorithms were optimized on a training set of seven cases, i.e. quantitatively assessed using real case data obtained from a radiologist. Finally, algorithms were validated using additional four real cases obtained from a radiologist, therefore accuracy of how their results are produced is known.

2. Methodology

2.1. Automatic Liver Segmentation

2.1.1. Importing DICOM Images

The segmentation procedure begins with importing the patient's images into the treatment planning software. The latter is a MATLAB application, developed in MATLAB R2012a (Mathworks, Nantick, MA, USA) using the *Image Processing Toolbox* and *Parallel Processing Toolbox*. The procedure for loading images loads all DICOM (Digital Imaging and Communications in Medicine) (National Electrical Manufacturers Association, 2009a) files from the user-defined folder, and reads their DICOM headers' *SeriesNumber* parameter in order to determine the number of different acquisition series present in the folder. Then, an image from every series is presented to the end-user (e.g. the attending physician); an image from every acquisition series is displayed and labeled using the original label that was stored at acquisition time and is read from the DICOM header as the string stored in the *SeriesDescription* parameter. Finally, the end-user determines which acquisition series will be used for planning of the electroporation-based treatment.

After that, all the images from the selected acquisition series are loaded and sorted according to their spatial location (i.e. according to their Z-index which can be read from the DICOM header as the *SliceLocation* parameter) using a common bubble-sorting algorithm. If all obtained Z-indexes after bubble-sorting are not evenly distributed, empty slices are inserted where the slices are detected as missing. However, since missing slices may indicate corruption of the patient's images collection, the software does not try to interpolate the missing slices but notifies the end-user instead.

Besides the image data, essential DICOM metadata is loaded; the metadata structure appended to the slices includes these parameters: *Width, Height, SliceThickness, PixelSpacing, Modality, AcquisitionDate*, *BitsAllocated,* and Volume of Interest (VOI) parameters *WindowCenter* (WC) and *WindowWidth* (WW) which are most important. Namely, WC and WW determine how source image data need to be interpreted when

displayed; therefore, an initial sigmoid transformation using parameters WC and WW needs to be performed first for the image data to be displayed correctly. The latter is done within the preprocessing procedure.

2.1.2. Preprocessing

For segmentation algorithms to perform without problems, the imported slices first need to be preprocessed. Preprocessing is a procedure which is executed on each slice separately; therefore, the procedure is non-recursive and can be run in parallel using multiple processors or processor cores. Since the preprocessing procedure comprises of several steps, the steps are marked for debugging and algorithm evaluation purposes by storing partial results (i.e. partially preprocessed slices) into separate *layers*, starting with the *source* slices (i.e. slices stored as DICOM data), which enables the developers of the algorithms to have a clear overview of the whole preprocessing procedure.

Interpretation of imported (i.e. *source*) slices is defined by the Volume-of-Interest (VOI) parameters (i.e. Window Center – WC, and Window Width – WW) that are stored as DICOM metadata. Since WC and WW differ from slice to slice, each slice first needs to be transformed from the imported data values (i.e. *source* layer) to the normal values (i.e. *original* layer) which are defined by the VOI parameters. The transformation can be performed using a sigmoid function as defined by the DICOM standard (National Electrical Manufacturers Association, 2009b); the transformation is described using Equation 1.

$$output = \frac{output\_range}{1 + e^{-4\frac{input - WC}{WW}}} \qquad \text{(Eq.1)}$$

As seen in Figure 1, such a transformation can be used for multiple purposes. When the WW parameter is small ($WW \to 1$), the sigmoid function (Figure 1B) changes into an approximation of a step function (Figure 1A) and can be used for thresholding, the WC parameter being the threshold value and the output value being Boolean with possible values (*0, output_range*). When the WW parameter is large (e.g. $WW > output\_range$), the sigmoid function changes into an approximation of a linear function (Figure 1C) and can

be used for linear transformations, the output value residing in the range (*0, output_range*) depending on the WC and WW parameter values.

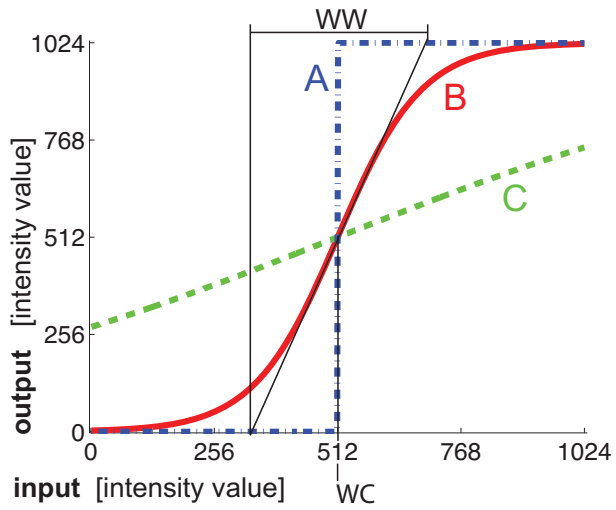

Figure 1. Sigmoid transformation function for preprocessing purposes.

Presented is an example sigmoid function (B), with approximations of the step function (A: WC = 512, WW = 1) and linear function (C: WC = 512, WW = 2048).

After transforming the *source* slices into *original* slices using the transformation from Eq.1 and parameter values (*WC*, *WW*, and *output_range*) from the DICOM metadata, the slices are then de-biased. De-biasing is a procedure that removes intensity inhomogeneity (Vovk et al., 2007) that is caused because the magnetic field in the area where the patient is positioned is not equally intense (i.e. the magnetic field is more homogeneous in the focal part of the device); a publicly available inhomogeneity correction algorithm was implemented for de-biasing (Zheng et al., 2009). Then, filtering of the slices, which is necessary for noise elimination, is performed by applying an average and a Gaussian blur filter ($\sigma = 3$), both with window sizes of 3x3 pixels. Finally, another sigmoid transformation is applied to the slices using fixed VOI parameters (*WC=20000, WW=100, output_range=*2^{16}) which ensures the intensity distribution of the slices is redistributed in the whole 16-bit range regardless of the *source* slices' range, and an adequate contrast which is dependent on the WW parameter. The fixed VOI values were selected based on our experience using real case data, and assure that the liver segment will have an appropriate intensity value range for the segmentation to be successful. After these procedures are

applied, the resulting slices are stored as *preprocessed* slices (i.e. on a separate layer) and are ready for segmentation.

2.1.3. Referential Slice

First, we define the *referential slice* as the slice in the patient's medical images collection with a high probability to include a large liver segment. We define Z_{REF} as the index (i.e. spatial location) of the referential slice using Equation 2:

$$Z_{REF} = ceil(0.65 \cdot Z_{MAX}) \quad \text{(Eq.2)}$$

where Z_{MAX} is the number of all the slices in the patient's medical images collection and the constant 0.65 was found empirically on real case data. Using Equation 2, we have a high probability of obtaining a *referential* slice with a liver segment that is morphologically similar to the liver segment shown in Figure 2B.

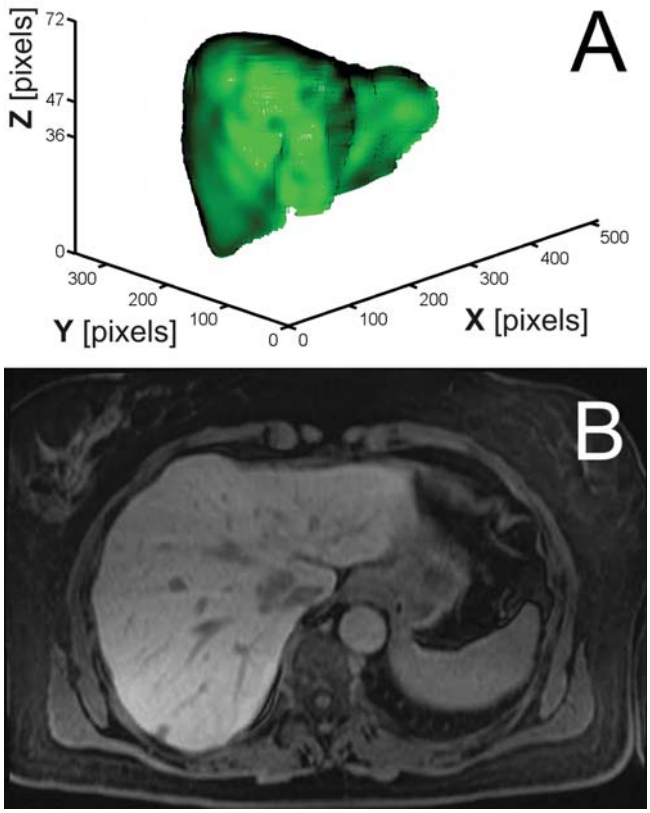

Figure 2. An example three-dimensional liver object.

The presented object consists of 72 slices (Z_{MAX}=72, A) and includes slice Z_{REF}=47 as the referential slice (B).

The identified *referential* slice serves as the beginning point of segmentation, i.e. the slice where segmentation is initiated, and its identification is independent of the chosen segmentation algorithm. Hence, there is a high probability that the *referential* slice will include a liver segment as the one shown in Figure 2B. For region growing, the *referential* slice is used as the slice that is presented to the end-user (e.g. attending physician) in order to place the initial seed on the slice; for adaptive threshold (and also for active contours which use adaptive threshold for contour initialization), the *referential* slice is used for comparing the dynamically thresholded slice to the presets that include similar liver segments, and marking the threshold value with the highest similarity to any of the presets as the initial liver segment.

2.1.4. Region Growing Segmentation Algorithm

We first implemented an intensity-based segmentation algorithm known as the region growing algorithm. The latter determines whether voxels are part of the target region or not by comparing their intensities to the intensity of the initial seed. The initial seed is a voxel manually selected by the end-user (e.g. the attending physician) at the beginning of the procedure; in our case, the *referential* slice is presented to the end-user who is required to click on the liver segment where there are no internal liver structures such as vessels or tumor nodules. The pixel clicked then serves as the initial seed voxel.

The region growing segmentation algorithm works in three dimensions and evaluates the voxels that are scheduled into the queue. At the beginning, a single voxel is added to the queue, namely the initial seed. The algorithm examines the *current* voxel in the queue by comparing the intensity of every *current* voxel's neighbor to the intensity of the *current* voxel, as shown in Figure 3 where an array of 3x3x3 voxels is displayed and the middle voxel represents the *current* voxel (i.e. 26-connected neighbors).

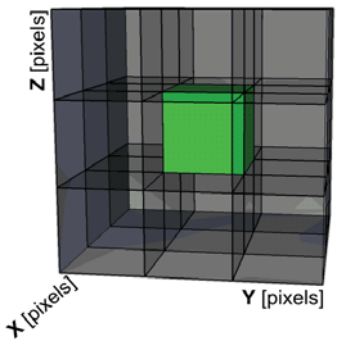

Figure 3. Representation of the initial seed voxel and its 26 neighbors.

Since intensity of the target region varies in all three dimensions due to inhomogeneity, it is imperative to allow some intensity deviation when evaluating if the neighboring voxels belong to the target region. The allowed intensity deviation is defined using a threshold deviation value (e.g. setting the threshold deviation value to 0.20, which is the value we used, determines the intensities that are acceptable for inclusion into the target region; the determined intensities reside in the range $0.8 \cdot I_{SEED} < I_{CURRENT} < 1.2 \cdot I_{SEED}$, where I denotes the voxel's intensity and a *bit* is its unit). Therefore, any of the evaluated neighbor voxels that have the intensity in the defined range are marked as part of the target region by being added to the queue. After all the neighbors of the *current* voxel are evaluated, the algorithm evaluates the next voxel in the queue; the next voxel becomes the *current* voxel and its neighbors are evaluated. The procedure is repeated until there are no voxels left in the queue. Finally, all the voxels that are stored in the queue represent the target region which in our case is the liver. Figure 4 displays progress of the segmentation based on region growing after 40.000 evaluated voxels (A), after 400.000 evaluated voxels (B), and after all the voxels in the queue have been evaluated (C).

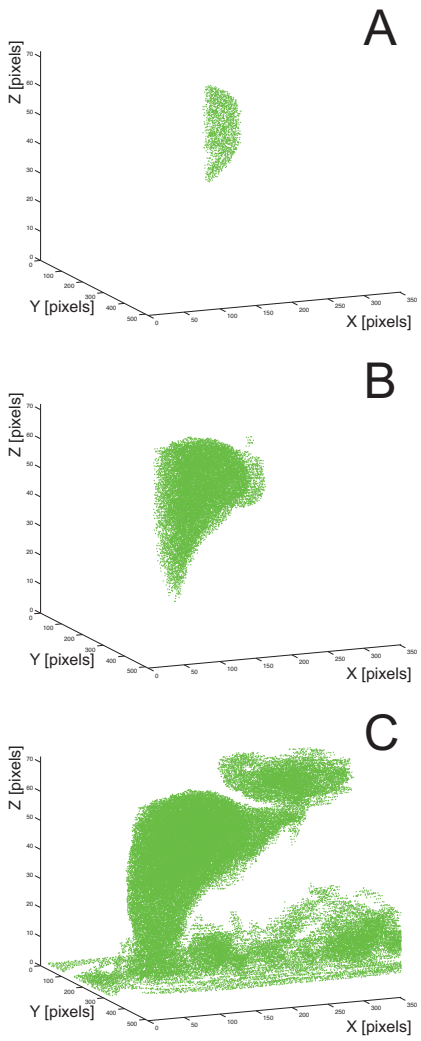

Figure 4. Progress of the region growing algorithm performing liver segmentation. *Presented is the functioning of the algorithm after 40.000 evaluated voxels (A), after 400.000 evaluated voxels (B), and after all the voxels have been evaluated (C). The initial seed is located at X=192, Y=209, Z=47.*

Due to leakage, region growing may include unwanted segments (e.g. the lower part of the heart, as seen in the upper right part of Figure 4C) which are later eliminated by the postprocessing procedure.

2.1.5. Adaptive Threshold Segmentation Algorithm

The second liver segmentation algorithm that we evaluated is adaptive threshold algorithm. We developed this algorithm as an upgraded threshold-based algorithm that executes filtering of the current slice using a threshold function while sweeping the intensity

threshold value and at the same time comparing the currently filtered slice to the previous already-segmented slice (i.e. the maximum similarity criterion). The intensity threshold value is swept over the whole intensity range, and the similarity comparison is done using normalized cross-correlation which performs segment area comparison (i.e. surface overlap). Similarity to the previous slice is chosen as the criterion for segment determination of adaptive threshold algorithm because the difference in liver shape and size between two neighboring slices is expected to be minimal; therefore, choosing similarity with the previous properly segmented slice as the criterion ensures that the current slice will also be segmented properly. Hence, the error of such a procedure is cumulative and shall the segmentation fail on one slice, all the following slices will be improperly segmented as well. The procedure is shown in Figure 5, where the current slice with three different threshold values (Figures 5A, 5B, and 5C) is compared to the previous slice (Figure 5D).

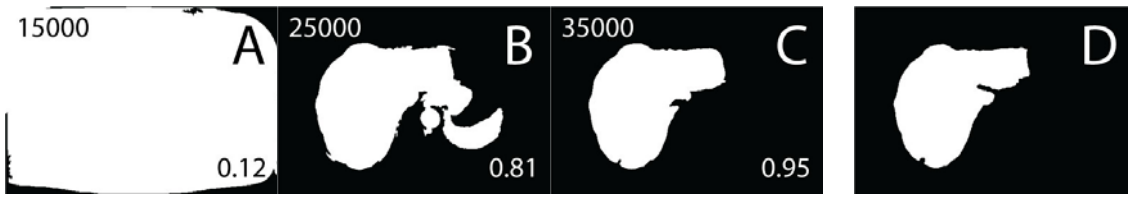

Figure 5. Adaptive threshold algorithm functioning.

Demonstrated is the functioning of the algorithm comparing a slice while sweeping the intensity threshold value; presented are three examples where the intensity threshold value is set to 15.000 bits and similarity is 0.12 (A), 25.000 bits and similarity is 0.81 (B) and 35.000 bits and similarity is 0.95 (C); the comparison is done to the previous already-segmented slice (D).

The comparison results (i.e. similarity) which are obtained using normalized cross-correlation are stored during sweep for each intensity threshold value. After the intensity threshold value sweep is done, the intensity threshold value with the highest similarity (i.e. the maximum normalized cross-correlation) is selected, and the current slice is, finally, transformed using the selected intensity threshold value. The procedure is started from the *referential* slice and repeated on the following slices until the end of the slices collection; then, the procedure is restarted from the *referential* slice to the beginning of the slices

collection. If the highest similarity is lower than a certain similarity threshold, the algorithms determines the segment has ended and empties the current and all the following (or previous, depending on the segmentation Z-direction) slices; in our case, the similarity threshold was set to 0.70 based on our experience on real case data. Moreover, since the *referential* slice has no prior slices it could be compared to, a set of six presets that include various possible liver segments is used instead, and the maximum similarity to any of the presets indicates the final intensity threshold value for the *referential* slice. Three out of six example presets that are used for thresholding the *referential* slice are shown in Figure 6.

Figure 6. Three example liver presets used by the adaptive threshold algorithm.
The preset are used for determining the final intensity threshold value of the referential slice.

2.1.6. Active Contours Segmentation Algorithm

The third algorithm for performing liver segmentation that we evaluated for electroporation-based treatment planning is the active contours segmentation, sometimes referred to as the *snakes* segmentation algorithm. This algorithm is based on placing a deformable (i.e. active) contour, which is a closed curve made of points, on the same location as certain voxels (i.e. the initial contour position). Then, for each point of the active contour (located at the *current* voxel), the energy of the *current* and all its neighboring voxels is calculated based on four energy contributions: elasticity of the contour's point in the *current* voxel, curvature of the contour's point in the *current* voxel, magnitude of intensity-based energy in the neighboring voxels, and direction of the intensity-based energy in the *current* voxel. Each point of the active contour is, then, moved to the voxel with the lowest energy. The procedure is repeated until the active contour reaches the desired location (e.g. after a defined number of iterations).

The active contours segmentation algorithm is initiated by placing an initial active contour on top of the *referential* slice. The active contour is attracted by the edges in the image (Kass et al., 1987); therefore, it is imperative to initialize the active contour by placing it near the edge of the desired segment (i.e. the liver). Hence, the adaptive threshold segmentation algorithm is used to generate the initial active contour by segmenting the *referential* slice and transforming the edge of the segment identified on the *referential* slice into a closed curve with points sorted according to their location on the segment's circumference. Moreover, the number of all the points in the active contour is reduced by decimation; in our case, the number of circumference pixels between two active contour points is limited to 8. Next, the image energy is calculated as the Gradient Vector Flow (GVF) of the image; a publicly-available GVF calculation algorithm (Xu and Prince, 1998) has been implemented using parameter μ=0.2 and run in 1.000 iterations. The calculation of the GVF is based on the edge map deriving from intensities in a slice; individual steps of this procedure are shown in Figure 7.

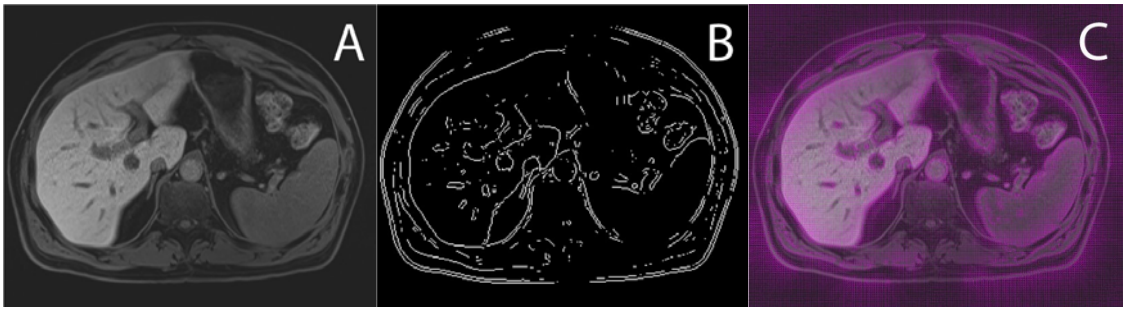

Figure 7. Active contours algorithm and the Gradient Vector Flow map.
Presented is an example original liver slice (A) with its edge map (B) and overlaid with a calculated Gradient Vector Flow (GVF) map (C).

The energy contributions to the total voxel energy are, based on our experience with optimizing algorithms using real case data, balanced using the coefficients 1, 3, 9, 3 for curve elasticity, curve curvature, GVF magnitude, GVF direction, respectively. All the energy contributions are normalized to reside within the range (0,1) in order for the energy coefficients to be properly balanced. In our segmentation algorithm, the *curve elasticity*

energy contribution is calculated based on Equation 3, while the *curve curvature* energy contribution is calculated based on Equation 4. The implemented GVF algorithm already ensures normalized energy results; the *GVF magnitude* energy contribution is calculated as the magnitude of the GVF vector in the evaluated voxel, while the *GVF direction* energy contribution is defined as representing low energy (0) in the neighboring voxel that is located in the direction the GVF vector of the evaluated voxel is pointing to, while all the other voxels have a high energy (1). In Equations 3 and 4, E denotes the energy contribution, while P_{CURR}, P_{PREV} and P_{NEXT} denote the current, the previous and the next points of the active contour, respectively.

$$E_{ELAST} = \frac{(\|P_{CURR}, P_{PREV}\| + \|P_{CURR}, P_{NEXT}\|)}{2} \quad \text{(Eq.3)}$$

$$E_{CURV} = \|\|P_{CURR}, P_{PREV}\| - \|P_{CURR}, P_{NEXT}\|\| \quad \text{(Eq.4)}$$

After the total energy on and around each active contour point is calculated, and balanced using energy contribution coefficients, the active contour points iteratively move toward the voxel with the lowest total energy. Since the energy depends on the active contour points' locations, the *curve elasticity* and *curve curvature* contributions are recalculated after every iteration, and the total energy is recalculated as well. The active contour movement is stopped after a predefined number of iterations (e.g. in our case, the active contour movement is limited to 100 iterations).

When the active contour movement is stopped on one slice, the procedure is repeated on another slice. The procedure is started from the *referential* slice and is repeated on the next slices until the end of the slices collection; then, the procedure is restarted from the *referential* slice to the beginning of the slices collection; therefore, the active contour segmentation algorithm may be split into two processing threads.

In order to perform segmentation using the active contours algorithm in three dimensions, the initial contour on the *current* slice is the same as the final active contour on the previous slice. Because the difference in liver shape and size between two neighboring slices is expected to be minimal on the slices where the organ that is subject to segmentation is

present, the previous slice's final active contour is a good initial contour for the *current* slice. Moreover, due to the expected minimal active contour movement, less iterations are required when calculating the image's GVF since edges will attract active contours in their vicinity even when the GVF is calculated in less iterations; therefore, the processing time of the active contour segmentation algorithm is reduced (e.g. in our case, we are calculating the GVF in 1000 iterations).

2.1.7. Postprocessing

After segmentation, a postprocessing algorithm needs to be executed to eliminate possible anomalies that may occur during segmentation (e.g. segment leakage). Postprocessing eliminates redundant segments that cannot be part of the final results; elimination is based on comparing neighboring slices in the direction of the third dimension (i.e. component Z) using normalized cross-correlation.

The postprocessing algorithm is initiated on the *referential* slice; namely, the probability that a slice includes only one identified segment is the highest on the *referential* slice, since segmentation was initiated on this slice regardless of the chosen segmentation algorithm: for region growing, the seed was placed on this slice; for adaptive threshold, the comparison with presets was made on this slice and also, the active contour was initiated using the adaptive threshold segmentation algorithm on the *referential* slice as well. Shall the morphological operations during segmentation split the segment on the *referential* slice into multiple segments, the first step of postprocessing eliminates such redundant segments by only keeping the largest segment on the *referential* slice.

Then, the postprocessed *referential* slice, i.e. $Z_{CURR}=Z_{REF}$, is used as the basis for performing normalized cross-correlation with the next, i.e. $Z_{CURR}+1$ or the previous, i.e. $Z_{CURR}-1$ slice, respectively. The template for the normalized cross-correlation is generated by intersecting each segment on the current slice, i.e. Z_{CURR}, with the finally postprocessed previous, i.e. $Z_{CURR}-1$ or next, i.e. $Z_{CURR}+1$ slice, respectively (depending on the postprocessing Z-direction). Then, each segment on the current slice is compared to its corresponding template generated from its neighboring slice using normalized cross-correlation; if the

result of the comparison exceeds a predefined threshold, the segment is kept on the slice, else it is discarded. In our case, we set the comparison threshold to 0.65 which was found empirically on real case data. The postprocessing procedure may be split into two processing threads, since it is symmetrically executed from $Z=Z_{REF}+1$ to $Z=Z_{MAX}$, and from $Z=Z_{REF}-1$ to $Z=1$ (i.e. the postprocessing Z-direction).

Moreover, if we compared the neighboring slices only by using the whole next or previous slice as the template for comparison to the current slice (i.e. without comparing separate segments on a slice), we would be unable to extract these separate segments and determine whether they derive from the target tissue (e.g. liver) or not; therefore, such comparison enables us to keep multiple segments on a slice with the possibility of eliminating segments that are not part of the target tissue. Besides, in order to allow separation of single segments that are in fact multiple segments connected by a thin bond (possibly due to leakage), all the slices are eroded before and dilated after the postprocessing procedure using a *disk* structuring element of 3x3 pixel size.

2.2. Validation

2.2.1. Optimization using Radiologist Data Set as a Training Set

Since segmentation algorithms are required to produce not only meaningful but also accurate results, validation of the algorithms is an imperative. In our case, validation was performed as a two-step procedure. In the first step, the algorithms were optimized using radiologist dataset as a training set, and then in the second step, the algorithms were validated after being optimized using another radiologist dataset.

In order to perform segmentation algorithms' optimization, seven sets of patient's liver manually segmented by a radiologist were used as a training set. For each segmentation algorithm, changeable parameters that significantly influence the functioning of the algorithms were defined, and their possible value ranges were defined based on our previous experience using real-case data. These changeable parameters were then subject to variation within optimization iterations; every of the seven cases that were already manually segmented by the radiologist was re-segmented using our three segmentation algorithms

(i.e. region growing, adaptive threshold, and active contours) in the optimization process. During this optimization process, variation of the defined changeable parameters was performed in order to each time automatically obtain a liver object that is most similar to the one segmented by the radiologist. Figure 8 demonstrates how manual segmentation was performed by the radiologist: an example slice during manual segmentation can be seen (Figure 8A), and a final three-dimensional liver object as a result of the manual segmentation by the radiologist (Figure 8B).

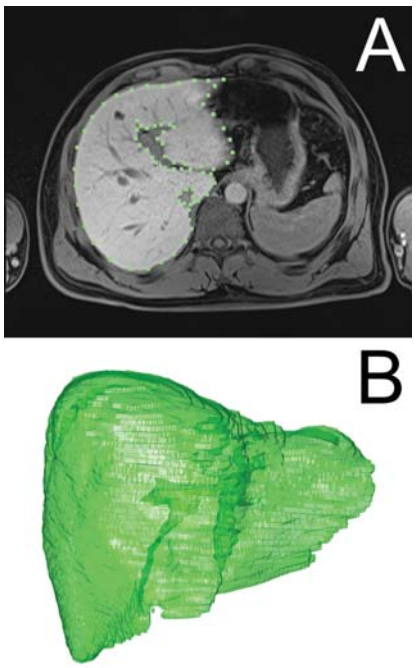

Figure 8. Radiologist manual segmentation procedure.

Presented is a defined liver segment on a slice (A) and a final three-dimensional liver object (B).

After acquiring the data obtained from the radiologist and arranging them into the form that was applicable to optimization and validation (i.e. changing the data syntax by converting them to a raw format, so that inclusion into optimization algorithms was seamless), value ranges of the changeable parameters were defined. For region growing, the parameters subject to variation during optimization were the size of the noise-elimination filter mask during preprocessing, and the threshold deviation value which determines the range of the intensities that are acceptable for inclusion into the target region during segmentation (for optimization purposes, the initial seed of the region growing algorithm

was chosen manually and fixed for each segmented case separately). For adaptive threshold, the parameters subject to variation during optimization were the size of the noise-elimination filter mask during preprocessing, and the initial coefficient that determines the targeted size of the referential segment (i.e. the initial liver segment on the referential slice) in the beginning of segmentation. For active contours, all four energy-contribution coefficients were varied during optimization.

Optimization was run on a workstation with Intel Core-i7 965 Extreme Edition processor (maximum frequency 3.46 GHz, 4 cores, 8 threads) with 12 GB of DDR3 memory (frequency 1.333 MHz), two 300 GB hard disk drives (velocity 10.000 rpm) running in stripe mode, and operating system Windows 7 Enterprise (64-bit). The segmented three-dimensional liver object that was produced in each iteration of optimization was compared to the corresponding model that was manually segmented by the radiologist; comparison was done on a slice-by-slice basis using normalized cross-correlation. Similarity (i.e. the results of the normalized cross-correlation) was stored together with the current values of the changeable parameters, and finally the iteration with the maximum similarity (i.e. the mean value of similarity of all slices), was chosen as the optimum (i.e. case-specific similarity, S_C in Table 1); the changeable parameters used in that iteration were marked as optimal parameters for the current case and currently evaluated segmentation algorithm. Moreover, optimal parameters of every evaluated segmentation algorithm were also determined for the whole evaluated series (i.e. all the seven cases) by comparing similarity of different cases with the same changeable parameters to the corresponding model that was manually segmented by the radiologist. These optimized parameters can be defined as globally-optimized parameters since their similarity (S_G in Table 1) to the training set was evaluated globally (i.e. for all the cases, and not using separate parameters for each case) and is, therefore, estimated that these globally-optimized parameters are optimal for every possible liver that needs to be segmented using our algorithms.

2.2.2. Final validation

After globally optimizing changeable parameters of all three evaluated segmentation algorithms, final validation was performed on additional four cases that were manually

segmented by the radiologist. As opposed to the optimization procedure, the changeable parameters were fixed during validation using values obtained from optimization and previously defined as globally-optimized parameters. Then, segmentation was performed and results were compared (i.e. validation similarity, S_{MN} and S_{MD} in Table 2) to the reference model that was manually segmented by the radiologist in the same manner as when performing optimization.

3. Results

The results of optimization, displayed as similarity to the training set, are shown in Table 1. Both the similarity using case-specific optimal parameters (S_C in Table 1) and using globally-optimized parameters (S_G in Table 1) are presented. The similarity was evaluated using two possible criteria: as the mean (Table 1A) or the median similarity (Table 1B) of all the slices within a case of the training set.

Table 1A. Optimization results of seven cases compared to radiologist data by mean values.

Presented are mean similarities of seven cases segmented using three segmentation algorithms and compared to models that were generated by radiologist manual segmentation. Every similarity (S) is the mean value of similarities from each slice of a case, and was evaluated using individual, case-specific parameters (S_C) or using globally-optimized parameters (S_G). Std stands for standard deviation of similarities of slices within a case.

case number	REGION GROWING				ADAPTIVE THRESHOLD				ACTIVE CONTOURS			
	S_C	std(S_C)	S_G	std(S_G)	S_C	std(S_C)	S_G	std(S_G)	S_C	std(S_C)	S_G	std(S_G)
2009122	91.2	*15.9*	**61.1**	*38.9*	72.2	*39.1*	**72.2**	*39.1*	88.2	*22.1*	**68.8**	*36.3*
2010093	92.7	*13.7*	**86.8**	*19.0*	70.1	*38.1*	**68.1**	*40.2*	89.7	*20.7*	**64.5**	*40.1*
2010122	84.7	*19.6*	**79.9**	*19.2*	73.4	*34.5*	**70.1**	*33.9*	84.6	*22.3*	**78.6**	*23.6*
2011022	81.1	*25.5*	**65.7**	*36.0*	74.0	*29.1*	**73.2**	*29.5*	79.4	*29.1*	**67.2**	*37.1*
2011042	86.6	*19.4*	**78.2**	*29.0*	60.0	*35.6*	**40.1**	*41.6*	64.8	*36.6*	**54.8**	*37.9*
2011062	94.4	*2.1%*	**94.2**	*2.9%*	80.2	*13.4*	**80.2**	*13.4*	87.6	*14.1*	**67.9**	*36.6*
2011070	92.5	*4.9%*	**92.5**	*4.9%*	69.3	*37.8*	**69.3**	*37.8*	80.3	*30.9*	**80.3**	*30.9*
mean			**79.8 %**	*12.7 %*			**67.6 %**	*12.8 %*			**68.8 %**	*8.6%*

Table 1B. Optimization results of seven cases compared to radiologist data by median values.

Presented are median similarities of seven cases segmented using three segmentation algorithms and compared to models that were generated by radiologist manual segmentation. Every similarity (S) is the median value of similarities from each slice of a case, and was evaluated using individual, case-specific parameters (S_C) or using globally-optimized parameters (S_G).

case number	REGION GROWING		ADAPTIVE THRESHOLD		ACTIVE CONTOURS	
	S_C	S_G	S_C	S_G	S_C	S_G
20091223	95.6%	**79.9%**	92.0%	**92.0%**	94.0%	**82.6%**
20100930	95.9%	**91.8%**	88.8%	**90.0%**	95.3%	**82.5%**
20101221	90.3%	**85.6%**	88.6%	**87.8%**	91.0%	**86.9%**
20110228	88.8%	**84.8%**	83.7%	**83.7%**	88.3%	**86.4%**
20110421	92.6%	**89.2%**	73.6%	**55.4%**	80.2%	**75.6%**
20110624	94.4%	**94.4%**	82.7%	**82.7%**	91.2%	**88.9%**
20110707	93.4%	**93.4%**	87.6%	**87.6%**	91.5%	**91.5%**
median		**89.2%**		**87.6%**		**86.4%**

As presented in Table 1A, after being globally optimized (i.e. for all cases) our implementation of region growing algorithm provides mean slice similarities (S_G in Table 1A) from 61.1% to 94.2% with the mean value of 79.8% (standard deviation 12.7%) which classifies the region growing as the most accurate algorithm evaluated based on the mean and also the median values of all the slices' similarities. Based on the data from Table 1B, median slice similarity values for the region growing algorithm vary from 84.8% to 94.4% with the median value of 89.2%, which is the highest among all three evaluated algorithms.

Our implementation of adaptive threshold algorithm provides globally optimized (i.e. for all cases) mean slice similarities (S_G in Table 1A) from 40.1% to 80.2% with the mean value of 67.6% (standard deviation 12.8%) which classifies the adaptive threshold algorithm as the least accurate algorithm evaluated based on the mean values of all the

slices' similarities. Based on the data from Table 1B, median slice similarity values for the adaptive threshold algorithm vary from 55.4% to 92.0% with the median value of 87.6%.

Our implementation of active contours algorithm provides globally optimized (i.e. for all cases) mean slice similarities (S_G in Table 1A) from 54.8% to 80.3% with the mean value of 68.8% (standard deviation 8.6%). Based on the data from Table 1B, median slice similarity values for the active contours algorithm vary from 75.6% to 91.5% with the median value of 86.4%.

The results of validation of the four additional cases manually segmented by the radiologist are shown in Table 2. The similarities are non-optimized: the segmentation results (S_V in Table 2) are validated using globally-optimized parameters (S_G in Table 1) without further modifications of these parameters in order to show functioning of our segmentation algorithms on models which previously were not used as a training set during the optimization procedure.

Table 2. Validation results of four cases compared to radiologist data by mean and median values.

Presented are validation results: mean and median similarities of four cases compared to manually-segmented data from the radiologist. Similarity (S) was evaluated on a slice-by-slice basis using validation-only parameters as mean (S_{MN}) or median (S_{MD}) of all the slices in a case. Std is the standard deviation of mean similarities of slices within a case.

case number	REGION GROWING			ADAPTIVE THRESHOLD			ACTIVE CONTOURS		
	S_{MN}	std(S_{MN})	S_{MD}	S_{MN}	std(S_{MN})	S_{MD}	S_{MN}	std(S_{MN})	S_{MD}
V1	**79.4%**	*24.8%*	**87.0%**	**67.3%**	*30.5%*	**76.4%**	**54.5%**	*43.0%*	**79.5%**
V2	**87.1%**	*18.0%*	**92.5%**	**64.5%**	*35.9%*	**79.0%**	**51.7%**	*42.6%*	**70.2%**
V3	**71.3%**	*33.1%*	**85.5%**	**67.5%**	*30.1%*	**78.0%**	**72.8%**	*28.5%*	**81.9%**
V4	**49.6%**	*38.1%*	**70.5%**	**65.9%**	*35.7%*	**81.9%**	**58.2%**	*43.6%*	**83.7%**
	71.9%	*16.2%*	**86.3%**	**66.3%**	*1.4%*	**78.5%**	**59.3%**	*9.4%*	**80.7%**

As presented in Table 2, the region growing algorithm achieves highest similarities (mean 71.9% with standard deviation 16.2%, or median 86.3%) of the validated models. The

standard deviation between different models segmented using the same algorithm is the smallest (i.e. 1.4%) using the adaptive threshold algorithm. Individual validation similarities (S_V in Table 2) on a slice basis are also presented in Figure 9.

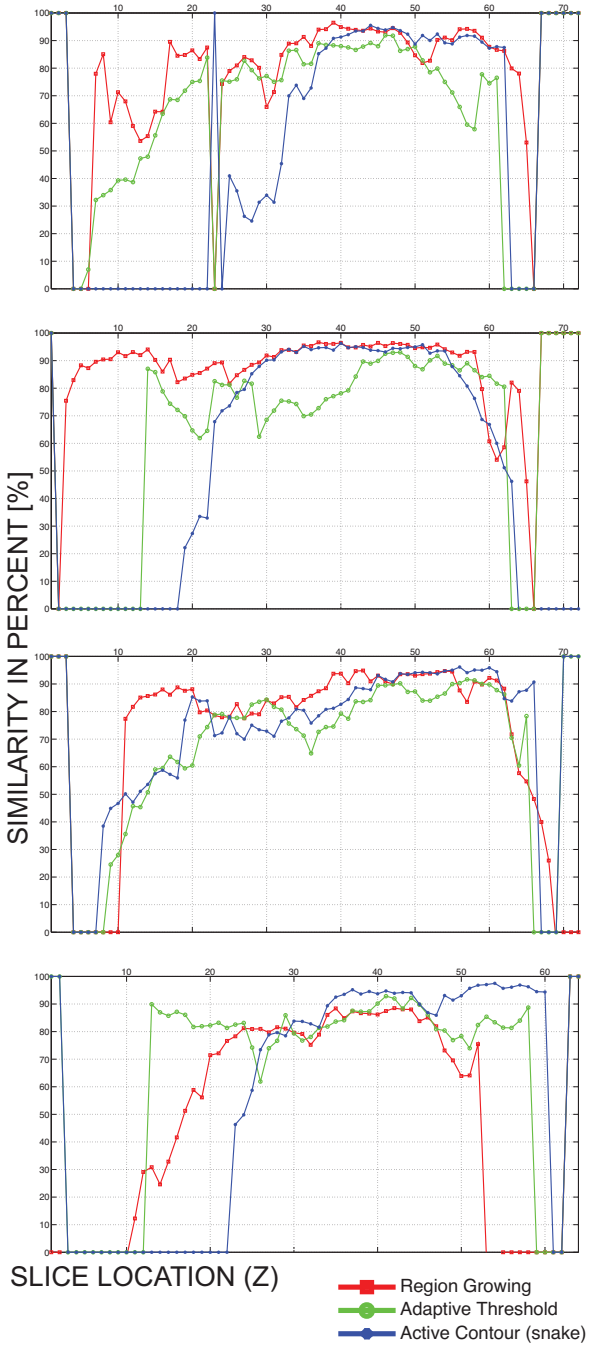

Figure 9. Final validation similarities of four cases (A, B, C, and D).

The similarities presented are on a slice-by-slice basis, i.e. the abscissa represents the location of a slice, while the value of the graphs is the similarity of the slice with the manually validated slice.

Figure 9 shows that although the four validation cases (A, B, C, and D) were not included in the training set, they could be segmented using our implementations of the region growing, adaptive threshold and active contours algorithms.

4. Discussion

The aim of this paper was to present three possible automatic liver segmentation algorithms and perform their evaluation by optimizing their functioning for an accurate liver segmentation; the optimization was based on seven-patients dataset segmented by the radiologist and used as a training set, while validation was performed using additional radiologist dataset consisting of four additional patients. As presented in the Results section, developing an automatic segmentation algorithm that generates accurate three-dimensional liver models is demanding, especially because of the variability of input data (i.e. liver in the patient's medical images). Nevertheless, because the region growing requires the end-user to place an initial seed (i.e. to click on the liver on one image), this segmentation algorithm cannot be classified as a fully-automatic algorithm but rather semi-automatic; however, an algorithm for automatically placing the initial seed could upgrade the region growing algorithm to a fully-automatic algorithm. The initial seed-placing algorithm can be developed based on the adaptive threshold segmentation algorithm (described in 2.1.5.) on the *referential* slice, with an additional task of selecting a pixel with a median intensity of the segment on the *referential* slice which should ensure avoidance to selecting vessels or nodules as the target region.

The liver includes or may include various inner structures (e.g. blood vessels, metastases, hemangioma, etc.) that do not have a predictable intensity range or texture; these structures may directly interfere with segmentation algorithms by possibly influencing the generation of segments. Also, certain organs near the liver (i.e. the spleen, the heart, the kidneys) have similar intensity ranges to the liver (Massoptier and Casciaro, 2008), which results in segmentation leakage for threshold-based segmentation methods (i.e. region growing and adaptive threshold). Moreover, active contours are attracted to edges, including the edges of the inner structures; therefore, straight-forward three-dimensional segmentation of the liver

using active contours would only be possible if the three-dimensional contour (i.e. the deformable surface) was initialized entirely near the edge of the liver. Besides, the soft transitions of the organs from one slice to another often prevent detection of the organ edges, which leads to an insufficient Gradient Vector Flow (GVF) map and consequently corrupting the generated segments of the active contours algorithm. All the identified difficulties demonstrate that accurate automatic liver segmentation is indeed a challenging task. Fortunately, highest accuracy of liver segmentation is not required for electroporation-based treatment planning since tissue of interest for electric field distribution actually represents the tumor tissue, and possibly large blood vessels which must be taken into account because of electric field calculations and electrode placement. The liver tissue, however, is only a medium that surrounds the tissue of interest, i.e. the tumor that resides in the liver, since electroporation-based treatment planning is required for tumor nodules that are inside or on the edge of the liver. Therefore, the main function of the generated three-dimensional liver model besides being the medium surrounding the tissue of interest is to provide instructions to the attending physician on how the electroporation-based treatment will be performed (i.e. where the tumor is located, since it cannot be seen as it is deep-seated), and serves as electrode-insertion approximate offline navigation for the clinician.

Since similarity comparisons using normalized cross-correlation were performed on each slice of a case separately, final results of each case are presented using two representations: the mean similarity of all the slices, and the median similarity of all the slices in a case. Two representations of the data were presented since there are many individual slices with a similarity of 0%, which means whether the radiologist marked a segment on that slice and the segmentation algorithm missegmented it, or vice-versa (i.e. the segmentation algorithm detected a segment that the radiologist did not identify). Hence, such slices significantly contribute to the final results of the comparison regardless of the size of the segment that caused the 0% similarity on the slice (i.e. even a segment of only few pixels detected by the segmentation algorithms and not identified by the radiologist would produce a 0% similarity of its slice). Since such slices significantly impact the quality of the final results, the mean similarity of all the slices in a case does not reflect success of the segmentation

algorithm enough. Therefore, the median similarity of the slices in a case was presented as well.

Optimization results presented in Table 1 show that using case-specific optimization parameters (i.e. parameters optimized for every case separately, S_C in Table 1), very good similarities to the training set can be obtained (median similarities of up to 95.9% using region growing, up to 80.2% using adaptive threshold, and up to 80.3% using active contours). However, results applying to case-specific parameters can only be achieved if a reference model which is part of the training set is available. Therefore, globally-optimized parameters are the parameters that give meaningful information on how accurate a segmentation algorithm is. Our implementation of region growing algorithm could be optimized to achieve an 89.2% median similarity (79.8% mean similarity with 12.7% standard deviation) to the training set, which classifies this algorithm as the most optimization-prone algorithm evaluated. The adaptive threshold algorithm could be optimized to achieve an 87.6% median similarity (67.6% mean similarity with 12.8% standard deviation), and our implementation of the active contours algorithm an 86.4% median similarity (68.8% mean similarity with 8.6% standard deviation), which shows that despite being more sophisticated, these two algorithms achieved lower results than region growing. The main reason is that region growing algorithm can be effectively optimized since the optimizable threshold-deviation parameter majorly influences segmentation (i.e. it significantly influences which voxels will be part of the final tissue segment). The adaptive threshold only has one most relevant parameter that could be optimized (i.e. the initial coefficient that determines the targeted size of the initial segment on the referential slice), which does not influence segmentation on further slices. Although the active contours algorithm includes four optimizable parameters (i.e. the four coefficients that balance energy contributions), it is almost impossible to influence the movement of the active contour (i.e. the snake). Namely, even if the four energy contributions are ideally balanced, the active contour movement needs to mostly rely on the edges in the image (i.e. the two coefficients representing GVF magnitude and directions). Therefore, if the edges of the target tissue were improperly detected after preprocessing (e.g. the target tissue does not

have clearly detectable edges), the movement of the active contour will produce unwanted results.

Results of the final validation that are presented in Table 2 show that new patient images that were not part of the optimization training set can be segmented using our implementations of segmentation algorithms (region growing, adaptive threshold, and active contours). The best results are provided by the region growing algorithm (median similarity 86.3%, mean similarity 71.9% with standard deviation 16.2%), while adaptive threshold (median similarity 78.5%, mean similarity 66.3% with standard deviation 1.4%) and active contours (median similarity 80.7%, mean similarity 59.3% with standard deviation 9.4%) provide lower similarity values. As it can be seen in Figure 9, there were many slices missegmented in all four cases. Most missegmented slices were produced using the active contours algorithm, while the least standard deviation is provided using the adaptive threshold algorithm. Although such missegmented slices would negatively influence not only generation of the liver model, but also detection of the tumors, this drawback is avoided using manual validation by the attending physician, which is discussed in the following paragraph. Finally, although the region growing was expected to be the least sophisticated and accurate algorithm, it proved to be the most robust of all the evaluated algorithms, providing highest accuracy and least missegmented slices.

Tumor detection from the patient's medical images is currently still in development and will be implemented as a semi-automatic procedure: identification of structures within the segmented liver (including its edge area) will be done automatically, but finally the end-user (i.e. the attending physician) will be required to manually determine which identified structures are tumors and are, therefore, subject to electroporation-based treatment. Therefore, the whole liver needs to be properly segmented, since tumors are detected as structures within or on the edge of the liver, and could be missed if some slices at the top or at the bottom of the liver are not segmented. Figure 10 demonstrates possible situations that are related to missegmenting liver segments at the beginning or at the end of the liver: Figure 10A shows an ideal case where all the slices are segmented with a high similarity to the radiologist data; in Figure 10B, there are three slices that do not include liver segments

but should include them (similarity of these slices is zero); Figure 10C shows a bad case where many slices that should include liver segments do not include them. The main reason for missing segments on such slices is intensity inhomogeneity in the Z direction (i.e. not on a single slice but through slices); although the latter is actually corrected when preprocessing the images applying the sigmoid transformation using Volume of Interest (VOI) parameters from the DICOM header, the anomaly is not completely removed, especially in the beginning and in the end of the series. Since this phenomenon cannot therefore be fully avoided, and because there are rare cases that can be automatically segmented as the case from Fig 10A, manual validation of the segmented slices is required at the end of electroporation-based treatment planning procedure. The validation can be combined with the attending physician's manual identification of the structures whether they are tumors or healthy tissue, which reduces the time needed to execute the whole treatment planning procedure. Hence, the attending physician manually validates the segmented images to ensure proper liver and tumor model generation, and manually corrects them if required.

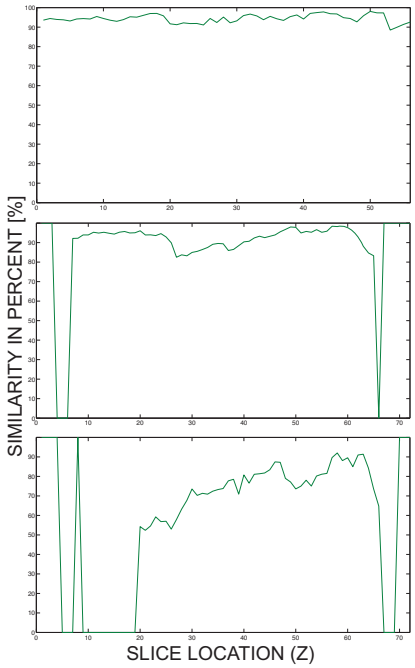

Figure 10. Possible miss situations when segmenting the liver.

Presented are the situations where all the slices are segmented (A), three slices have been missegmented (B) or many slices have been missegmented (C).

Currently, only Magnetic Resonance Imaging (MRI) images are segmented for electroporation-based treatment planning, as MRI is preferred in clinical practice for the liver. Namely, MRI is a non-invasive procedure (i.e. there is no ionizing radiation present during MRI) and using a contrast medium it can provide satisfactory images of the liver for electroporation-based treatment planning. Hence, our algorithms are currently written and optimized only for MRI images; the preprocessing procedures are prepared for expected intensity ranges and Volume-of-Interest (VOI) values that derive from MRI sources, and could therefore not perform segmentation of e.g. Computed Tomography (CT) images. However, since the modality of obtained images can be easily determined from the header of the DICOM files, and because only minor modifications of the preprocessing algorithms would be required, a modification allowing non-MRI image segmentation would not be demanding to implement.

Further steps of our research in the field of electroporation-based treatment planning include improved algorithms for tumor detection and, also, automatic vessel segmentation. Namely, segmentation of tumors and vessels needs to be also developed since algorithms for liver segmentation (i.e. region growing, adaptive threshold, and active contours) cannot be used for this purpose without thorough modifications of the algorithms. We expect to develop vessel segmentation algorithms as a combination of intensity- and morphology-based methods with the aim of extracting line-like structures from the liver.

We plan to develop electroporation-based treatment planning as a web application that will be remotely accessible from a web browser and will allow generating treatment plans by allowing the attending physician to upload the DICOM images of the patient and, after calculations and manual validation of the results, obtaining a directly applicable treatment plan. Hence, besides the automatic liver segmentation, the treatment planning software will also need to include electrode insertion and calculation of the electric field distribution with electrode position optimization in order for the treatment plan to comprise all the required information. The treatment planning procedure will be simplified in order to minimize the input of the clinician: because the segmentation of the tissue is automatic, the clinician will only need to validate the segmentation results (and if required, correct the segmentation by

dragging the produced contours towards desired positions on each slice) and, finally, determine the entry direction of the electrodes. Namely, the electrodes will be automatically inserted towards the gravitational center of the tumor (or tumors), and the required number of electrodes will be proposed by the software based on the shape and size of the tumor (or tumors). Therefore, the clinician will only need to rotate the electrode array towards the excepted intraoperative entry direction, which will simplify the procedure.

Finally, since automatic liver segmentation can be implemented for other applications (Conversano et al., 2011; Crocetti et al., 2008; Massoptier and Casciaro, 2008) beside electroporation-based treatments, we opt towards extending the functioning of our web-based treatment planning software for electroporation-based treatments onto related fields of surgical liver intervention planning.

Acknowledgements

The first author would like to thank prof. dr. Bostjan Likar for extensive discussion on image segmentation and dr. Barbara Mali for the brief discussion on statistical methods.

References

Agerholm-Larsen, B., Iversen, H.K., Ibsen, P., Moller, J.M., Mahmood, F., Jensen, K.S., Gehl, J., 2011. Preclinical Validation of Electrochemotherapy as an Effective Treatment for Brain Tumors. Cancer Research 71, 3753–3762.

Aström, M., Zrinzo, L.U., Tisch, S., Tripoliti, E., Hariz, M.I., Wårdell, K., 2009. Method for patient-specific finite element modeling and simulation of deep brain stimulation. Med Biol Eng Comput 47, 21–28.

Beichel, R., Pock, T., Janko, C., Zotter, R.B., Reitinger, B., Bornik, A., Palagyi, K., Sorantin, E., Werkgartner, G., Bischof, H., Sonka, M., 2004. Liver segment approximation in CT data for surgical resection planning 1435–1446.

Birkfellner, W., 2010. Applied Medical Image Processing: A Basic Course, Har/Com. ed. Taylor & Francis.

Casciaro, S., Franchini, R., Massoptier, L., Casciaro, E., Conversano, F., Malvasi, A., Lay-Ekuakille, A., 2012. Fully Automatic Segmentations of Liver and Hepatic Tumors From 3-D Computed Tomography Abdominal Images: Comparative Evaluation of Two Automatic Methods. IEEE Sensors Journal 12, 464–473.

Chi, Y., Liu, J., Venkatesh, S.K., Huang, S., Zhou, J., Tian, Q., Nowinski, W.L., 2011. Segmentation of Liver Vasculature From Contrast Enhanced CT Images Using Context-Based Voting. IEEE Transactions on Biomedical Engineering 58, 2144 – 2153.

Conversano, F., Franchini, R., Demitri, C., Massoptier, L., Montagna, F., Maffezzoli, A., Malvasi, A., Casciaro, S., 2011. Hepatic Vessel Segmentation for 3D Planning of Liver Surgery: Experimental Evaluation of a New Fully Automatic Algorithm. Academic Radiology 18, 461 – 470.

Crocetti, L., Lencioni, R., DeBeni, S., See, T., Della Pina, C., Bartolozzi, C., 2008. Targeting Liver Lesions for Radipfrequency Ablation - an Experimental Feasibility Study Using a CT-US Fusion Imaging System. Investigative Radiology 33–39.

Čorović, S., Lacković, I., Šuštaršič, P., Šuštar, T., Rodič, T., Miklavčič, D., 2013. Modeling of electric field distribution in tissues during electroporation. BioMedical Engineering Online in press.

Daugimont, L., Baron, N., Vandermeulen, G., Pavselj, N., Miklavcic, D., Jullien, M.-C., Cabodevila, G., Mir, L.M., Préat, V., 2010. Hollow Microneedle Arrays for Intradermal Drug Delivery and DNA Electroporation. J. Membrane Biol. 236, 117–125.

Davalos, R., Rubinsky, B., 2008. Temperature considerations during irreversible electroporation. International Journal of Heat and Mass Transfer 51, 5617–5622.

Davalos R, Mir LM, Rubinsky B (2005) Tissue ablation with irreversible electroporation. Annals of Biomedical Engineering 33: 223-231.

De Pasquale, F., Stander, J., 2009. A Multi-Scale Template Method for Shape Detection with Bio-Medical Applications. Pattern Analysis and Applications 179–192.

Edhemovic, I., Gadzijev, E.M., Brecelj, E., Miklavcic, D., Kos, B., Zupanic, A., Mali, B., Jarm, T., Pavliha, D., Marcan, M., Gasljevic, G., Gorjup, V., Music, M., Vavpotic, T.P., Cemazar, M., Snoj, M., Sersa, G., 2011. Electrochemotherapy: A New Technological Approach in Treatment of Metastases in the Liver. Technol. Cancer Res. Treat 10, 475–485.

Fini, M., Tschon, M., Alberghini, M., Bianchi, G., Mercuri, M., Campanacci, L., Cavani, F., Ronchetti, M., De Terlizzi, F., Cadossi, R., 2011. Cell Electroporation in Bone Tissue, in: Kee, S.T., Gehl, J., Lee, E.W. (Eds.), Clinical Aspects of Electroporation. Springer New York, New York, NY.

Frangi, A., Niessen, W., Vincken, K., Viergever, M., 1998. Multiscale vessel enhancement filtering, in: Wells, W., Colchester, A., Delp, S. (Eds.), Medical Image Computing and Computer-Assisted Intervention, Lecture Notes in Computer Science. Presented at the MICCAI'98, Springer-Verlag, Berlin, Germany, pp. 130–137.

Garcia, P., Pancotto, T., Rossmeisl, J., Henao-Guerrero, N., Gustafson, N., Daniel, G., Robertson, J., Ellis, T., Davalos, R., 2011. Non-Thermal Irreversible Electroporation (N-TIRE) and Adjuvant Fractionated Radiotherapeutic Multimodal Therapy for Intracranial Malignant Glioma in a Canine Patient. Technology in Cancer Research & Treatment 73–83.

Gilbert, R., Jaroszeski, M.J., Heller, R., 1997. Novel electrode designs for electrochemotherapy. Biochimica et Biophysica Acta 1334, 9–14.

Golberg, A., Rubinsky, B., 2012. Towards Electroporation Based Treatment Planning Considering Electric Field Induced Muscle Contractions. Technology in Cancer Research & Treatment 11, 189–201.

Gusbeth, C., Frey, W., Volkmann, H., Schwartz, T., Bluhm, H., 2009. Pulsed Electric Field Treatment for Bacteria Reduction and Its Impact on Hospital Wastewater. Chemosphere 228–233.

Heimann, T., Thorn, M., Kunert, T., Meinzer, H.P., 2004. New methods for leak detection and contour correction in seeded region growing segmentation, in: International Archives of the Photogrammetry, Remote Sensing, Vol. 35. Presented at the ISPRS Congress, Istanbul, Turkey, pp. 317–322.

Heller, L., Heller, R., 2010. Electroporation Gene Therapy Preclinical and Clinical Trials for Melanoma. Current Gene Therapy 10, 312–317.

Heymann, M., Degani, A., 2007. Formal Analysis and Automatic Generation of User Interfaces: Approach, Methodology, and an Algorithm. Human Factors 311–330.

Kapur, J.N., Sahoo, P.K., Wong, A.K.C., 1985. A new method for gray-level picture thresholding using the entropy of the histogram. Computer Vision, Graphics, and Image Processing 29, 140 –.

Kass, M., Witkin, A., Terzopoulos, D., 1987. Snakes - active contour models. Int. J. of Comp. Vis 1, 321–331.

Kos, B., Zupanic, A., Kotnik, T., Snoj, M., Sersa, G., Miklavcic, D., 2010. Robustness of Treatment Planning for Electrochemotherapy of Deep-Seated Tumors. Journal of Membrane Biology 236, 147–153.

Kotnik, T., Bobanovic, F., Miklavcic, D., 1997. Sensitivity of Transmembrane Voltage Induced by Applied Electric Fields - a Theoretical Analysis. Bioelectrochemistry and Bioenergetics 43, 285–291.

Kotnik, T., Pucihar, G., Miklavcic, D., 2010. Induced Transmembrane Voltage and Its Correlation with Electroporation-Mediated Molecular Transport. Journal of Membrane Biology 236, 3–13.

Lecchi, M., Fossati, P., Elisei, F., Orecchia, R., Lucignani, G., 2008. Current Concepts on Imaging in Radiotherapy. European Journal of Nuclear Medicine and Molecular Imaging 35, 821–837.

Linguraru, M.G., Pura, J.A., Pamulapati, V., Summers, R.M., 2012. Statistical 4D graphs for multi-organ abdominal segmentation from multiphase CT. Medical Image Analysis 16, 904–914.

Linnert, M., Iversen, H., Gehl, J., 2012. Multiple brain metastases - current management and perspectives for treatment with electrochemotherapy. Radiology and Oncology 2012, 1–8.

Mahmood, F., Gehl, J., 2011. Optimizing clinical performance and geometrical robustness of a new electrode device for intracranial tumor electroporation. Bioelectrochemistry 81, 10–16.

Mali, B., Jarm, T., Snoj, M., Sersa, G., Miklavcic, D., 2013. Antitumor effectiveness of electrochemotherapy: A systematic review and meta-analysis. European Journal of Surgical Oncology (EJSO) 39, 4 – 16.

Maor, E., Ivorra, A., Rubinsky, B., 2009. Non Thermal Irreversible Electroporation: Novel Technology for Vascular Smooth Muscle Cells Ablation. PLOS One 4.

Marty, M., Sersa, G., Garbay, J., Gehl, J., Collins, C., Snoj, M., Billard, V., Geertsen, P., Larkin, J., Miklavcic, D., Pavlovic, I., Paulin-Kosir, S., Cemazar, M., Morsli, N., Rudolf, Z., Robert, C., O'Sullivan, G., Mir, L., 2006. Electrochemotherapy - an Easy, Highly Effective and Safe Treatment of Cutaneous and Subcutaneous Metastases: Results of ESOPE (European Standard Operating Procedures of Electrochemotherapy) Study. EJC Supplements 4, 3–13.

Massoptier, L., Casciaro, S., 2008. A new fully automatic and robust algorithm for fast segmentation of liver tissue and tumors from CT scans. European Radiology 18, 1658–1665.

Miklavcic, D., 2012. Network for Development of Electroporation-Based Technologies and Treatments: COST TD1104. Journal of Membrane Biology 245, 591–598.

Miklavcic, D., Beravs, K., Semrov, D., Cemazar, M., Demsar, F., Sersa, G., 1998. The Importance of Electric Field Distribution for Effective in Vivo Electroporation of Tissues. Biophysical Journal 2152–2158.

Miklavcic, D., Corovic, S., Pucihar, G., Pavselj, N., 2006. Importance of Tumour Coverage by Sufficiently High Local Electric Field for Effective Electrochemotherapy. EJC Supplements 4, 45–51.

Miklavcic, D., Snoj, M., Zupanic, A., Kos, B., Cemazar, M., Kropivnik, M., Bracko, M., Pecnik, T., Gadzijev, E., Sersa, G., 2010. Towards Treatment Planning and Treatment of Deep-Seated Solid Tumors by Electrochemotherapy. Biomedical Engineering Online 9, -.

Miklavčič, D., Serša, G., Brecelj, E., Gehl, J., Soden, D., Bianchi, G., Ruggieri, P., Rossi, C.R., Campana, L.G., Jarm, T., 2012. Electrochemotherapy: technological advancements for efficient electroporation-based treatment of internal tumors. Medical & Biological Engineering & Computing 50, 1213–1225.

Mir, L., Gehl, J., Sersa, G., Collins, C., Garbay, J., Billard, V., Geertsen, P., Rudolf, Z., O'Sullivan, G., Marty, M., 2006. Standard operating procedures of the electrochemotherapy: Instructions for the use of bleomycin or cisplatin administered either systemically or locally and electric pulses delivered by the Cliniporator (TM) by means of invasive or non-invasive electrodes. EJC Supplements 4, 14–25.

Mir, L.M., Orlowski, S., Belehradek, J., Paoletti, C., 1991. Elecrochemotherapy potentiation of antitumor effect of bleomycin by local electric pulses. European Journal of Cancer 27, 68–72.

National Electrical Manufacturers Association, 2009a. Digital Imaging and Communications in Medicine (DICOM).

National Electrical Manufacturers Association, 2009b. CP-467 addition to DICOM.

Neal, II, R.E., Rossmeisl, Jr., J.H., Garcia, P.A., Lanz, O.I., Henao-Guerrero, N., Davalos, R.V., 2011. Successful Treatment of a Large Soft Tissue Sarcoma With Irreversible Electroporation. Journal of Clinical Oncology 29, E372–E377.

Neumann, E., Schaeferridder, M., Wang, Y., Hofschneider, P., 1982. Gene-Transfer into Mouse Lyoma Cells by Electroporation in High Electric-Fields. EMBO Journal 841–845.

Olsen, D., Bruland, O., Davis, B., 2000. Telemedicine in radiotherapy treatment planning: requirements and applications. Radiotherapy and Oncology 54, 255–259.

Pahr, D., Zysset, P., 2009. From high-resolution CT data to finite element models: development of an integrated modular framework. Comput Methods Biomech Biomed Engin 12, 45–57.

Paulides, M.M., Bakker, J.F., Linthorst, M., Van der Zee, J., Rijnen, Z., Neufeld, E., Pattynama, P.M.T., Jansen, P.P., Levendag, P.C., Van Rhoon, G.C., 2010. The clinical feasibility of deep hyperthermia treatment in the head and neck: new challenges for positioning and temperature measurement. Physics in Medicine and Biology 55, 2465.

Pavliha, D., Kos, B., Županič, A., Marčan, M., Serša, G., Miklavčič, D., 2012. Patient-specific treatment planning of electrochemotherapy: Procedure design and possible pitfalls. Bioelectrochemistry 87, 265–273.

Pavselj, N., Bregar, Z., Cukjati, D., Batiuskaite, D., Mir, L.M., Miklavcic, D., 2005. The Course of Tissue Permeabilization Studied on a Mathematical Model of a Subcutaneous Tumor in Small Animals. IEEE Trans. Biomed. Eng. 52, 1373–1381.

Puc, M., Corovic, S., Flisar, K., Petkovsek, M., Nastran, J., Miklavcic, D., 2004. Techniques of signal generation required for electropermeabilization: Survey of electropermeabilization devices. Bioelectrochemistry 64, 113–124.

Sel, D., Cukjati, D., Batiuskaite, D., Slivnik, T., Mir, L., Miklavcic, D., 2005. Sequential finite element model of tissue electropermeabilization. IEEE Transactions on Biomedical Engineering 52, 816–827.

Sersa, G., Miklavcic, D., Cemazar, M., Rudolf, Z., Pucihar, G., Snoj, M., 2008. Electrochemotherapy in Treatment of Tumours. EJSO 34, 232–240.

Serša, G., Miklavčič, D., 2008. Electrochemotherapy of Tumors. Journal of Visualized Experiments 22.

Toepfl, S., Heinz, V., Knorr, D., 2007. High intensity pulsed electric fields applied for food preservation. Chemical Engineering and Processing 46, 537–546.

Ušaj, M., Trontelj, K., Miklavčič, D., Kandušer, M., 2010. Cell–Cell Electrofusion: Optimization of Electric Field Amplitude and Hypotonic Treatment for Mouse Melanoma (B16-F1) and Chinese Hamster Ovary (CHO) Cells. J. Membrane Biol. 236, 107–116.

Vovk, U., Pernuš, F., Likar, B., 2007. A review of methods for correction of intensity inhomogeneity in MRI. IEEE Transactions on Image Processing 26, 405–421.

Xu, C., Prince, J., 1998. Snakes, shapes, and gradient vector flow. IEEE Trans Imag Proc 7, 359–369.

Zheng, Y., Grossman, M., Awate, S.P., Gee, J.C., 2009. Automatic Correction of Intensity Nonuniformity from Sparseness of Gradient Distribution in Medical Images, in: Proceedings of the 12th International Conference on Medical Image Computing and Computer-Assisted Intervention: Part II, MICCAI '09. Springer-Verlag, Berlin, Heidelberg, pp. 852–859.

Županič, A., Kos, B., Miklavčič, D., 2012. Treatment planning of electroporation-based medical interventions: electrochemotherapy, gene electrotransfer and irreversible electroporation. Physics in Medicine and Biology 57, 5425–5440.

Županič, A., Čorović, S., Miklavčič, D., 2008. Optimization of Electrode Position and Electric Pulse Amplitude in Electrochemotherapy. Radiology and Oncology 42, 93–101.

Županič, A., Miklavčič, D., 2009. Optimization and Numerical Modeling in Irreversible Electroporation Treatment Planning, in: Irreversible Electroporation. Springer, Berlin, pp. 203–222.

Županič, A., Miklavčič, D., 2011. Tissue heating during tumor ablation with irreversible electroporation. Electrotechnical Review 2011, 42–47.

ARTICLE 3

Title: Planning of electroporation-based treatments using web-based treatment planning software

Authors: PAVLIHA Denis, KOS Bor, MARČAN Marija, ŽUPANIČ Anže, SERŠA Gregor, MIKLAVČIČ Damijan

Publication: Journal of Membrane Biology

DOI: Under review; the paper was submitted on January 10th, 2013.

Year: /

Volume: /

Number: /

Pages: /

Impact factor: 1.808

Ranking:

Category name	Total journals in category	Journal rank in category	Quartile in category
biochemistry & molecular biology	290	211	Q3
cell biology	181	140	Q4
physiology	79	51	Q3

Planning of electroporation-based treatments using web-based treatment planning software

Denis Pavliha[1], Bor Kos[1], Marija Marčan[1], Anže Županič[1], Gregor Serša[2], Damijan Miklavčič[1]

[1] University of Ljubljana, Faculty of Electrical Engineering, Tržaška c. 25, SI-1000 Ljubljana, Slo.

[2] Institute of Oncology Ljubljana, Zaloška c. 2, SI-1000 Ljubljana, Slovenia

Abstract

Electroporation-based treatment combining high voltage electric pulses and poorly permanent cytotoxic drugs, i.e. electrochemotherapy (ECT), is currently used for treating superficial tumor nodules by following standard operating procedures. Besides ECT, another electroporation-based treatment termed non-thermal irreversible electroporation (N-TIRE) is also efficient in treating deep-seated tumors. To perform ECT or N-TIRE of deep-seated tumors, following standard operating procedures is not sufficient and patient-specific treatment planning is required for a successful treatment. Treatment planning is required because of the use of individual long needle electrodes and due to diverse shape, size and location of deep-seated tumors. Many institutions that already perform ECT of superficial metastases could benefit from treatment planning software that would enable the preparation of patient-specific treatment plans. To this end, we have developed a web-based treatment planning software for planning electroporation-based treatments that does not require prior engineering knowledge from the user (e.g. the clinician). The software includes algorithms for automatic tissue segmentation and, after segmentation the generation of the 3D model of the tissue. The procedure allows the user to define how the electrodes will be inserted. Finally, electric field distribution is computed and position of electrodes and voltage to be applied are optimized using the 3D model, and a downloadable treatment plan is made available to the user.

1. Introduction

Electroporation is the phenomenon that occurs when a cell is exposed to a sufficiently high external electric field (Kotnik et al. 2012). During and after exposure, the plasma membrane is transiently permeabilized, thus allowing the material from outside to enter the cell, which would be otherwise impeded (Kotnik et al. 1997). The phenomenon is considered to be a universal method and platform technology because all types of cells (animal, plant, and microorganisms) are affected by electroporation (Miklavcic 2012). In fact, many electroporation-based applications have already been identified and developed, such as electrochemotherapy of tumors (Serša and Miklavčič 2008), non-thermal irreversible ablation of tumors (Garcia et al. 2011; Maor et al. 2009), gene therapy (Heller and Heller 2010), food preservation (Toepfl et al. 2007), and others (Daugimont et al. 2010; Gusbeth et al. 2009; Ušaj et al. 2010).

Electrochemotherapy (ECT), which is currently most developed electroporation-based therapy (Mali et al. 2013; Sersa et al. 2008), improves chemotherapy outcome by increasing the plasma membrane permeability to cytotoxic drugs with exposure of target cells (i.e. tumor) to a high-strength electric field (Serša and Miklavčič 2008) The electric field is caused by high-voltage electric pulses that are delivered to the target tissue (i.e. tumor) using electrodes (Mir et al. 1991). ECT is already used in clinical practice for treating metastases of skin melanoma in more than 100 clinical institutions in Europe (Miklavčič et al. 2012), and has already been introduced to clinical trials for treating deep-seated metastases in liver (Edhemovic et al. 2011), brain (Agerholm-Larsen et al. 2011; Linnert et al. 2012; Mahmood and Gehl 2011), bone (Fini et al. 2011), and soft tissue (Neal, II et al. 2011). While following standard operating procedures (Mir et al. 2006) ensures safe and successful treatment of skin melanoma metastases (Marty et al. 2006), patient-specific treatment planning is nevertheless required for ECT of deep-seated tumors (Pavliha et al. 2012). Namely, deep-seated tumors are very diverse in shape, size and location in the body, and because of the use of long needle electrodes for treating such tumors, coverage of the whole target tissue (i.e. tumor) with a sufficiently high electric field (which is a prerequisite for successful ECT) (Miklavcic et al. 2006; Miklavcic et al. 1998)

can currently only be assured by means of numerical modeling of electric field distribution based on representative input data is performed and image guided insertion of electrodes is used (Kos et al. 2010; Miklavcic et al. 2010).

Similarly to ECT, Non-Thermal Irreversible Electroporation (N-TIRE) is another electroporation-based application that is used for ablation of pathological tissue (i.e. tumor) using electrodes (Davalos and Rubinsky 2008; Garcia et al. 2011; Županič and Miklavčič 2009). N-TIRE performs tissue ablation using electric field strengths above values used for electrochemotherapy and/or with a greater number of electric pulses and, therefore, destroys target tissue without the use of chemotherapeutic drug or heat (Davalos and Rubinsky 2008). N-TIRE has been in use for treating e.g. brain metastases (Garcia et al. 2011) or soft-tissue sarcoma (Neal, II et al. 2011) and would also benefit from patient-specific treatment planning (Golberg and Rubinsky 2012).Although N-TIRE is very similar to ECT, it also requires calculations of temperature increase to be included in treatment planning procedure (Županič and Miklavčič 2011).

Patient-specific treatment planning of electroporation-based treatments such as ECT and N-TIRE is based on medical images of the patient which are used to generate a three-dimensional model of the target tissue (i.e. tumor) and the organ surrounding the target tissue (Pavliha et al. 2012). Then, the three-dimensional model is used for calculation of the electric field distribution during the electroporation-based treatment (Zupanic et al. 2012). Since the standard for medical imaging transfer and storage, i.e. Digital Imaging and Communications in Medicine (DICOM) (National Electrical Manufacturers Association 2009) represents a common format for storage and transfer of medical images, the images can be transferred over the internet and, due to the standard format, the receiver will be able to display them properly. This facilitates treatment planning by developing treatment planning software as a web application, which allows remote generation of treatment plans (Olsen et al. 2000). Moreover, the treatment planning software should be as automated as possible, since without treatment planning software a clinician (i.e. a medical doctor – MD) may otherwise need about six hours to manually perform segmentation of a patient

(Paulides et al. 2010).The advance from treating skin metastases to treating deep-seated tumors would be facilitated by user-friendly treatment planning software that would allow clinicians to prepare patient-specific treatment plans without the need of an engineer or a medical physicist or specialized engineering knowledge (Pavliha et al. 2012). In our present paper, we describe implementation of treatment planning tool including developed methods for image segmentation, model building and determination of electroporation as a web-based application for treatment planning of electroporation-based therapies such as electrochemotherapy and non-thermal irreversible electroporation.

2. Materials and Methods

2.1. Web-based Graphical User Interface (GUI)

The functioning of the web-based treatment planning software for electroporation-based treatments is presented in Figure 1.

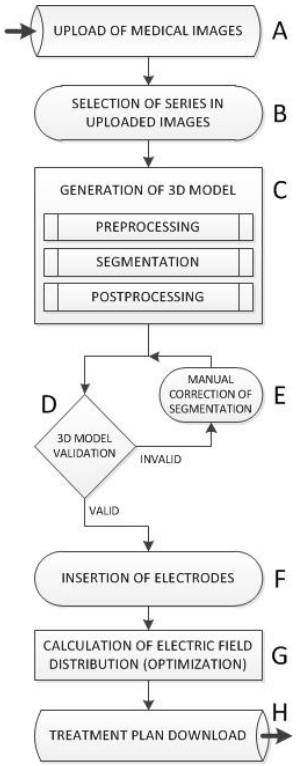

Figure 1: Flow diagram of web-based treatment planning for electroporation-based treatments.

The treatment planning procedure consists of the following subprocedures: upload of medical images (Figure 1a), selection of series used for planning (Figure 1b), generation of 3D model (which is done by preprocessing, segmentation, and postprocessing of the images – Figure 1c), 3D model validation (Figure 1d), manual correction of segmentation (if decided by the user that it is required – Figure 1e), virtual insertion of electrodes into the model (Figure 1f), calculation of electric field distribution (with optimization of parameters: voltages and electrode positions – Figure 1g), and download of the treatment plan (Figure 1h). In case the images have been previously segmented (Figure 1i), steps (c, d, and e) are not executed and pregenerated segments are loaded instead.

In order to develop easy-to-use treatment planning software, user interaction (i.e. the number of parameters, events, or actions the user needs to execute or monitor) should be minimal (Heymann and Degani 2007). Therefore, the most demanding subprocedures (i.e. generation of the 3D model and calculation of the electric field distribution on Figures 1c and 1g, respectively) are developed so that they do not require any user interaction. Namely, the subprocedures of 3D model generation and electric field distribution calculation require engineering knowledge, such as medical image processing (Birkfellner 2010) and numerical modeling based on the finite element method (FEM) in order to perform them. Since users of web-based treatment planning software for electroporation-based treatments are expected to be clinicians, all subprocedures are presented in a non-engineering way, so that users are able to generate treatment plans effortlessly.

First, the user is required to upload the medical images of the patient (Figure 1a) by selecting the DICOM files that contain image slices of the body area with the target tissue (i.e. one or more metastases). After uploading the medical images, treatment planning software automatically examines them by reading metadata of the DICOM files (i.e. the DICOM header). Parameters *SeriesNumber*, *SeriesDescription* and *SliceLocation* are read from the header and, then, the images are grouped by the series they belong to (i.e. *SeriesNumber* parameter) and labeled using the original series name (i.e. *SeriesDescription* parameter). Within each group, the images are sorted according to their spatial location (i.e. according to their Z-index, i.e. *SliceLocation* parameter). Afterwards, one median image

from each group (i.e. each detected series) is presented to the user who, finally, by clicking on the corresponding series' image selects which series will be used for planning the electroporation-based treatment (Figure 1b).

2.2. Automatic segmentation of medical images

Web-based treatment planning for electroporation-based treatments is based on algorithms for automatic segmentation of medical images (Figure 1c). First, the selected series (Figure 1b) of the uploaded medical images (Figure 1a) is preprocessed; all the images (slices) are first transformed using a sigmoid function, described in Equation 1.

$$output = \frac{output\_range}{1 + e^{-4 \cdot \frac{input - WC}{WW}}} \quad \text{(Eq.1)}$$

Parameters Window Center (WC) and Window Width (WW) are part of the Volume-of-Interest (VOI) metadata located in the DICOM header of each image. The *output_range* parameter defines the maximum value of the preprocessed image. Parameters *input* and *output* are the source and preprocessed data, respectively. All the parameters' values are *bits*. After transforming each slice using the transformation from Eq. 1, the slices are de-biased using a publicly available inhomogeneity correction algorithm (Zheng et al. 2009). Then, each slice is filtered using an average and a Gaussian blur filter (σ= 3), both with window sizes of 3x3 pixels. Finally, a fixed-value sigmoid transformation (*WC=20000, WW=100, output_range=*2^{16}) is applied to each slice in order to ensure appropriate intensity distribution which is necessary for segmentation; fixed values were defined empirically using real-case data.

After preprocessing, image segmentation is performed. Currently, three possible liver segmentation methods are implemented: region growing, adaptive threshold, and active contours (i.e. snakes) algorithms. Region growing is a semi-automatic algorithm (because it requires the user to place an initial seed, i.e. to click on the liver on a single slice) while adaptive threshold and active contours are automatic algorithms that generate 3D liver models without user interaction. Three liver segmentation algorithms have been implemented because different segmentation algorithms provide different results (De Pasquale and Stander 2009) and user requirements on how the 3D model is constructed may vary. After the liver is segmented, segmentation of tumors and vessels is executed.

Algorithms for segmentation of tumors and vessels combine intensity-based and morphological characteristics of given objects to identify them in source images. The basis of the algorithms is a multi-scale filter, described in (Frangi et al. 1998) which detects local second-order structures based on relationship between their eigenvalues. The filter distinguishes between linear (or cylindrical in 3D) and round (or spherical in 3D) structures, which can be used for detection of vessels and tumors, respectively. Results of filtering are two image layers: the first includes enhanced tumors while the other includes enhanced vessel structures. After filtering, the resulting enhanced image layers of tumors and vessels are thresholded using a method based on maximization of entropy (Kapur et al. 1985).

Additionally, region growing is performed in 3D based on thresholding results in order to collect neighboring voxels with intensity values within and below the threshold, as these voxels are also part of the segmented structure (Beichel et al. 2004). Region growing is performed iteratively with lowering of the threshold by factor 0.001 in each step. The procedure stops once no new voxels have been added in an iteration step. Segmentation of tumors and vessels is performed based on segmentation of the organ that includes them (i.e. the liver) since the segmented target organ is used as a mask for tumor and vessel segmentation. Therefore, the tumors are detected if they are in or on the boundary of the organ.

When the segmentation is finished, the user has to validate the generated 3D model (Figure 1d): segmented layers with the liver, tumor and vessels are presented and manual correction of the generated segments is possible for each slice by dragging the overlaid contours of the generated segments to desired positions (Figure 1e). In the final stage, the electrodes are inserted into the 3D model (Figure 1f). For each identified tumor, a selection of basic electrodes' configurations is presented to the user. The electrodes are positioned relative to the center of gravity of the tumor at appropriate depth (Kos et al. 2010) and are parallel to each other. Depending on the planned direction of access, the user can change the direction of insertion of the electrode array, number of electrodes, rotation of the outer electrodes with respect to the electrodes inserted in the tumors, the distance between electrodes, as

well as basic electrode configuration and number of electrodes. When initial positions of all electrode arrays are defined, electric field distribution calculation and optimization of electrode voltage and position is performed.

2.3. Electric field distribution calculation and optimization

The electric field distribution is the most important predictor of electroporation (Miklavcic et al. 2006; Miklavcic et al. 1998). The electric field distribution can be determined by solving the Laplace equation for electric potential (V) in the static case, described in Equation 2.

$$-\nabla \cdot (\sigma \cdot \nabla V) = 0 \qquad \text{(Eq. 2)}$$

Comsol Multiphysics (Comsol AB, Stockholm, Sweden) is used with the connection to Matlab (Mathworks, Nantick, MA, USA) to automatically build the patient-specific model by using the segmented images for setting location-specific electric properties (Aström et al. 2009), including the electrodes, and solving the electric field distribution. Briefly, the automatic process (Figure 1g) proceeds as follows: the conductivity of the region of interest is set as a location-based function. The electrodes are then inserted as conductive cylinders of appropriate dimensions (Figure 1f) and boundary conditions are set. When electrodes are active (i.e. potential is present on them) they are considered as fixed potential, while the non-active electrodes are left floating with an undefined potential. The simulations are run with a sequential algorithm for increasing conductivities during pulse application (Pavselj et al. 2005; Sel et al. 2005). The electric field and current density are extracted in the next step and the simulations are repeated for all the electrode pairs. The postprocessing of the computed electric fields and currents is handled by Matlab using built-in Comsol functions for extracting the electric fields and integrating the current density. The Matlab-Comsol integration provides easy coupling with optimization algorithms, which have access to the output of the models, as well as the ability to subsequently modify electrode positions and applied voltages (Zupanic et al. 2012; Županič et al. 2008). Finally, the results of treatment planning can be downloaded as a Portable Document Format (PDF) file (Figure 1h).

3. Results and Discussion

Treatment planning software for electroporation-based treatments is developed as a web application. The front-end uses Hyper-Text Markup Language 5 (HTML5) and JavaScript (JS) for content generation and user interaction, while the back-end is a Matlab (Mathworks, Nantick, MA, USA) application invoked by the front-end using *Asynchronous JS and XML* (AJAX) and *PHP Hyper-Text Preprocessor* (The PHP Group, 2001-2012). Three-dimensional visualization is performed using *X Toolkit* (XTK, The X Toolkit Developers, 2012) which is a *Web Graphics Library* (WebGL) based toolkit for scientific visualization. The graphical user interface (GUI) of the treatment planning software for electroporation-based treatments is presented in Figure 2, where three example screens are shown: the initial screen (Figure 2a), the interface for series selection (Figure 2b, procedure from Figure 1b), and an example generated 3D model of the liver with vessels and an identified tumor (Figure 2c).

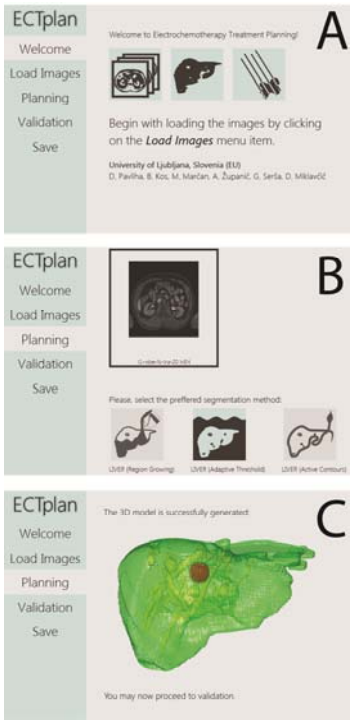

Figure 2: Graphical User Interface (GUI) of the web-based treatment planning software for electroporation-based treatments. Presented are three example screens: initial screen (A), interface for series selection (B), and an example generated 3D model of liver with a tumor and major vessels (C).

While the GUI is rendered at the client-side (i.e. in the user's web browser), all the processing that involves 3D model generation (Figure 1c) and electric field distribution calculations (Figure 1f) is executed on the treatment planning server and, therefore, the user's computer is not loaded by the functioning of the treatment planning software.

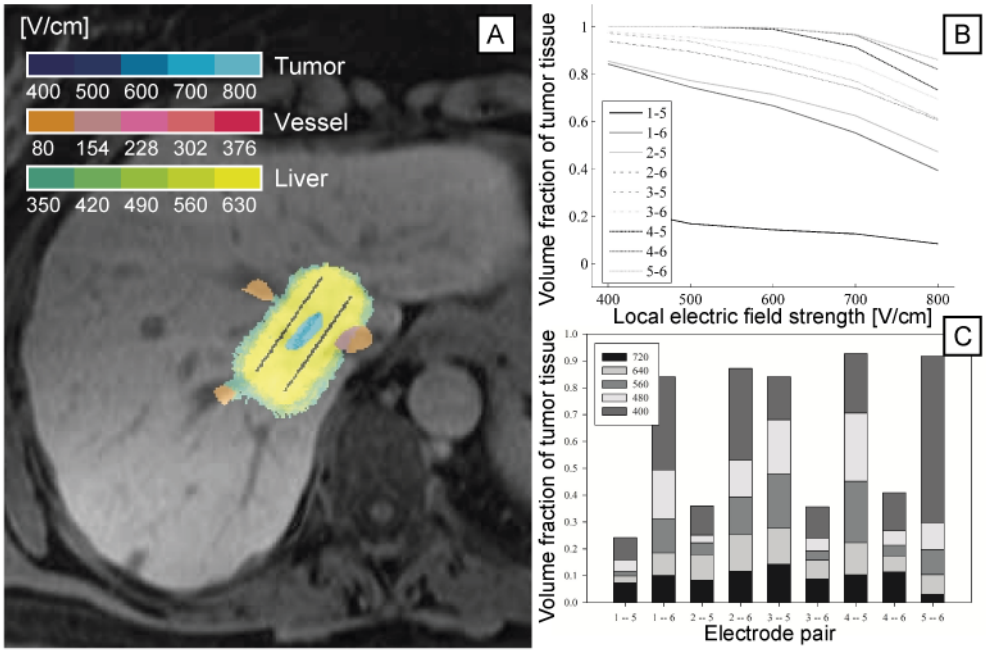

Figure 3: Example of generated treatment plan, showing electroporation cross section overlaid with the original patient image (A), cumulative coverage curves showing the volume fraction of tumor treated above a certain electric field (B) and electrode pair contributions indicating contribution of each individual electrode pair (C).

In this paper, we presented the possibility of generating treatment plans for electroporation-based treatments remotely (Olsen et al. 2000), i.e. using web-based treatment planning software, and without prior engineering knowledge or help of an engineer. The software is based on algorithms for automatic segmentation; currently, three different algorithms for liver segmentation are implemented. Because the software is developed as modular, future inclusion of additional segmentation modules is possible with instantaneous deployment. Namely, the developed software provides a modular framework that allows inclusion of

additional segmentation algorithms; therefore, modules for segmentation of other tissue (e.g. bone, soft-tissue sarcoma, etc.) may be additionally included in the web application. Computation of electric fields in additional tissues is also possible, since segmented images are used as postprocessing and electric property masks in the simulation step. The only possible limitation is the availability of data on electrical properties of tissues and data on changes of electric conductivity during pulse application which however can be obtained through iterative procedure (i.e. modeling and measurements) or by inverse analysis (Čorović et al. 2013).

The presented software allows loading cases that were previously segmented (Figure 1i) which is important for historical evaluation of patients that were already treated. The possibility of loading presegmented cases brings two major benefits: 1. the clinicians can perform historical evaluation of cases that were previously treated with ECT or N-TIRE and evaluate if there is correlation between the calculated coverage of the tumor with the electric field, and 2. the software is able to perform calculations of the electroporation-based treatment regardless of the tissue/organ that is subject to treatment provided that segmentation data is available. If the segmentation is performed by radiologists, the presented treatment planning software allows calculations and optimization of the electric field distribution in the segmented tissue/organ. In Figure 4, an example of model geometry representing the prostate is shown. The model was previously segmented by a radiologist; then, segments were imported into the treatment planning software and, finally, a treatment plan for N-TIRE was calculated.

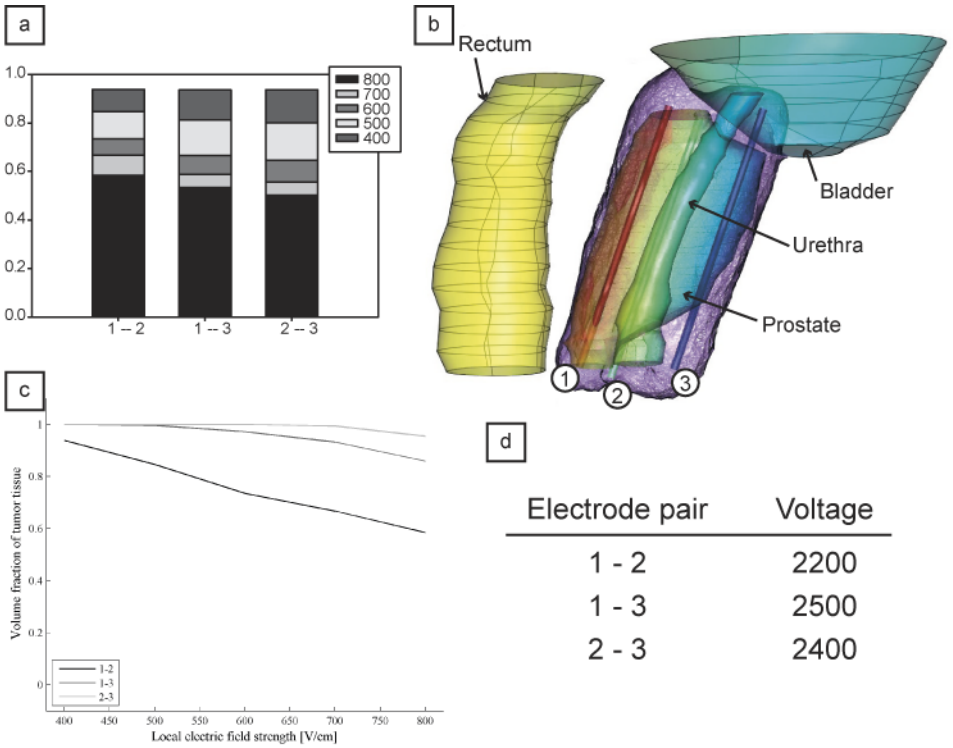

Figure 4: Excerpt from a prepared treatment plan for N-TIRE of prostate cancer. A) Electrode pair contribution, b) model with three needle electrodes, c) cumulative coverage curves showing that the whole tumor is covered with fields in excess of 700 V/cm and over 95 % of tumor is covered with fields in excess of 800 V/cm, d) voltages used in the proposed treatment plan

Algorithms for segmentation of tumor and vessel structures need to be robust, especially with respect to different imaging modalities of source images. Based on our experience with real case data, MRI images may include representations of tumors and vessels with very similar intensities. Therefore, intensity-based segmentation methods such as thresholding cannot successfully separate tumors from vessels in MRI images. This hinder can be overcome by incorporating structural information into the segmentation algorithm: by observing the structures in three dimensions through all slices, it is possible to separate blob-like structures which might be tumors from line structures which are typical for vessels. After the execution of the segmentation algorithm which detects blobs, an additional step is required to define whether the identified structures are tumors or healthy tissue. Such verification is performed in the validation step (Figure 1d), where segmentation of all the tissues is manually validated by the user who has the possibility of

accepting the segmentation results or correcting them manually (i.e. each slice) before continuing with virtual electrode insertion.

Finally, the results of treatment planning that are produced by electric field distribution optimization need to be presented in understandable and human-readable form. We have previously developed several novel visualization methods, allowing the visualization of the contribution of each electrode pair towards the total treatment and the visualization of coverage of tissues above a certain electric field (as well as visualization of predicted electroporation) overlaid on the original medical images. In the future, the treatment plan can be transferred directly to electroporation devices (e.g. electroporators or devices for robots-assisted surgery), which will facilitate electroporation-based treatments even more.

Optimization of the electric field distribution is performed using a custom written genetic algorithm, with the entry direction of electrodes specified as an input parameter. The relative electrode positions are optimized, along with the applied voltages (Županič et al. 2008). The constraints of the electric pulse generator (electroporator) are also taken into account. The resulting treatment plans have also been evaluated for robustness to variations in electrode positions and voltages (Kos et al. 2010). The computation of temperature rise can also be included if treatment plans for N-TIRE are desired (Županič and Miklavčič 2011).

Conclusion

Because a well-defined target (i.e. tumor or other pathological tissue) needs to be determined when planning electroporation-based treatments (such as ECT or N-TIRE) of deep-seated tumors (Pavliha et al. 2012), and distribution of the electric field in biological tissue is the most important predictor of electroporation (Miklavcic et al. 2006; Miklavcic et al. 1998), clinicians and eventually patients can greatly benefit from the web-based treatment planning software we developed. Namely, the software allows generation of electroporation-based treatment plans without prior engineering knowledge and generates 3D models based on patient images that are used for calculation and optimization of the electric field distribution during electroporation. Moreover, it is possible to import previously segmented cases, which allows historical evaluation of patients that were already treated as well as preparation of treatment plans for tissue types which are currently not

supported by the automatic segmentation algorithms but could also benefit from web-based treatment planning. Finally, the treatment plan is presented in a clearly understandable human readable form. Therefore, the web-based treatment planning software could contribute to faster advance of clinicians already practicing electroporation-based treatments of superficial tumor nodules towards treating deep-seated tumors, such as bone metastasis and soft-tissue sarcoma (Miklavčič et al. 2012)

Acknowledgments

This work was supported by the Slovenian Research Agency (ARRS). Research was conducted in the scope of the Electroporation in Biology and Medicine (EBAM) European Associated Laboratory (LEA). The authors thank dr. Robert Hudej from the Institute of Oncology, Ljubljana, for providing data that was used for preparing the treatment plan for N-TIRE of prostate cancer.

References

Agerholm-Larsen B, Iversen HK, Ibsen P, et al. (2011) Preclinical Validation of Electrochemotherapy as an Effective Treatment for Brain Tumors. Cancer Research 71:3753–3762. doi: 10.1158/0008-5472.CAN-11-0451

Aström M, Zrinzo LU, Tisch S, et al. (2009) Method for patient-specific finite element modeling and simulation of deep brain stimulation. Med Biol Eng Comput 47:21–28. doi: 10.1007/s11517-008-0411-2

Beichel R, Pock T, Janko C, et al. (2004) Liver segment approximation in CT data for surgical resection planning. 1435–1446. doi: 10.1117/12.535514

Birkfellner W (2010) Applied Medical Image Processing: A Basic Course, Har/Com. Taylor & Francis

Čorović S, Lacković I, Šuštaršič P, et al. (2013) Modeling of electric field distribution in tissues during electroporation. BioMedical Engineering Online in press.

Daugimont L, Baron N, Vandermeulen G, et al. (2010) Hollow Microneedle Arrays for Intradermal Drug Delivery and DNA Electroporation. J Membrane Biol 236:117–125. doi: 10.1007/s00232-010-9283-0

Davalos R, Rubinsky B (2008) Temperature considerations during irreversible electroporation. International Journal of Heat and Mass Transfer 51:5617–5622. doi: 10.1016/j.ijheatmasstransfer.2008.04.046

Edhemovic I, Gadzijev EM, Brecelj E, et al. (2011) Electrochemotherapy: A New Technological Approach in Treatment of Metastases in the Liver. Technol Cancer Res Treat 10:475–485.

Fini M, Tschon M, Alberghini M, et al. (2011) Cell Electroporation in Bone Tissue. Clinical Aspects of Electroporation

Frangi A, Niessen W, Vincken K, Viergever M (1998) Multiscale vessel enhancement filtering. In: Wells W, Colchester A, Delp S (eds) Medical Image Computing and Computer-Assisted Intervention. Springer-Verlag, Berlin, Germany, pp 130–137

Garcia P, Pancotto T, Rossmeisl J, et al. (2011) Non-Thermal Irreversible Electroporation (N-TIRE) and Adjuvant Fractionated Radiotherapeutic Multimodal Therapy for Intracranial Malignant Glioma in a Canine Patient. Technology in Cancer Research & Treatment 73–83.

Golberg A, Rubinsky B (2012) Towards Electroporation Based Treatment Planning Considering Electric Field Induced Muscle Contractions. Technology in Cancer Research & Treatment 11:189–201.

Gusbeth C, Frey W, Volkmann H, et al. (2009) Pulsed Electric Field Treatment for Bacteria Reduction and Its Impact on Hospital Wastewater. Chemosphere 228–233.

Heller L, Heller R (2010) Electroporation Gene Therapy Preclinical and Clinical Trials for Melanoma. Current Gene Therapy 10:312–317.

Heymann M, Degani A (2007) Formal Analysis and Automatic Generation of User Interfaces: Approach, Methodology, and an Algorithm. Human Factors 311–330.

Kapur JN, Sahoo PK, Wong AKC (1985) A new method for gray-level picture thresholding using the entropy of the histogram. Computer Vision, Graphics, and Image Processing 29:140 –. doi: 10.1016/S0734-189X(85)90156-2

Kos B, Zupanic A, Kotnik T, et al. (2010) Robustness of Treatment Planning for Electrochemotherapy of Deep-Seated Tumors. Journal of Membrane Biology 236:147–153. doi: 10.1007/s00232-010-9274-1

Kotnik T, Bobanovic F, Miklavcic D (1997) Sensitivity of Transmembrane Voltage Induced by Applied Electric Fields - a Theoretical Analysis. Bioelectrochemistry and Bioenergetics 43:285–291.

Kotnik T, Kramar P, Pucihar G, et al. (2012) Cell membrane electroporation- Part 1: The phenomenon. IEEE Electrical Insulation Magazine 28:14 –23. doi: 10.1109/MEI.2012.6268438

Linnert M, Iversen H, Gehl J (2012) Multiple brain metastases - current management and perspectives for treatment with electrochemotherapy. Radiology and Oncology 2012:1–8. doi: 10.2478/v10019-012-0042-y

Mahmood F, Gehl J (2011) Optimizing clinical performance and geometrical robustness of a new electrode device for intracranial tumor electroporation. Bioelectrochemistry 81:10–16. doi: 10.1016/j.bioelechem.2010.12.002

Mali B, Jarm T, Snoj M, et al. (2013) Antitumor effectiveness of electrochemotherapy: A systematic review and meta-analysis. European Journal of Surgical Oncology (EJSO) 39:4 – 16. doi: 10.1016/j.ejso.2012.08.016

Maor E, Ivorra A, Rubinsky B (2009) Non Thermal Irreversible Electroporation: Novel Technology for Vascular Smooth Muscle Cells Ablation. PLOS One. doi: 10.1371/journal.pone.0004757

Marty M, Sersa G, Garbay J, et al. (2006) Electrochemotherapy - An easy, highly effective and safe treatment of cutaneous and subcutaneous metastases: Results of ESOPE (European Standard Operating Procedures of Electrochemotherapy) study. Eur J Cancer Suppl 4:3–13. doi: 10.1016/j.ejcsup.2006.08.002

Miklavcic D (2012) Network for Development of Electroporation-Based Technologies and Treatments: COST TD1104. Journal of Membrane Biology 245:591–598. doi: 10.1007/s00232-012-9493-8

Miklavcic D, Beravs K, Semrov D, et al. (1998) The Importance of Electric Field Distribution for Effective in Vivo Electroporation of Tissues. Biophysical Journal 2152–2158.

Miklavcic D, Corovic S, Pucihar G, Pavselj N (2006) Importance of Tumour Coverage by Sufficiently High Local Electric Field for Effective Electrochemotherapy. EJC Supplements 4:45–51.

Miklavcic D, Snoj M, Zupanic A, et al. (2010) Towards Treatment Planning and Treatment of Deep-Seated Solid Tumors by Electrochemotherapy. Biomedical Engineering Online 9:-.

Miklavčič D, Serša G, Brecelj E, et al. (2012) Electrochemotherapy: technological advancements for efficient electroporation-based treatment of internal tumors. Medical & Biological Engineering & Computing 50:1213–1225. doi: 10.1007/s11517-012-0991-8

Mir L, Gehl J, Sersa G, et al. (2006) Standard operating procedures of the electrochemotherapy: Instructions for the use of bleomycin or cisplatin administered either systemically or locally and electric pulses delivered by the Cliniporator (TM) by means of invasive or non-invasive electrodes. EJC Supplements 4:14–25. doi: 10.1016/j.ejcsup.2006.08.003

Mir LM, Orlowski S, Belehradek J, Paoletti C (1991) Elecrochemotherapy potentiation of antitumor effect of bleomycin by local electric pulses. European Journal of Cancer 27:68–72.

National Electrical Manufacturers Association (2009) Digital Imaging and Communications in Medicine (DICOM).

Neal, II RE, Rossmeisl, Jr. JH, Garcia PA, et al. (2011) Successful Treatment of a Large Soft Tissue Sarcoma With Irreversible Electroporation. Journal of Clinical Oncology 29:E372–E377. doi: 10.1200/JCO.2010.33.0902

Olsen D, Bruland O, Davis B (2000) Telemedicine in radiotherapy treatment planning: requirements and applications. Radiotherapy and Oncology 54:255–259. doi: 10.1016/S0167-8140(99)00185-1

De Pasquale F, Stander J (2009) A Multi-Scale Template Method for Shape Detection with Bio-Medical Applications. Pattern Analysis and Applications 179–192.

Paulides MM, Bakker JF, Linthorst M, et al. (2010) The clinical feasibility of deep hyperthermia treatment in the head and neck: new challenges for positioning and temperature measurement. Physics in Medicine and Biology 55:2465.

Pavliha D, Kos B, Županič A, et al. (2012) Patient-specific treatment planning of electrochemotherapy: Procedure design and possible pitfalls. Bioelectrochemistry 87:265–273.

Pavselj N, Bregar Z, Cukjati D, et al. (2005) The Course of Tissue Permeabilization Studied on a Mathematical Model of a Subcutaneous Tumor in Small Animals. IEEE Trans Biomed Eng 52:1373–1381. doi: 10.1109/TBME.2005.851524

Sel D, Cukjati D, Batiuskaite D, et al. (2005) Sequential finite element model of tissue electropermeabilization. IEEE Transactions on Biomedical Engineering 52:816–827. doi: 10.1109/TBME.2005.845212

Sersa G, Miklavcic D, Cemazar M, et al. (2008) Electrochemotherapy in Treatment of Tumours. EJSO 34:232–240.

Serša G, Miklavčič D (2008) Electrochemotherapy of Tumors. Journal of Visualized Experiments 22.

Toepfl S, Heinz V, Knorr D (2007) High intensity pulsed electric fields applied for food preservation. Chemical Engineering and Processing 46:537–546. doi: 10.1016/j.cep.2006.07.011

Ušaj M, Trontelj K, Miklavčič D, Kandušer M (2010) Cell–Cell Electrofusion: Optimization of Electric Field Amplitude and Hypotonic Treatment for Mouse Melanoma (B16-F1) and Chinese Hamster Ovary (CHO) Cells. J Membrane Biol 236:107–116. doi: 10.1007/s00232-010-9272-3

Zheng Y, Grossman M, Awate SP, Gee JC (2009) Automatic Correction of Intensity Nonuniformity from Sparseness of Gradient Distribution in Medical Images. Proceedings of the 12th International Conference on Medical Image Computing and Computer-Assisted Intervention: Part II. Springer-Verlag, Berlin, Heidelberg, pp 852–859

Zupanic A, Kos B, Miklavcic D (2012) Treatment planning of electroporation-based medical interventions: electrochemotherapy, gene electrotransfer and irreversible electroporation. Physics in Medicine and Biology 57:5425–5440. doi: 10.1088/0031-9155/57/17/5425

Županič A, Čorović S, Miklavčič D (2008) Optimization of Electrode Position and Electric Pulse Amplitude in Electrochemotherapy. Radiology and Oncology 42:93–101.

Županič A, Miklavčič D (2009) Optimization and Numerical Modeling in Irreversible Electroporation Treatment Planning. Irreversible Electroporation. Springer, Berlin, pp 203–222

Županič A, Miklavčič D (2011) Tissue heating during tumor ablation with irreversible electroporation. Electrotechnical Review 42–47.

DISCUSSION

ELECTROCHEMOTHERAPY TREATMENT PLANNING PROCEDURE

In *Article 1*, we described the development of the electrochemotherapy (ECT) treatment planning procedure that can provide clinicians with the information needed to effectively perform electroporation-based treatments in the clinical setting. Because following standard operating procedures (Mir et al., 2006) cannot ensure successful treatment when treating deep-seated tumors with ECT, it is important to prepare a patient-specific treatment plan (Pavliha et al., 2012). However, treatment planning of ECT is an interdisciplinary procedure that requires knowledge from the fields of biomedicine, engineering and oncology. Therefore, in order to make ECT treatment planning available to clinicians, the procedure needs to be simplified from the user's point of view. Hence, the required user interaction to perform treatment planning should be minimal (Heymann and Degani, 2007; Stupak et al., 2010).

In order for clinicians to adopt ECT treatment planning procedure, the latter has been designed based on the radiotherapy example (Lecchi et al., 2008) where treatment planning is well-established and not only known, but also accepted to be of paramount importance for successful treatment (Tannock et al., 2005). We exposed parallelisms to radiotherapy when conceptually designing ECT treatment planning, and although the established protocols and algorithms have been intended specifically for ECT of deep-seated tumors, they are general enough to be useful for all electroporation-based therapies given that application-specific details are added to the procedure. Since electric field distribution is the most important predictor of successful electroporation (Miklavčič et al., 2006, 1998), electric field distribution-specific parameters (i.e. the objective function) need to be modified in order to use the treatment planning procedures for other electroporation-based therapies than ECT (Županič et al., 2010). Namely, when planning ECT the tumor is required to be covered with a sufficiently strong electric field (above 460 V/cm, i.e. the reversible threshold) minimizing also damage to healthy tissue due to irreversible electroporation (i.e. the irreversible threshold). Moreover, voltage and electrode position/geometry with respect to the distance between electrodes need to be such as to

ensure adequate electric field strengths (i.e. above reversible and below irreversible thresholds). Similarly, the resulting electric field strength in the target tissue is required to exceed the irreversible threshold when planning non-thermal irreversible electroporation (N-TIRE) for ablation to be successful. It is however important to avoid tissue damage due to thermal effects (i.e. Joule heating) (Davalos et al., 2003). All these issues demonstrate that, given that all the required parameters are adequately chosen and application-specific requirements are met, the described treatment planning procedure can be indeed used for every electroporation-based treatment (Županič et al., 2012).

LIVER SEGMENTATION ALGORITHMS AND VALIDATION

In order to simplify the treatment planning procedure, algorithms for automatic liver segmentation were developed. As part of automatic segmentation, some preprocessing techniques were implemented; since e.g. debiasing is required when processing MRI images but developing of such algorithms can represent a demanding task (Likar et al., 2001), publicly available code was used to perform this procedure (Zheng et al., 2009). In *Article 2*, three possible automatic liver segmentation algorithms were presented and evaluated by optimizing their functioning for accurate liver segmentation. Optimization was done on a dataset consisting of seven patients that were manually segmented by the radiologist and used as a training set. Furthermore, validation was performed using an additional radiologist dataset of four patients that were previously not included in the training set. Development of automatic segmentation algorithm for accurate three-dimensional liver model generation is a challenging task: the variability of the input data (i.e. liver in the patient's medical images) namely makes segmentation difficult to perform. To explore different segmentation possibilities, three algorithms were implemented and further improved by developing and applying a postprocessor.

We first evaluated the region growing algorithm that, although not being fully automatic due to the need for a manual initial seed placement, can provide satisfactory segmentation results (Mancas et al., 2005). The main drawback of the region growing algorithm, i.e. segment leakage, was eliminated by the postprocessor as the final step of liver segmentation. Although considered overly simplistic, region growing provided best similarity results to the

radiologist dataset, as presented in *Table 2* of *Article 2*. Moreover, the algorithm could be upgraded to a fully automatic algorithm by programmatically defining the initial seed location, e.g. based on determining the expected intensity of the target segment on the *referential slice* (as defined in chapter 2.1.3. of *Article 2*) using another segmentation algorithm, e.g. adaptive threshold. In that way, the implemented region growing algorithm could be upgraded to perform automatically, i.e. without the need of user interaction.

As second we evaluated the adaptive threshold segmentation algorithm that was developed because of its intuitive approach; the algorithm is based on the physical property of the organ subject to segmentation, i.e. continuity of the tissue on two neighboring slices. Namely, due to tissue continuity the difference between segments on two neighboring slices is expected to be minimal. Therefore, the developed algorithm processes the currently-segmented slice by a thresholding function with an adaptive (i.e. changing in every iteration) threshold to the previous already-segmented slice; the global maximum of similarity (i.e. normalized cross-correlation) of the neighboring slices determines the finally used threshold, and segmentation proceeds to the next slice. Adaptive threshold, like the region growing algorithm, can also be exposed to segment leakage since it is intensity-based. Therefore, the use of the postprocessor proved to be necessary, since otherwise some organs (e.g. the spleen, the heart, the kidneys) may be detected as liver segments due to their similar intensity ranges to the liver (Massoptier and Casciaro, 2008). The initialization of the adaptive threshold algorithm is another important step: since the initial slice has no predecessors which it could be compared to, a set of presets (i.e. approximate shapes of the target organ's segment that is expected to be detected in the initial slice) is used for the first comparison instead. Although only six liver presets were available in our implementation of the adaptive threshold algorithm, the initial segment was properly detected on every case during optimization and validation procedures.

We evaluated active contours, sometimes referred to as the *snakes* algorithm (Kass et al., 1987), as the third segmentation algorithm; our implementation of the active contours algorithm is based on the Gradient Vector Flow (GVF) (Xu and Prince, 1998). Active contours algorithm has the benefit of not being susceptible to intensity-related anomalies, such as intensity inhomogeneity. However, the active (i.e. deformable) contour, that finally

determines the segment, is attracted to edges including those of the structures within the target organ. Therefore, it is imperative to properly initialize the active contour, i.e. place it in the near vicinity of the target segment, since otherwise it may get attracted by edges of internal organ structures (e.g. blood vessels, metastases, hemangioma etc.) instead of external organ edges. Besides, soft transitions of the tissue between two neighboring slices also represent a drawback of the active contours algorithm, because its current implementation is based on the Gradient Vector Flow (GVF) map which is dependent on the edges detected in the images. Namely, soft transitions of the tissue prevent proper edge detection in the images, which further prevents proper GVF map generation; finally, due to improper GVF map the active contours do not align on the external organ edges since edges were not properly detected. Therefore, active contours are aligned to edges of surrounding organs instead, which causes improper segment detection.

All the described issues demonstrate that despite of the used algorithm, liver segmentation for electrochemotherapy (ECT) is a complex procedure. Fortunately, highest accuracy of the relevant tissue (e.g. liver) is not required for electric field distribution calculation of ECT since from the modeling point of view, the liver only represents the medium that surrounds the target tissue, i.e. the tumor. Moreover, during surgery the liver tends to deform and, therefore, the organ may differ from the model geometry in the treatment plan (Clements et al., 2011). It is however important the tumor being accurately segmented. Although the ECT treatment planning we established is based on radiotherapy treatment planning, there is a certain radiotherapy-specific feature related to tumor segmentation that should not be replicated when planning ECT. Namely, in radiotherapy treatment planning, the tumor (i.e. target tissue for the radiation beam) is segmented using a safety margin (i.e. some healthy tissue around the tumor is exposed to the radiation beam as well). The safety margin is used to assure complete beam coverage of the target tissue. Nevertheless, in ECT treatment planning such increase of tumor volume is not acceptable because the tumor tissue's conductivity significantly differs from the conductivity of the healthy tissue (Kos et al., 2010) and calculations of the electric field distribution would be improper if the tumor was oversegmented. Hence the need for accurate tumor segmentation. Currently, tumor segmentation is performed manually (i.e. by manual

contour delineation) because automatic tumor segmentation is a challenging task due to variability of shape, size and location of tumors (Barbosa et al., 2012). However, we are considering implementing an algorithm for segmentation of internal structures (i.e. residing within the liver which is achieved by masking the input data using the obtained liver segments) that detects line-like and blob-like structures and identifies them as blood vessels and possible tumor objects, respectively. The multi-scale algorithm (Frangi et al., 1998) described in *Article 3* serves as the base for blood vessel and tumor segmentation; since tumor segmentation is a demanding procedure (Ahmed et al., 2011; Foo et al., 2011; Wang, 2011) and because high accuracy is required, manual validation of the generated segments is necessary at the end of the segmentation procedure, which enables the end-user (i.e. the clinician) to approve the results obtained. Such manual validation gives the clinician the possibility of not only determining which blob-like structures are tumors and performing manual error correction of segmentation, but also taking liability for the generated segmentation results, which is of great importance for clinical use of electroporation-based therapies' treatment planning.

An important step of developing treatment planning software with embedded automatic segmentation algorithms is validation of the developed procedures. Namely, the implemented segmentation algorithms need to provide accurate results (i.e. correctly detected tissue segments) which designates the requirement for algorithm validation. Before validation of the algorithms, their optimization was performed using a set of seven patient cases manually segmented by the radiologist (i.e. the training set). The training set allowed optimization of algorithm parameters: deviation of the intensity that is included in the region (region growing), initial coefficient that determines targeted size of the initial segment (adaptive threshold), and energy contribution coefficients (active contours). The automatically generated (i.e. using segmentation algorithms) results were compared to data from the training set using normalized cross-correlation (i.e. similarity) on a slice basis. Optimization results presented in *Table 1* of *Article 2* demonstrated that our implementation of region growing was the most optimization-prone algorithm evaluated, since it could be optimized to achieve 89.2% median similarity (79.8% mean similarity with 12.7% standard deviation) to the training set. Adaptive threshold algorithm could be

optimized to achieve 87.6% median similarity (67.6% mean similarity with 12.8% standard deviation), and our implementation of the active contours algorithm 86.4% median similarity (68.8% mean similarity with 8.6% standard deviation), which shows that despite being more sophisticated, these two algorithms achieved lower optimization results (i.e. similarity to the training set) than region growing. Region growing allowed good optimization possibilities because the parameter that influences what intensity range is included in the segment (i.e. deviation of the intensity) was subject to optimization. Adaptive threshold algorithm lacks changeable parameters that influence segmentation, as it mainly relies on the tissue continuity feature and in this implementation, no other parameters could be set. An improvement could be made by replacing the threshold function of the adaptive threshold algorithm with a bandpass function (i.e. instead of including intensities that exceed the threshold, intensities between two boundary thresholds would be included instead), which would enable more parameters (lower and upper boundaries, and width of the included intensity range) of the adaptive threshold algorithm to be optimized. Finally, four parameters of the active contours algorithm were optimized (i.e. energy contributions of the deformable contour: elasticity, curvature, GVF magnitude and GVF direction). Although such optimization should provide good fit to the training set, it is rather difficult to accurately influence the movement of the active contour since the movement is mostly relying on GVF-related parameters. Namely, the active contour aligns itself mainly to edges in the image (e.g. external organ edges). If the edges of the target tissue are improperly detected after preprocessing (e.g. the target tissue does not have clearly detectable edges), the movement of the active contour will be unforeseeable and optimization is trivial.

After optimization, a final validation step of the algorithms was performed. The validation of the algorithms was done on four patient cases manually segmented by a radiologist that were not part of the training set (i.e. validation data set). Like optimization, validation was also done by comparing similarities of the automatically generated results by the segmentation algorithms to the data from the validation data set using normalized cross-correlation on a slice basis. The total similarity (i.e. similarity of a patient case, comprising of similarities of each slice) was determined using mean or median similarity of all slice

similarities within a case. Two data representations (i.e. mean and median) were presented because during optimization and validation, many slices with 0% similarity were detected. Zero-similarity is detected when comparing two slices where an automatically generated slice or the manually (i.e. by the radiologist) segmented slice does not contain any segments while the other does. Therefore, if only a few pixels are detected by the segmentation algorithm but are not identified by the radiologist (or vice versa), the result of such slice comparison will be 0% similarity. Hence, such slices significantly impact the overall outcome of the assessment and using the mean value of all slices, the success of a segmentation algorithm may not be reflected enough. Therefore, besides the mean similarity, the median similarity of the slices of a case is presented as well.

INTEGRATED SOFTWARE WITH GRAPHICAL USER INTERFACE

To facilitate electrochemotherapy (ECT) treatment planning, the procedure that includes algorithms for automatic segmentation was developed as web-based treatment planning software that is operated by the end-user (i.e. clinician) using a graphical user interface (GUI). The GUI is rendered at the client-side (i.e. in the user's web browser), while all the processing that involves 3D model generation and electric field distribution calculation and optimization is executed on the treatment planning server. Such implementation permits that the client computer is not loaded by the processing, and also allows centralization of all generated treatment plans. The latter is of great importance because it permits generating a database of not only segmented but also validated patient cases of various tissues; namely, since the software allows manual validation of the segmentation algorithms at the end of the procedure (i.e. the end-user manually corrects segmentation outcome) the data can serve as a new training set that keeps expanding with the use of the software. Finally, the training set could be used by the software to automatically learn segmentation and optimize its own functioning.

Because of its modular design, the ECT treatment planning software also allows new segmentation algorithms to be included subsequently. Namely, the software currently allows segmentation of liver (using three possible liver segmentation algorithms: region growing, adaptive threshold, and active contours) and bone (using fixed thresholding).

Moreover, it is possible to import pre-segmented DICOM images which include segment structures in a standard DICOM file. In that way, segmentation can be done using external software (or archived medical images can be reused for evaluation) and ECT treatment planning software is, then, only used for post-segmentation procedures (i.e. virtual electrode insertion and electric field distribution calculation). These data could also become part of a new training set that could allow development of new algorithms for segmenting tissue that has not been included in automatic segmentation procedure. Also, loading already-segmenting cases allows historical evaluation of patients that were already treated with the purpose of correlating the calculated coverage of the tumor with the electric field to the treatment outcome. The latter is of great importance for improving electroporation-based treatments in clinical practice.

CONCLUSION

In this doctoral dissertation, we establish treatment planning procedure for electrochemotherapy (ECT) of deep-seated tumors. Furthermore, because the developed procedures are primarily based on knowledge about the electroporation phenomenon, they are not ECT-specific and are, therefore, applicable to other electroporation-based treatments, e.g. non-thermal irreversible electroporation (N-TIRE) for tumor ablation.

Treatment planning allows users of electroporation-based treatments (i.e. clinicians) better insight on the importance of accurate treatment planning due to direct correlation of tumor coverage with sufficiently high electric field strength to the treatment outcome. Moreover, the possibility of generating treatment plans for cases that were previously segmented and already treated allows historical evaluation of performed treatments, which is of great importance for further improvements of performing electroporation-based treatments in the clinical setting.

Finally, development of easy-to-use web-based treatment planning software with integrated algorithms for automatic tissue segmentation greatly improves the availability of ECT or N-TIRE treatment planning procedures to end-users (i.e. clinicians) who can use the software to prepare accurate treatment plans remotely and without the need of engineers. Consequently, more treatments can be performed and better treatment outcome can be expected, which at the end results in improved patients' quality of life.

ORIGINAL CONTRIBUTIONS

Based on results in this doctoral dissertation I claim for the recognition of the following original scientific contributions to the research area:

DESIGN OF PATIENT-SPECIFIC ELECTROCHEMOTHERAPY TREATMENT PLANNING PROCEDURES FOR TREATING DEEP-SEATED TUMORS

We designed patient-specific treatment planning for electrochemotherapy of deep-seated tumors; treatment planning procedures are based on radiotherapy treatment planning. The designed treatment planning procedures rely on patient medical images processing and tissue segmentation: relevant organ (e.g. liver), pathological tissue (i.e. tumor), and other relevant tissue (e.g. blood vessels). The developed procedures allow efficient electrochemotherapy treatment of deep-seated tumors.

OPTIMIZATION AND VALIDATION OF AUTOMATIC LIVER SEGMENTATION ALGORITHMS FOR PATIENT-SPECIFIC ELECTROCHEMOTHERAPY TREATMENT PLANNING

We developed algorithms for automatic liver segmentation from the medical images; segmentation algorithms are used for patient-specific electrochemotherapy treatment planning-purposes. The developed algorithms (region growing, adaptive threshold, and active contours) are validated using radiological expert opinion using seven models for functioning optimization and additional four models for final validation of the optimized algorithms.

DEVELOPMENT OF INTEGRATED SOFTWARE FOR PATIENT-SPECIFIC ELECTROCHEMOTHERAPY TREATMENT PLANNING

We developed integrated software that embeds all the procedures that are required for electrochemotherapy treatment planning: interface for patient's medical images import, algorithms for automatic segmentation, interface for virtual electrode insertion, algorithms for electric field distribution in tissue, and interface for treatment plan presentation.

Currently, the software allows segmentation of two tissue types: liver (with blood vessels) and bones. Due to its modular design, inclusion of segmentation algorithms for other tissue types is possible. The software is controlled using easy-to-use graphical user interface that is developed as a web application which, therefore, allows remote treatment planning (i.e. telemedicine).

REFERENCES

Agerholm-Larsen, B., Iversen, H.K., Ibsen, P., Moller, J.M., Mahmood, F., Jensen, K.S., Gehl, J., 2011. Preclinical Validation of Electrochemotherapy as an Effective Treatment for Brain Tumors. Cancer Research 71, 3753–3762.

Ahmed, S., Iftekharuddin, K., Vossough, A., 2011. Efficacy of Texture, Shape, and Intensity Feature Fusion for Posterior-Fossa Tumor Segmentation in MRI. IEEE Transactions on Information Technology in Biomedicine 15, 206–213.

Barbosa, D., Dietenbeck, T., Schaerer, J., D'hooge, J., Friboulet, D., Bernard, O., 2012. B-Spline Explicit Active Surfaces: An Efficient Framework for Real-Time 3-D Region-Based Segmentation. IEEE Transactions on Image Processing 21, 241–251.

Charpentier, K.P., Wolf, F., Noble, L., Winn, B., Resnick, M., Dupuy, D.E., 2010. Irreversible electroporation of the pancreas in swine: a pilot study. HPB 12, 348–351.

Charpentier, K.P., Wolf, F., Noble, L., Winn, B., Resnick, M., Dupuy, D.E., 2011. Irreversible electroporation of the liver and liver hilum in swine. HPB 13, 168–173.

Clements, L., Dumpuri, P., Champan, W., Dawant, B., Galloway, R., Miga, M., 2011. Organ surface deformation measurement and analysis in open hepatic surgery: method and preliminary results from 12 clinical cases. IEEE Transactions on Biomedical Engineering PP, 1–1.

Daugimont, L., Baron, N., Vandermeulen, G., Pavselj, N., Miklavcic, D., Jullien, M.-C., Cabodevila, G., Mir, L.M., Préat, V., 2010. Hollow Microneedle Arrays for Intradermal Drug Delivery and DNA Electroporation. J. Membrane Biol. 236, 117–125.

Davalos, R., Rubinsky, B., 2008. Temperature considerations during irreversible electroporation. International Journal of Heat and Mass Transfer 51, 5617–5622.

Davalos, R., Rubinsky, B., Lir, L., 2003. Theoretical analysis of the thermal effects during in vivo tissue electroporation. Bioelectrochemistry 61, 99–107.

Edhemović, I., Gadžijev, E.M., Brecelj, E., Miklavčič, D., Kos, B., Županič, A., Mali, B., Jarm, T., Pavliha, D., Marčan, M., Gašljevič, G., Gorjup, V., Mušič, M., Vavpotič, T.P., Čemažar, M., Snoj, M., Serša, G., 2011. Electrochemotherapy: A New Technological Approach in Treatment of Metastases in the Liver. Technol. Cancer Res. Treat 10, 475–485.

Fini, M., Tschon, M., Alberghini, M., Bianchi, G., Mercuri, M., Campanacci, L., Cavani, F., Ronchetti, M., De Terlizzi, F., Cadossi, R., 2011. Cell Electroporation in Bone Tissue, in: Kee, S.T., Gehl, J., Lee, E.W. (Eds.), Clinical Aspects of Electroporation. Springer New York, New York, NY.

Foo, J., Miyano, G., Lobe, T., Winer, E., 2011. Tumor Segmentation from Computed Tomography Image Data Using a Probabilistic Pixel Selection Approach. Computers in Biology and Medicine 41, 56–65.

Frangi, A., Niessen, W., Vincken, K., Viergever, M., 1998. Multiscale vessel enhancement filtering, in: Wells, W., Colchester, A., Delp, S. (Eds.), Medical Image Computing and Computer-Assisted Intervention, Lecture Notes in Computer Science. Presented at the MICCAI'98, Springer-Verlag, Berlin, Germany, pp. 130–137.

Garcia, P., Pancotto, T., Rossmeisl, J., Henao-Guerrero, N., Gustafson, N., Daniel, G., Robertson, J., Ellis, T., Davalos, R., 2011. Non-Thermal Irreversible Electroporation (N-TIRE) and Adjuvant Fractionated Radiotherapeutic Multimodal Therapy for Intracranial Malignant Glioma in a Canine Patient. Technology in Cancer Research & Treatment 73–83.

Gusbeth, C., Frey, W., Volkmann, H., Schwartz, T., Bluhm, H., 2009. Pulsed Electric Field Treatment for Bacteria Reduction and Its Impact on Hospital Wastewater. Chemosphere 228–233.

Heller, L., Heller, R., 2010. Electroporation Gene Therapy Preclinical and Clinical Trials for Melanoma. Current Gene Therapy 10, 312–317.

Heymann, M., Degani, A., 2007. Formal analysis and automatic generation of user interfaces: Approach, methodology, and an algorithm. Human Factors 49, 311–330.

Kass, M., Witkin, A., Terzopoulos, D., 1987. Snakes - active contour models. Int. J. of Comp. Vis 1, 321–331.

Kos, B., Županič, A., Kotnik, T., Snoj, M., Serša, G., Miklavčič, D., 2010. Robustness of Treatment Planning for Electrochemotherapy of Deep-Seated Tumors. Journal of Membrane Biology 236, 147–153.

Kotnik, T., Pucihar, G., Miklavčič, D., 2010. Induced Transmembrane Voltage and Its Correlation with Electroporation-Mediated Molecular Transport. Journal of Membrane Biology 236, 3–13.

Lecchi, M., Fossati, P., Elisei, F., Orecchia, R., Lucignani, G., 2008. Current Concepts on Imaging in Radiotherapy. European Journal of Nuclear Medicine and Molecular Imaging 35, 821–837.

Likar, B., Viergever, M., Pernuš, F., 2001. Retrospective correction of MR intensity inhomogeneity by information minimization. IEEE Transactions on Medical Imaging 20, 1398–1410.

Linnert, M., Iversen, H., Gehl, J., 2012. Multiple brain metastases - current management and perspectives for treatment with electrochemotherapy. Radiology and Oncology 2012, 1–8.

Maček-Lebar, A., Serša, G., Čemažar, M., Miklavčič, D., 1998. Elektroporacija. Medicinski Razgledi 37, 339–354.

Mahmood, F., Gehl, J., 2011. Optimizing clinical performance and geometrical robustness of a new electrode device for intracranial tumor electroporation. Bioelectrochemistry 81, 10–16.

Mali, B., Jarm, T., Snoj, M., Serša, G., Miklavčič, D., 2013. Antitumor effectiveness of electrochemotherapy: A systematic review and meta-analysis. European Journal of Surgical Oncology (EJSO) 39, 4 – 16.

Mancas, M., Gosselin, B., Macq, B., 2005. Segmentation Using a Region Growing Thresholding, in: Image Processing: Algorithms and Systems IV. San Jose, CA, USA.

Marty, M., Serša, G., Garbay, J., Gehl, J., Collins, C., Snoj, M., Billard, V., Geertsen, P., Larkin, J., Miklavčič, D., Pavlović, I., Paulin-Košir, S., Čemažar, M., Morsli, N., Rudolf, Z., Robert, C., O'Sullivan, G., Mir, L., 2006. Electrochemotherapy - an Easy, Highly Effective and Safe Treatment of Cutaneous and Subcutaneous Metastases: Results of ESOPE (European Standard Operating Procedures of Electrochemotherapy) Study. EJC Supplements 4, 3–13.

Massoptier, L., Casciaro, S., 2008. A new fully automatic and robust algorithm for fast segmentation of liver tissue and tumors from CT scans. European Radiology 18, 1658–1665.

Miklavčič, D., Beravs, K., Šemrov, D., Čemažar, M., Demšar, F., Serša, G., 1998. The Importance of Electric Field Distribution for Effective in Vivo Electroporation of Tissues. Biophysical Journal 2152–2158.

Miklavčič, D., Čorović, S., Pucihar, G., Pavšelj, N., 2006. Importance of Tumour Coverage by Sufficiently High Local Electric Field for Effective Electrochemotherapy. EJC Supplements 4, 45–51.

Miklavčič, D., Serša, G., Brecelj, E., Gehl, J., Soden, D., Bianchi, G., Ruggieri, P., Rossi, C.R., Campana, L.G., Jarm, T., 2012. Electrochemotherapy: technological advancements for efficient electroporation-based treatment of internal tumors. Medical & Biological Engineering & Computing 50, 1213–1225.

Miklavčič, D., Snoj, M., Zupanic, A., Kos, B., Cemazar, M., Kropivnik, M., Bracko, M., Pecnik, T., Gadzijev, E., Sersa, G., 2010. Towards treatment planning and treatment of deep-seated solid tumors by electrochemotherapy. BioMed Eng OnLine 9, 10.

Miklavčič, D., Šemrov, D., Mekid, H., Mir, L.M., 2000. A validated model of in vivo electric field distribution in tissues for electrochemotherapy and for DNA electrotransfer for gene therapy. Biochimica et Biophysica Acta 1523, 73–83.

Mir, L., Gehl, J., Sersa, G., Collins, C., Garbay, J., Billard, V., Geertsen, P., Rudolf, Z., O'Sullivan, G., Marty, M., 2006. Standard operating procedures of the electrochemotherapy: Instructions for the use of bleomycin or cisplatin administered either systemically or locally and electric pulses delivered by the Cliniporator (TM) by means of invasive or non-invasive electrodes. EJC Supplements 4, 14–25.

Mir, L., Orlowski, S., Belehradek, J., Paoletti, C., 1991. Electrochemotherapy Potentiation of Antitumor Effect of Bleomycin by Local Electric Pulses. European Journal of Cancer 68–72.

National Electrical Manufacturers Association, 2009. Digital Imaging and Communications in Medicine (DICOM).

Neal, R.E., Rossmeisl, Jr., J.H., Garcia, P.A., Lanz, O.I., Henao-Guerrero, N., Davalos, R.V., 2011. Successful Treatment of a Large Soft Tissue Sarcoma With Irreversible Electroporation. Journal of Clinical Oncology 29, E372–E377.

Neumann, E., Schaeferridder, M., Wang, Y., Hofschneider, P., 1982. Gene-Transfer into Mouse Lyoma Cells by Electroporation in High Electric-Fields. EMBO Journal 841–845.

Orlowski, S., Belehradek, J., Paoletti, C., Mir, L.M., 1988. Transient Electropermeabillization of Cells in Culture - Increase of Cyto-Toxicity of Anticancer Drugs. Biochemical Pharmacology 37, 4727–4733.

Paulides, M.M., Bakker, J.F., Linthorst, M., Van der Zee, J., Rijnen, Z., Neufeld, E., Pattynama, P.M.T., Jansen, P.P., Levendag, P.C., Van Rhoon, G.C., 2010. The clinical feasibility of deep hyperthermia treatment in the head and neck: new challenges for positioning and temperature measurement. Physics in Medicine and Biology 55, 2465.

Pavešić, N., 2000. Razpoznavanje vzorcev: uvod v analizo in razumevanje vidnih in slušnih signalov. Fakulteta za elektrotehniko, Ljubljana.

Pavliha, D., Kos, B., Županič, A., Marčan, M., Serša, G., Miklavčič, D., 2012. Patient-specific treatment planning of electrochemotherapy: Procedure design and possible pitfalls. Bioelectrochemistry 87, 265–273.

Puc, M., Čorović, S., Flisar, K., Petkovšek, M., Nastran, J., Miklavčič, D., 2004. Techniques of signal generation required for electropermeabilization: Survey of electropermeabilization devices. Bioelectrochemistry 64, 113–124.

Rubinsky, B., Onik, G., Mikus, P., 2007. Irreversible electroporation: A new ablation modality - Clinical implications. Technology in Cancer Research & Treatment 6, 37–48.

Serša, G., Čemažar, M., Miklavčič, D., 1995. Antitumor effectivness of electrochemotherapy with cis-diamminedichloroplatinium (II) in mice. Cancer Research 55, 3450–3455.

Serša, G., Miklavčič, D., 2008. Electrochemotherapy of Tumors. Journal of Visualized Experiments 22.

Serša, G., MIklavčič, D., Čemažar, M., Rudolf, Z., Pucihar, G., Snoj, M., 2008. Electrochemotherapy in treatment of tumours. Eur. J. Surg. Oncol. 34, 232–240.

Stupak, N., DiFonzo, N., Younge, A.J., Homan, C., 2010. SOCIALSENSE: Graphical User Interface Design Considerations for Social Network Experiment Software. Computers in Human Behavior 26, 365–370.

Šel, D., Cukjati, D., Batiuskaite, D., Slivnik, T., Mir, L., Miklavčič, D., 2005. Sequential finite element model of tissue electropermeabilization. IEEE Transactions on Biomedical Engineering 52, 816–827.

Tannock, I.F., Hill, R.P., Bristow, R.G., Harrington, L., 2005. The Basic Science of Oncology, 4th ed. McGraw-Hill Medical.

Toepfl, S., Heinz, V., Knorr, D., 2007. High intensity pulsed electric fields applied for food preservation. Chemical Engineering and Processing 46, 537–546.

Ušaj, M., Trontelj, K., Miklavčič, D., Kandušer, M., 2010. Cell–Cell Electrofusion: Optimization of Electric Field Amplitude and Hypotonic Treatment for Mouse Melanoma (B16-F1) and Chinese Hamster Ovary (CHO) Cells. J. Membrane Biol. 236, 107–116.

Vovk, U., Pernuš, F., Likar, B., 2007. A review of methods for correction of intensity inhomogeneity in MRI. IEEE Transactions on Image Processing 26, 405–421.

Wang, C., 2011. Robust Automated Tumour Segmentation on Histological and Immunohistochemical Tissue Images. PLOS One 6.

Xu, C., Prince, J., 1998. Snakes, shapes, and gradient vector flow. IEEE Trans Imag Proc 7, 359–369.

Zheng, Y., Grossman, M., Awate, S.P., Gee, J.C., 2009. Automatic Correction of Intensity Nonuniformity from Sparseness of Gradient Distribution in Medical Images, in: Proceedings of the 12th International Conference on Medical Image Computing and Computer-Assisted Intervention: Part II, MICCAI '09. Springer-Verlag, Berlin, Heidelberg, pp. 852–859.

Županič, A., Čorović, S., Miklavčič, D., 2008. Optimization of Electrode Position and Electric Pulse Amplitude in Electrochemotherapy. Radiology and Oncology 42, 93–101.

Županič, A., Čorović, S., Miklavčič, D., Pavlin, M., 2010. Numerical optimization of gene electrotransfer into muscle tissue. BioMed Eng OnLine 9, 66.

Županič, A., Kos, B., Miklavčič, D., 2012. Treatment planning of electroporation-based medical interventions: electrochemotherapy, gene electrotransfer and irreversible electroporation. Physics in Medicine and Biology 57, 5425–5440.

Županič, A., Miklavčič, D., 2009. Optimization and Numerical Modeling in Irreversible Electroporation Treatment Planning, in: Irreversible Electroporation. Springer, Berlin, pp. 203–222.

Županič, A., Miklavčič, D., 2011. Tissue heating during tumor ablation with irreversible electroporation. Electrotechnical Review 42–47.

DECLARATION

The author hereby declares that the content of the thesis is a result of his own research work supervised by prof. Damijan Miklavčič. The results, which were collected in collaboration with other colleagues, are published in the presented papers. The assistance from other colleagues is stated in the Acknowledgments. The published results of other authors are presented in the literature.

Denis Pavliha, B.Sc.

IZJAVA

Izjavljam, da sem doktorsko disertacijo izdelal sam, pod mentorstvom prof. dr. Damijana Miklavčiča. Rezultati, ki so nastali v sodelovanju z drugimi sodelavci, so bili objavljeni v predstavljenih člankih. Izkazano pomoč ostalih sodelavcev sem v celoti navedel v zahvali. Že objavljeni dosežki drugih avtorjev so navedeni v spisku literature.

Denis Pavliha, univ.dipl.inž.el.